

THE CELESTIAL REFERENCE FRAME AT 24 AND 43 GHz. II. IMAGING

P. CHARLOT^{1,2}, D. A. BOBOLTZ³, A. L. FEY³, E. B. FOMALONT⁴, B. J. GELDZAHLER⁵,
 D. GORDON⁶, C. S. JACOBS⁷, G. E. LANYI⁷, C. MA⁸, C. J. NAUDET⁷,
 J. D. ROMNEY⁹, O. J. SOVERS¹⁰, AND L. D. ZHANG⁷

Draft version July 17, 2021, accepted by the Astronomical Journal

ABSTRACT

We have measured the sub-milli-arcsecond structure of 274 extragalactic sources at 24 and 43 GHz in order to assess their astrometric suitability for use in a high frequency celestial reference frame (CRF). Ten sessions of observations with the Very Long Baseline Array have been conducted over the course of ~ 5 years, with a total of 1339 images produced for the 274 sources. There are several quantities that can be used to characterize the impact of intrinsic source structure on astrometric observations including the source flux density, the flux density variability, the source structure index, the source compactness, and the compactness variability. A detailed analysis of these imaging quantities shows that (1) our selection of compact sources from 8.4 GHz catalogs yielded sources with flux densities, averaged over the sessions in which each source was observed, of about 1 Jy at both 24 and 43 GHz, (2) on average the source flux densities at 24 GHz varied by 20%–25% relative to their mean values, with variations in the session-to-session flux density scale being less than 10%, (3) sources were found to be more compact with less intrinsic structure at higher frequencies, and (4) variations of the core radio emission relative to the total flux density of the source are less than 8% on average at 24 GHz. We conclude that the reduction in the effects due to source structure gained by observing at higher frequencies will result in an improved CRF and a pool of high-quality fiducial reference points for use in spacecraft navigation over the next decade.

Subject headings: astrometry — quasars: general — radio continuum: galaxies — surveys

1. INTRODUCTION

The International Celestial Reference Frame (ICRF) was formally adopted as the fundamental celestial reference frame (CRF) by the International Astronomical Union (IAU) in 1997. The catalog includes precise astrometric positions of over 600 extragalactic compact radio sources distributed uniformly over the sky. These positions were determined from the analysis of thousands of dual-frequency S/X-band (2.3/8.4 GHz) Very Long Baseline Interferometry (VLBI) observational sessions recorded between 1979 and 1995. The frame itself was defined by the 212 highest-quality “defining” sources with typical position accuracies of 0.25 milli-arcseconds (mas), while the axes of the frame are accurate to 0.02 mas (Ma et al. 1998). In addition to the 212 defining sources, positions for 294 less observed “candidate” sources along with 102 “other” sources with excessive po-

sition variation, were also given to increase the density of the frame (Ma et al. 1998). Since its adoption, incremental updates to the catalog of sources have occurred in the form of two extensions to the ICRF (Fey et al. 2004) using hundreds of additional sessions along with improved analysis and modeling techniques. However, the positions of the original 212 defining sources have remained constant through these extensions.

The compact extragalactic radio sources that comprise the ICRF have been the subject of extensive study since the inception of VLBI techniques. In the standard theory, (e.g. Blandford & Königl 1979), the jet-like emission from quasars and active galactic nuclei is assumed to be powered by a central engine where energetic phenomena occur. The observed, frequency dependent, intrinsic structure of extragalactic radio sources typically consists of a flat spectrum ($S \propto \nu^\alpha, \alpha \approx 0$) unresolved core at the base of the jet where the optical depth is near unity ($\tau \approx 1$) and extended emission in the form of multiple steep spectrum ($\alpha \approx -0.5$ to -1.5) jet components. These components often move away from the core along the direction of the jet, sometimes at apparent superluminal speeds. The emission outside of the core has been shown to be extended on scales larger than the accuracy of the astrometric position measurements (Fey et al. 1996). This extended emission, or intrinsic source structure, contributes to the uncertainty in the measured astrometric positions of sources that comprise the ICRF. In addition to extended emission, frequency dependent opacity effects can contribute to variations in the measured astrometric positions of extragalactic radio sources. In particular, opacity conditions in the region near the base of the jet can cause the measured core position to move inward along the jet direction as a function of in-

¹ Université de Bordeaux, Observatoire Aquitain des Sciences de l’Univers, BP 89, 33271 Floirac Cedex, France

² CNRS, Laboratoire d’Astrophysique de Bordeaux – UMR 5804, BP 89, 33271 Floirac Cedex, France

³ U.S. Naval Observatory, 3450 Massachusetts Ave., NW, Washington, DC 20392-5420

⁴ National Radio Astronomy Observatory, 520 Edgemont Rd., Charlottesville, VA 22903

⁵ National Aeronautics and Space Administration, 300 E. St., SW, Washington, DC 20546

⁶ NVI Inc./NASA Goddard Space Flight Center, Greenbelt, MD 20771

⁷ Jet Propulsion Laboratory, Caltech, 4800 Oak Grove Dr., Pasadena, CA 91109

⁸ NASA Goddard Space Flight Center, Greenbelt, MD 20771

⁹ National Radio Astronomy Observatory, P.O. Box O, Socorro, NM 87801

¹⁰ Remote Sensing Analysis Systems, 2092 Sinaloa Ave., Alameda, CA 94501

creasing radio frequency of the observations. Such core shifts have been measured for some compact sources (e.g. Lobanov 1998; Kovalev et al. 2008).

Based upon the discussion above, there are potential advantages to observing astrometric sources at radio frequencies higher than the typical S/X band observations. First, the resolution of the observations is increased, thus improving the astrometric accuracy. Second, the effects due to intrinsic source structure may be reduced since the core and jet components have different spectral characteristics and the core is expected to be more dominant at high frequencies. We have undertaken a program to observe a number of extragalactic sources at K band (24 GHz) and Q band (43 GHz) using the 10 stations of the Very Long Baseline Array (VLBA). At these higher frequencies, only the VLBA provides the stability, imaging capabilities and frequency coverage to enable such a program. The long term goals of the program include: 1) developing a high-frequency CRF with a variety of applications including improved deep space navigation, 2) providing the astronomical community with an extended catalog of calibrator sources for VLBI observations at 24 and 43 GHz, and 3) studying the effects of the intrinsic structure of extragalactic sources to improve the astrometric accuracy of future high-frequency reference frames. A detailed discussion of the program and the astrometric results is contained in a companion paper (Lanyi et al. 2009, hereafter Paper I). In this paper, we concentrate on the imaging aspects of the program and the effects of observed source structure and variability on astrometric accuracy.

Theoretically, an optimal CRF would be composed of sources with strong, non-variable, point-like emission. In reality, however, virtually all sources possess some structure and intrinsic variability in the emission over time. In addition, there is the potential for sudden flaring events even for normally quiescent sources. Thus it is highly desirable to characterize and monitor the nature of the sources used in a CRF through periodic VLBI imaging. The VLBA has previously been used to make simultaneous dual-frequency S/X-band (2.3/8.4 GHz) observations of a total of 389 ICRF sources (Fey et al. 1996; Fey & Charlot 1997, 2000). To date, approximately 90% of the ICRF sources north of -20° declination have been imaged at least once at both 2.3 and 8.4 GHz. Based on the initial work of Charlot (1990), the database of VLBA X-band and S-band images was analyzed by Fey & Charlot (1997, 2000) in order to quantitatively improve our understanding of the relationship between extended source structure and the astrometric positions determined from VLBI. Here we discuss our growing database of high-frequency images of potential extragalactic reference frame sources. We apply similar analysis techniques in an attempt to characterize the impact of extended source structure on the astrometric accuracy of the catalog of source positions obtained from our VLBA high-frequency data (Paper I).

2. OBSERVATIONS AND DATA REDUCTION

We observed a total of 351 extragalactic radio sources using the 10 antennas of the VLBA (Napier et al. 1994) of

the National Radio Astronomy Observatory (NRAO)¹¹ over the course of 10 sessions spanning five years from 2002–2007. In all 10 of the sessions, observations were recorded at K-band (24 GHz). Additionally, in four of the 10 sessions, observations were also recorded at Q-band (43 GHz). In two of the sessions, dual S/X-band (2.3/8.4 GHz) observations were interspersed with the K-band observations to investigate potential ionospheric correction methods. A summary of the VLBA K- and Q-band observations relevant to the imaging program is presented in Table 1.

The frequency information listed in Table 1 reflects the changing observing strategy over the course of the 10 VLBA sessions. For the first two sessions, four 8 MHz bands each at 24 and 43 GHz were recorded simultaneously for each scan using 2 bit sampling yielding a total bandwidth of 32 MHz. The remaining sessions used eight 8 MHz bands with 1 bit sampling for a total bandwidth of 64 MHz. For these sessions, scans alternated between K and Q bands (sessions 3 and 5), simultaneous S/X band and K band (sessions 6 and 8), or just K band alone (sessions 4, 9, and 10). The first K-only session observed a large number of potential sources found in other VLBI surveys in order to expand the total number of available high-frequency astrometric targets. In the final two K-only sessions, candidate sources near the ecliptic plane were added for potential future use in deep space navigation. A detailed discussion of the evolving observing strategy and its relevance to the astrometric goals of the program is presented in Paper I.

All of the observations were made in a bandwidth synthesis mode to facilitate group delay measurements for astrometry – the multiplicity of channels allows for the determination of a precise group delay (Rogers 1970). Observations in this mode also allow snapshot imaging. Source scans were typically 2 minutes in duration at K band and 3 minutes for Q band. Most sources were observed in three or more scans – the one exception being the K-band survey session on 2003 May 22 in which many of the sources were observed only once or twice. The raw data bits were correlated with the VLBA correlator at the Array Operations Center in Socorro, New Mexico.

The correlated data were calibrated and corrected for residual delay and delay rate using the NRAO’s Astronomical Image Processing System (AIPS). Initial amplitude calibration for each intermediate frequency (IF) was accomplished using system temperature measurements taken during the observations combined with NRAO supplied gain curves. Fringe-fitting was done in AIPS using solution intervals equal to the scan durations and a point source model in all cases. After correction for residual delay and delay rate, the data were written to FITS disk files. All subsequent image processing was carried out using the Caltech VLBI imaging software, primarily DIFMAP.

The visibility data for each frequency band were self-calibrated, Fourier inverted, and CLEANed using DIFMAP in an automatic mode (Pearson et al. 1994). DIFMAP combines the visibilities for each IF of an observation in the (u,v) -plane during gridding, taking into

¹¹ The National Radio Astronomy Observatory is a facility of the National Science Foundation operated under cooperative agreement by Associated Universities, Inc.

account frequency differences. However, DIFMAP makes no attempt to correct for spectral index effects. The spanned bandwidth of the IFs in each band is relatively small (0.5 GHz – 2% of the fractional bandwidth), so we assume that source structure and flux density variations across each of the two frequency bands are negligible. After phase self-calibration with a point source model, the 4 s correlator records were coherently averaged to 12 s records. The averaged data were subsequently edited to remove outliers due to poor data and times in which the antennas were not on source.

The amplitude calibration within each particular session at each frequency band was improved through observations of a strong, compact source. A single amplitude gain correction factor was derived for each antenna for each IF, based on fitting a simple Gaussian source model to the visibility data of these compact sources after applying only the initial calibration based on the measured system temperatures and gain curves. Gain correction factors were calculated based on the differences between the observed and model visibilities. The resulting amplitude gain correction factors were typically less than 5% and were applied to the visibility data of all sources.

The data were self-calibrated following the hybrid-mapping technique (Pearson & Readhead 1984) to correct for residual amplitude and phase errors. The data were initially phase self-calibrated and mapped using uniform weighting in the u, v -plane before switching to natural weighting after several iterations. A point source model was used as a starting model for the iterative procedure in all cases. Convergence was defined basically as the iteration when the peak in the residual image became less than about six to eight times the root-mean-square (rms) noise of the residual image from the previous iteration. The 1%–2% of sources with emission structure too complex or too extended for the automatic imaging script to handle were imaged by hand, i.e. in an interactive mode, following the same prescription as that for the automatic mode. Convergence for these sources was subjective and was based on the iteration at which it was judged that further self-calibration would not significantly improve the resultant image.

Subsequent to the calibration and imaging process, an analysis of the variations in the flux density scaling from one session to the next was performed using 65 sources observed in at least 6 of 10 sessions at K band and 31 sources observed in at least 3 of 4 sessions at Q band. For this analysis, the mean and standard deviation of the flux density for the ensemble of sources at each band were computed. The results showed that, on average, the relative flux density scaling from one session to the next varied by $\sim 5\%$ at K band and $\sim 9\%$ at Q band.

3. IMAGING RESULTS AND ANALYSIS

Table 1 provides a summary of the number of sources successfully imaged (out of the 351 total) from the 10 sessions of K-band observations and four sessions of Q-band observations recorded as part of the high-frequency CRF program. The results of the imaging part of the program are presented graphically in the form of contour plots available via the USNO Radio Reference Frame Image Database (RRFID)¹². Shown in Figures 1 and 2 are

example contour maps from the most recent session of each of the 274 sources imaged at K band and of each of the 132 sources imaged at Q band. For convenience, the resulting K-band maps are identified by only a single fiducial frequency (either ~ 23.9 or 24.4 GHz depending on session) even though they come from data using all frequency channels. Similarly, the Q-band maps are also identified by only a single fiducial frequency (~ 43.1 GHz).

Tables 2 and 3 list the parameters relevant to the final images at each frequency including: the observation session, the elliptical beam size and position angle, the peak flux density (S_{peak}), the total flux density (S_{total}), the rms of the residuals of the flux density (S_{rms}), and the contour levels in the maps shown in Figures 1 and 2. The total flux density is the sum of all CLEAN component model flux densities obtained from the source images (Clark 1980). From the data in the table, we determined the minimum, maximum and average dynamic range ($S_{\text{peak}}/S_{\text{rms}}$) for all of the K-band images to be $\sim 40:1$, $\sim 1720:1$, and $\sim 340:1$, respectively. The average rms noise at K band is ~ 2.8 mJy beam $^{-1}$. The minimum, maximum, and average dynamic range for the Q-band images are $\sim 60:1$, $\sim 910:1$, and $\sim 250:1$, respectively. The average rms noise at Q band is ~ 5.0 mJy beam $^{-1}$. For comparison, the expected thermal noise at K band assuming 6 minutes on source (~ 2 minutes per scan times three scans) is estimated to be ~ 0.7 mJy beam $^{-1}$. At Q band, assuming 9 minutes on source (~ 3 minutes per scan times three scans) the expected thermal noise is ~ 1.6 mJy beam $^{-1}$.

The CLEAN component models were also used to determine two additional parameters, the source structure index (SI) and the source compactness (C). The structure index is described in detail in § 3.2. The source compactness is defined as the percentage of the total CLEANed flux density contained within a radius approximately equal to one synthesized beam width centered on the peak emission in the image.

3.1. Source Flux Density

For a source to be an effective astrometric reference (e.g. for spacecraft tracking and astronomical phase referencing) it must be detectable within a coherence time at the observing frequency; typically less than 2 minutes at K and Q bands. Sources should, therefore, have sufficient flux density for the given observational sensitivity, and sufficiently small variability so as not to fall below the detection threshold. From the CLEAN components models described above, the total source flux densities (S_{total}) were determined for all of the sources in all sessions in both frequency bands. From S_{total} we computed the mean flux density (\bar{S}) per source averaged over all sessions in which the source was observed. Plotted in Figure 3 are the distributions of \bar{S} for all of the sources imaged in the program including 138 sources at X band, 274 sources at K band, and 132 sources at Q band. The mean (median) values of the distributions are approximately 1.5 (0.8) Jy at X band, 1.1 (0.7) Jy at K band, and 1.4 (0.9) Jy at Q band. Shown in Figure 4 are the same distributions of \bar{S} for only those 97 sources that are common to all three bands. Here the mean (median) values are 1.7 (0.9), 1.5 (0.9) and 1.5 (1.0) Jy at X, K

¹² <http://rorf.usno.navy.mil/rrfid.shtml>

and Q bands, respectively.

It is not surprising that for the case of all sources and for the 97 sources in common that the mean flux densities at X band are the highest, especially since the strongest (> 300 mJy) most compact sources in the S/X-band ICRF program were selected for the K/Q-band observations in order to optimize the probability of detection at the higher frequencies (Paper I). This selection effect is also, very likely, the reason that, on average, the Q-band mean flux densities are larger than those at K band for all sources (Figure 3). The Q-band sources were drawn strictly from this pool of strong, compact, ICRF sources. However, as Table 1 shows, a significant fraction of the K-band sources were observed in a single-session survey that occurred on 2003 May 22. For this survey, the X-band flux density criterion was relaxed from a nominal value of 300 mJy to 200 mJy in order to include more sources. For the 97 sources in common to all three bands, the selection effect is reduced since many of the K-band survey sources are excluded. Figure 4 shows the K- and Q-band mean flux densities to be consistent with each other to within the $\sim 10\%$ session-to-session flux density scale variations mentioned previously.

The extent to which the total flux density varies over time can be characterized by the flux density variability index (σ_S/\bar{S}), which is the standard deviation of the measured flux densities divided by the mean. A minimum value, $\sigma_S/\bar{S} = 0.0$, indicates no variation in the flux density with time. Since a number of the sources at K and Q bands were observed in multiple sessions, it is possible to determine σ_S/\bar{S} for these sources. This was not the case for X band where only 25 sources were observed in both of the two X-band sessions. Distributions for the flux density variability index for the 235 sources at K band and 82 sources at Q band observed in two or more sessions are shown in Figure 5. The mean and median values of σ_S/\bar{S} at K band are 0.18 and 0.16, respectively. The Q-band mean and median values of the flux density variability for sources observed in two or more sessions are 0.19 and 0.15, respectively.

Given of the relatively few number of sessions thus far observed, the values above represent lower limits to the flux density variability. Increasing the cutoff for the minimum number of sessions per source to five, reduces the number of available K-band sources to 87 and yields a mean value of σ_S/\bar{S} of 0.23. Further increasing the minimum cutoff to 10 sessions, reduces the number of sources to 18 and results in a mean flux density variability of 0.24. At Q band there were 22 sources with data available from all four observing sessions. The mean flux density variability for these 22 sources was 0.28. Our preliminary results therefore indicate that on average the flux density varied by 20%–25% at K band, and 20%–30% at Q band. These results are limited to the ~ 5 year period over which our data were recorded and by the $\sim 10\%$ variations in the flux density scaling mentioned previously.

In addition to the flux density variability index, we also determined the ratio of the maximum to minimum flux density (S_{\max}/S_{\min}) for each source observed in more than one session. Distributions for S_{\max}/S_{\min} at K band and Q band are plotted in Figure 6, with the mean and median ratio for each distribution indicated. For the two distributions, the mean (median) values are 1.7 (1.5) at K band, and 1.7 (1.4) at Q band. The figure shows that over

the five-year period in which the sources were monitored, the maximum to minimum flux density ratio was greater than a factor of 2 for roughly 23% of the sources at K band and 24% of the sources at Q band. The ratio is greater than a factor of 3 for only 6% of the sources at K band and 4% of the sources at Q.

Our flux density results can be compared to other extragalactic source monitoring programs. The 14-m telescope at the Metsahovi Radio Observatory has monitored the flux densities of active galactic nuclei at 22, 37, and 87 GHz over the course of 25+ years (Teräsranta et al. 2005, and reference therein). Statistical analysis of this data using several different methods (Hovatta et al. 2008, 2007) has shown that smaller flux density variations occur on shorter timescales of 1–2 years, while larger outbursts are rare occurring on average every 6 years. Their sample consisted of 80 sources with a minimum flux density of 1 Jy and a minimum monitoring time of ten years. Although the time span of our data is shorter, the sampling much sparser, and the minimum flux density lower at 200–300 mJy, our K- and Q-band results seem to be consistent with the Metsahovi data. The variability index results show that the variations are relatively small over the five-year monitoring period, while the S_{\max}/S_{\min} results indicate very few large-scale outbursts over the same time period.

3.2. Source Structure Index

As previously demonstrated by Charlot (1990), the contribution of intrinsic source structure to a VLBI bandwidth synthesis delay measurement can be significant. It depends on the exact form of the spatial brightness distribution of the extended radio source relative to the geometry of the VLBI baseline vector projected onto the plane of the sky. The overall magnitude of the source structure effect for a given source is most easily estimated by calculating corrections to the bandwidth synthesis delay based upon the observed source structure, for a range of (u, v) coordinates (u and v are coordinates of the baseline vector projected onto the plane of the sky and are expressed in units of the observing wavelength). Following such a scheme, Fey & Charlot (1997) defined a source “structure index” according to the median value of the structure delay corrections, τ_{median} , calculated for all projected VLBI baselines that could be possibly observed with Earth-based VLBI (i.e., for all baselines with $\sqrt{u^2 + v^2}$ less than the diameter of the Earth), separating the sources into four classes as follows:

$$\text{Structure Index} = \begin{cases} 1, & \text{if } 0 \text{ ps} \leq \tau_{\text{median}} < 3 \text{ ps}, \\ 2, & \text{if } 3 \text{ ps} \leq \tau_{\text{median}} < 10 \text{ ps}, \\ 3, & \text{if } 10 \text{ ps} \leq \tau_{\text{median}} < 30 \text{ ps}, \\ 4, & \text{if } 30 \text{ ps} \leq \tau_{\text{median}} < \infty. \end{cases}$$

Based on this definition, the structure index at each of the three bands (X, K, and Q) was obtained for each source/session, thus providing an indication of the magnitude of the effects of intrinsic source structure in the session of observation. Detailed information regarding the computation of the structure delay corrections and the source structure index may be found in Charlot (1990) and Fey & Charlot (1997). False color images of the structure corrections as a function of (u, v) distance are available for each source via the Bordeaux VLBI Im-

age Database¹³.

From the source CLEAN components models, structure indices for 165 images of 138 sources imaged at X band, 1072 images of 274 sources at K band, and 267 images of 132 sources at Q band have been determined in a manner similar to that presented in Fey & Charlot (1997, 2000). For each source that was successfully observed, Table 4 lists the number of sessions imaged along with the minimum and maximum values of the source structure index over the course of those sessions at each of the three frequency bands. In most of the cases, the difference between the maximum and minimum SI is either 0 or 1 for X, K and Q bands. For a few sources at K and Q, the difference is 2, while there are no sources with a difference of 3. Although the data are limited in number of sessions, this seems to indicate that the SI is relatively stable over time.

As reported in §3, average image dynamic ranges were $\sim 340:1$ and $\sim 250:1$ for K and Q band, respectively. The effects of dynamic range on SI were investigated by varying the number of low-level image CLEAN components used to determine the median structure corrections and the structure index classification. Variation of the CLEAN components resulted in changes in the median structure correction on the order of a few tenths of a picosecond (0.7 ps rms), with changes larger than 1 ps occurring for only about 5% of the 1073 images at K band. These changes in the median structure correction resulted in a change in SI by 1 unit for roughly 4% of the 1073 structure indices computed. Results for Q band were similar to those at K band. Thus, the structure indices determined in this study are not significantly affected by the dynamic range of the images.

Figures 7 and 8 compare the distributions of the source structure indices derived from our VLBA observations at the three bands, X, K, and Q. In Figure 7 we plot histograms of the maximum SI measured for all sources in each of the three bands. The maximum is drawn from all available sessions in which the structure index for a particular source was determined. There were a total of 138 sources at X band, 274 sources at K band and 132 sources at Q band for which the SI was measured. The figure shows a greater number of $SI = 1, 2$ (the most compact) sources at progressively higher frequencies. The percentage of $SI = 1, 2$ sources is 71, 85, and 92% for X-, K-, and Q-band, respectively. Figure 8 plots histograms of the maximum structure index measured for only the 97 sources common to all three frequencies in our VLBA observations. Again, the obvious trend toward lower structure index at higher frequencies is seen. For the 97 common sources, the percentage having $SI = 1, 2$ is 71% at X, 87% at K, and 93% at Q band. These results indicate that the impact of source structure should be reduced at higher frequencies.

3.3. Source Compactness

The source structure index and its underlying quantity, the median structure delay correction, have proven to be highly useful measures of source structure and its effects on astrometric observations (Charlot et al. 2005; Fey et al. 2004; Sovers et al. 2002). In addition to these quantities, we introduce here a second indicator of structure

called the source compactness, C , described earlier in § 3. The compactness, which is proportional to $S_{\text{beam}}/S_{\text{total}}$, provides an indication of how point-like or extended the radio emission from a particular source is on a continuous scale from 0.0 to 1.0, where 1.0 represents a source with no extended emission.

The compactness was determined for all sources in all sessions for each of the three observing frequencies. Session-based compactness values were used to determine the average compactness over all sessions (\bar{C}) for each source. Shown in Figure 9 are the distributions for \bar{C} for all sources imaged in the program including 138 sources at X band, 274 sources at K band, and 132 sources at Q band. The mean and median values of the distributions at X band are 0.83 and 0.86, or greater than 80% of the maximum possible compactness $\bar{C} = 1.0$. The mean and median values at K band are slightly lower with values of 0.81 and 0.83, respectively. For Q band, the results are nearly identical to those at K band, with a value of 0.81 for both the mean and median of the distribution of \bar{C} . In Figure 10 the distributions of \bar{C} are plotted for the 97 sources common to all three observing bands. The results here are very similar to those shown for all sources with mean (median) values of 0.84 (0.87), 0.79 (0.81), and 0.80 (0.80) for the X-, K-, and Q-band distributions, respectively. While these results suggest only minor differences between the distributions of the mean source compactness at the three frequencies, one should recall that the compactness is dependent upon the flux density contained within one beam-width, S_{beam} , which, in turn, is dependent upon the frequency of the observations. Therefore, a constant value for the compactness with increasing frequency still implies a reduced intrinsic source size.

The source compactness also provides a convenient way to track changes in the source structure from one observing session to the next. To measure these changes, we computed the source compactness variability index (σ_C/\bar{C}), which is simply the standard deviation of the compactness divided by its mean. A minimum value, $\sigma_C/\bar{C} = 0.0$, corresponds to no variation in the compactness over time. Shown in Figure 11 are the distributions of source compactness variability index for sources imaged in more than one session at K and Q bands, respectively. The mean (median) compactness variability for the 235 sources at K band is 0.08 (0.06). For the 82 sources at Q band mean (median) values of σ_C/\bar{C} are slightly smaller 0.07 (0.05). These variations are small (no more than about 8% on average), however the probability that the compactness variability is significantly different from zero has not been determined. As in the case of the flux density variability, the compactness variability results are limited to the ~ 5 yr period over which our VLBA data were recorded.

4. COMPARISONS AND DISCUSSION

In the previous section, we discussed results for several quantities that emerged from our analysis of the VLBA images, namely: the source flux density, the source structure index, the source compactness, and the time variability of each of these quantities. In this section, we compare the source structure index to the compactness in order to verify that the two quantities are related.

¹³ <http://www.obs.u-bordeaux1.fr/BVID/>

In addition, we compare both the structure index and the compactness to two astrometric quantities derived in Paper I, namely: the formal position uncertainties and position variability of the sources. These comparisons were made to determine whether the reduced structure effects seen at high frequency correspond to more precise astrometric positions.

4.1. Structure Index and Source Compactness

As an initial test of the source compactness, we compared \bar{C} to the source structure index, SI , at each of the two frequencies. Shown in Figure 12 are the distributions of the mean source compactness for the 274 sources imaged at K band separated in terms of maximum source structure index. Figure 13 shows similar distributions for the 132 sources imaged at Q band. The three panels in each figure show $SI = 1, 2$ and 3 sources, respectively. There are two sources at K band and one source at Q band with $SI = 4$ that are not shown in the figures. In both figures, it is evident that the distributions in compactness among the three structure indices are quite different with the distribution for $SI = 1$ being strongly peaked at both frequencies, and the distributions broadening with increasing values of SI . Within each panel of Figures 12 and 13 the mean and median of the distribution are given. These values are also summarized in Table 5. From the table we see that for both frequencies, the mean and median source compactness is directly related to structure index. The correspondence between SI and \bar{C} is not unexpected, since both quantities provide an indication of the source structure as derived from the VLBI imaging.

We also compared the compactness variability index to the source structure index and the results are shown in Figure 14. Plotted in the figure is σ_C/\bar{C} at K band as a function of each of the three structure indices, $SI = 1, 2$ and 3 . Recall that the compactness variability index was determined for only those sources observed in more than one session (235 sources at K band and 82 sources at Q band). The equivalent plot for the Q band data was not produced because of the greatly reduced number of sources. As in the case of the source compactness, the variability in the compactness shows a clear trend with SI , with the σ_C/\bar{C} distribution being the most narrow for $SI = 1$ and the broadest for $SI = 3$. The mean (median) values for each distribution are 0.04 (0.04), 0.08 (0.07) and 0.15 (0.14) for the $SI = 1, 2$ and 3 sources, respectively. A variability index $\sigma_C/\bar{C} = 0$ indicates no variability in the source compactness from one session to the next. This relationship between the compactness variability index and the structure index suggests that the sources with the most structure as measured by SI exhibit increased variability in their structure as measured by σ_C/\bar{C} .

4.2. Structure Index, Compactness and Source Position Uncertainty

The impact of source structure on the high-frequency CRF can be further studied by comparing structure index with the formal precision of the source positions comprising a potential CRF. The formal position uncertainties were taken from the K-band astrometric solution detailed in Paper I. For this solution, we used

the CALC/SOLVE software package maintained by the NASA Goddard Space Flight Center (GSFC) to perform a least-squares astrometric solution for the K-band data. The 10 diurnal K-band experiments encompassed 82,334 measurements of bandwidth synthesis (group) delay and phase delay rate. Geodetic parameters estimated for each session include: station positions, 20-minute piecewise linear continuous troposphere zenith parameters, tropospheric gradients in the east–west and north–south directions, linear in time, estimated once per 24 hr session, quadratic clock polynomials to model the gross clock behavior, and 60-minute piecewise linear continuous clock parameters. Corrections for ionospheric refraction drawn from Global Positioning System (GPS) total electron content (TEC) maps were applied to K-band data as discussed in Paper I. Positions for sources having three or more measurements of group delay were the only global parameters that were estimated.

The K-band catalog derived from the astrometric solution is comprised of positions and associated formal uncertainties for 268 sources. Because there were too few sources at Q-band (131) to separate into the four structure index categories, we chose only to compare the K-band uncertainties with structure index and compactness. An initial comparison of all 268 sources showed the position uncertainties plotted as a function of SI category to be sensitive to a few outliers with relatively few observations. We, therefore, decided to restrict the comparison to sources with 100 or more group delay measurements. This same restriction was used by Fey & Charlot (2000) in a similar study performed at X band.

Shown in Figure 15 are the distributions of the formal position uncertainties in a) $\alpha \cos \delta$ and b) δ for 193 sources with 100 or more group delay measurements at K band. The distributions are separated into the three SI categories 1, 2, and 3. There were two $SI = 4$ sources with greater than 100 delay measurements that are not shown. There is good agreement between the mean and median values suggesting little or no dependence on outliers. The results show no significant difference in the mean and median position uncertainties from one structure index category to the next. In addition, we find the mean and median position uncertainties in δ are roughly twice the uncertainties in $\alpha \cos \delta$ for all three SI categories.

In Fey & Charlot (2000), it was shown that the mean and median X-band source position uncertainties in both $\alpha \cos \delta$ and δ increased regularly as a function of structure index from $SI=1$ to 4. In addition to the 100 group delay measurement restriction, Fey & Charlot (2000) used the formal position uncertainties from Ma et al. (1998), which were adjusted by the standard ICRF inflation factor described therein. In order to accurately compare our K-band values, we applied the same inflation factor (the root sum square (rss) of 1.5 times the formal uncertainty and 0.25 mas) to the K-band formal uncertainties. Table 6 lists the mean and median position uncertainties at both X and K bands as a function of SI category. Again we see that there is no increase in position uncertainty from structure index 1 to 3 at K-band unlike the earlier findings at X-band. More importantly, the table shows that for a similar number of sources, the inflated mean/median position uncertainties are smaller at K band than at X band for all structure index categories.

It should be noted, that there have been significant improvements in both the number and quality of the VLBI observations since the construction of the ICRF, and the Fey & Charlot (2000) values reported in Table 6 do not reflect the accuracy of the current X-band CRF.

In addition to the comparison of the SI and the formal uncertainties, we compared the mean source compactness (\bar{C}) to the formal uncertainties. Recall that the maximum possible value of the source compactness $C = 1.0$ indicates that all of the source flux density is contained within one synthesized beam. The mean compactness is just an average over all of the sessions in which the source was imaged. Figure 16 shows the formal uncertainties in the position versus the source compactness. The plotted formal position uncertainty is the rss of the uncertainties in $\alpha \cos \delta$ and δ . The figure also shows the structure index for each source by point color and type, with green circles, blue triangles, and red squares indicating maximum SI values of 1, 2, and 3 respectively. Figure 16 does not show a clear trend in the formal position uncertainty versus compactness. This is to be expected since it was previously shown that the \bar{C} and SI are correlated, and no significant relationship was found for the position uncertainty as a function of SI (e.g. Figure 15).

4.3. Structure Index, Compactness, and Source Position Stability

Another useful comparison can be made between the stability of the source positions over time and the source structure as traced by either the structure index or the source compactness. Time variation of the astrometric coordinates of CRF sources has previously been attributed to variability in the intrinsic source structure (c.f. Charlot 1994, 2002; Fey et al. 1997; Fey & Charlot 2000). Thus, it is natural to search for any relationship between such variations and the structure index at higher frequencies. A measure of source position stability is the weighted root-mean-square (wrms) position variation. These variations were obtained from a series of K-band astrometric solutions described in Paper I. In these solutions, a fraction of the sources were treated as local parameters (i.e. an estimate of the position was derived for each session in which the source was observed) with the remaining sources treated as global. The estimation of source position stability was limited to 88 sources that were observed in five or more of the 10 VLBA sessions. Five was considered a sufficient number of sessions (position estimates) per source to derive reliable statistics.

From these solutions, a time series of source positions was generated for each source, and from these time series the wrms position variations were computed. Shown in Figure 17 are the distributions of the wrms position variations in $\alpha \cos \delta$ (a) and δ (b), respectively. The figure also lists the mean and median position variations for each distribution. In $\alpha \cos \delta$, the mean and median of the distribution are 0.14 and 0.12 mas, respectively. For δ the mean and median are roughly twice as large at 0.30 and 0.25 mas, respectively. As stated in Paper I, the larger wrms position variations in δ are likely due to the combination of ionospheric/tropospheric effects and network geometry, specifically the lack of long north-south baselines for the VLBA.

It would have been desirable to separate the wrms position variations into structure index categories, and to

plot the distributions as a function of SI as was done in §4.2. Because the structure index is quantized into four categories, there were simply too few sources observed in five or more sessions to determine reliable statistics for the separate SI categories. Instead, in Figure 18, we plot the wrms variation against the mean source compactness previously described in §3.3. The wrms variation plotted is the rss of the variations in $\alpha \cos \delta$ and δ . In addition, the structure index for each source is shown by point type with green circles, blue triangles, and red squares indicating maximum SI of 1, 2, and 3 respectively. Figure 18 does not suggest a clear trend in the compactness and wrms position stability. While it does appear that there are a number of sources clustered in a region of high compactness and low wrms variations, there are also sources that are less compact with equally low wrms variations. A more quantitative comparison between the SI and the position stability will have to wait for additional high-frequency observations.

5. SUMMARY

We have produced a combined total of 1339 K- and Q-band images of 274 extragalactic sources from 10 sessions of VLBA data observed as part of a program to select high-frequency sources for use in spacecraft navigation and future CRFs. A detailed analysis of the images has allowed us to determine several quantities that can serve as useful indicators of both detectability and astrometric quality including: source flux density, flux density variability, structure index, source compactness, and compactness variability. The results of our imaging and analysis can be summarized as follows:

1. The sources described herein were selected from previous catalogs at lower (e.g. 8.4 GHz) frequencies. The distributions of source flux density at X, K, and Q bands show mean values greater than 1 Jy for each of the three bands. These results suggest a sufficient number of suitable sources for astrometric use at high frequencies.
2. For sources imaged at 24 GHz, we find that, on average, 1σ variations in the session-to-session flux density were 20%–25% over the five-year period of our observations. Comparatively, variations of the flux density scale from one session to the next were less than 10%. Variations in the source flux density are, thus, relatively small and it should be expected that sources will be observable from one session to the next.
3. There is a clear dependence of source structure index on observational frequency. The percentage of sources with $SI = 1, 2$ (the most compact) increases from $\sim 70\%$ at X band, to $\sim 85\%$ at K band, and to $\sim 92\%$ at Q band. This suggests that the higher resolution afforded by the higher observing frequencies yields less structure at a fixed angular scale. This result is corroborated by the mean source compactness which shows that 80% of the total flux density is contained within the core at all three frequencies.
4. On average, the 1σ variations in the source compactness at K and Q-band were no more than about

- 8% at either frequency over the five-year period of our VLBA observations.
5. For the K-band data, we find a trend between the source compactness variability index (i.e., the variation of the compactness over time) and the source structure index indicating that sources with larger values of SI exhibit increased variation in the structure as measured by σ_C/\bar{C} .
 6. No clear trend was found between the formal uncertainties in the astrometric source positions and the source structure index at K band in contrast to the trend found at X band by Fey & Charlot (2000).

The implications of the above results with regards to spacecraft navigational needs are twofold. First, there

are numerous sources available at high frequencies, and these sources persist over relatively long (five years) periods of time. Second, the sources are more compact at these higher frequencies and should provide high-quality astrometric reference points for spacecraft navigation. Such sources also provide a foundation upon which to build a future CRF and are of benefit to radio astronomy, in general, as fiducial references. Future imaging observations should continue to improve our understanding of source structure at K and Q band and allow us to better characterize the variability of the structure over time and its effect on astrometric positional stability.

This research was partially supported through NASA contracts with the California Institute of Technology and the U.S. Naval Observatory. This research made use of the USNO Radio Reference Frame Image Database (RRFID).

REFERENCES

- Blandford, R. D. & Königl, A. 1979, ApJ, 232, 34
 Charlot, P. 1990, AJ, 99, 1309
 Charlot, P. 1994, in Proc. of Int. Symp.: VLBI Technology - Progress and Future Observational Possibilities, Kyoto, Japan, 1993 September, ed. T. Sasao, S. Manabe, O. Kameya & M. Inoue (Tokyo: Terra Scientific Publishing Company), 287
 Charlot, P. 2002, in International VLBI Service for Geodesy and Astrometry: General Meeting Proc., 2002 May, ed. N. R. Vandenberg & K. D. Baver, NASA/CP-2002-210002, 233
 Charlot, P., Fey, A. L., Jacobs, C. S., Ma, C., Sovers, O. J., & Baudry, A. 2005, Journées 2004-systèmes de référence spatio-temporels, 21
 Clark, B. G. 1980, A&A, 89, 37
 Fey, A. L., & Charlot, P. 1997, ApJS, 111, 95
 Fey, A. L., & Charlot, P. 2000, ApJS, 128, 17
 Fey, A. L., Clegg, A. W., & Fomalont, E. B. 1996, ApJS, 105, 299
 Fey, A. L., Eubanks, T. M., & Kingham, K. A. 1997, AJ, 114, 2284
 Fey, A. L., et al. 2004, AJ, 127, 3587
 Hovatta, T., Lehto, H. J., & Tornikoski, M. 2008, A&A, 488, 897
 Hovatta, T., Tornikoski, M., Lainela, M., Lehto, H. J., Valtaoja, E., Torniainen, I., Aller, M. F., & Aller, H. D. 2007, A&A, 469, 899
 Kovalev, Y. Y., Lobanov, A. P., Pushkarev, A. B., & Zensus, J. A. 2008, A&A, 483, 759
 Lanyi, G. E., et al. 2009, AJ, submitted. (Paper I)
 Lobanov, A. P. 1998, A&A, 330, 79
 Ma, C., et al. 1998, AJ, 116, 516
 Napier, P. J., Bagri, D. S., Clark, B. G., Rogers, A. E. E., Romney, J. D., Thompson, A. R., & Walker, R. C. 1994, Proceedings of the IEEE, 82, 658
 Pearson, T. J., & Readhead, A. C. S. 1984, ARA&A, 22, 97
 Pearson, T. J., Shepherd, M. C., Taylor, G. B., & Myers, S. T. 1994, BAAS, 26, 1318
 Rogers, A. E. E. 1970, Radio Science, 5, 1239
 Sovers, O. J., Charlot, P., Fey, A. L., & Gordon, D. 2002, in International VLBI Service for Geodesy and Astrometry: General Meeting Proc., 2002 May, ed. N. R. Vandenberg & K. D. Baver, NASA/CP-2002-210002, 243
 Teräsranta, H., Wiren, S., Koivisto, P., Saarinen, V., & Hovatta, T. 2005, A&A, 440, 409

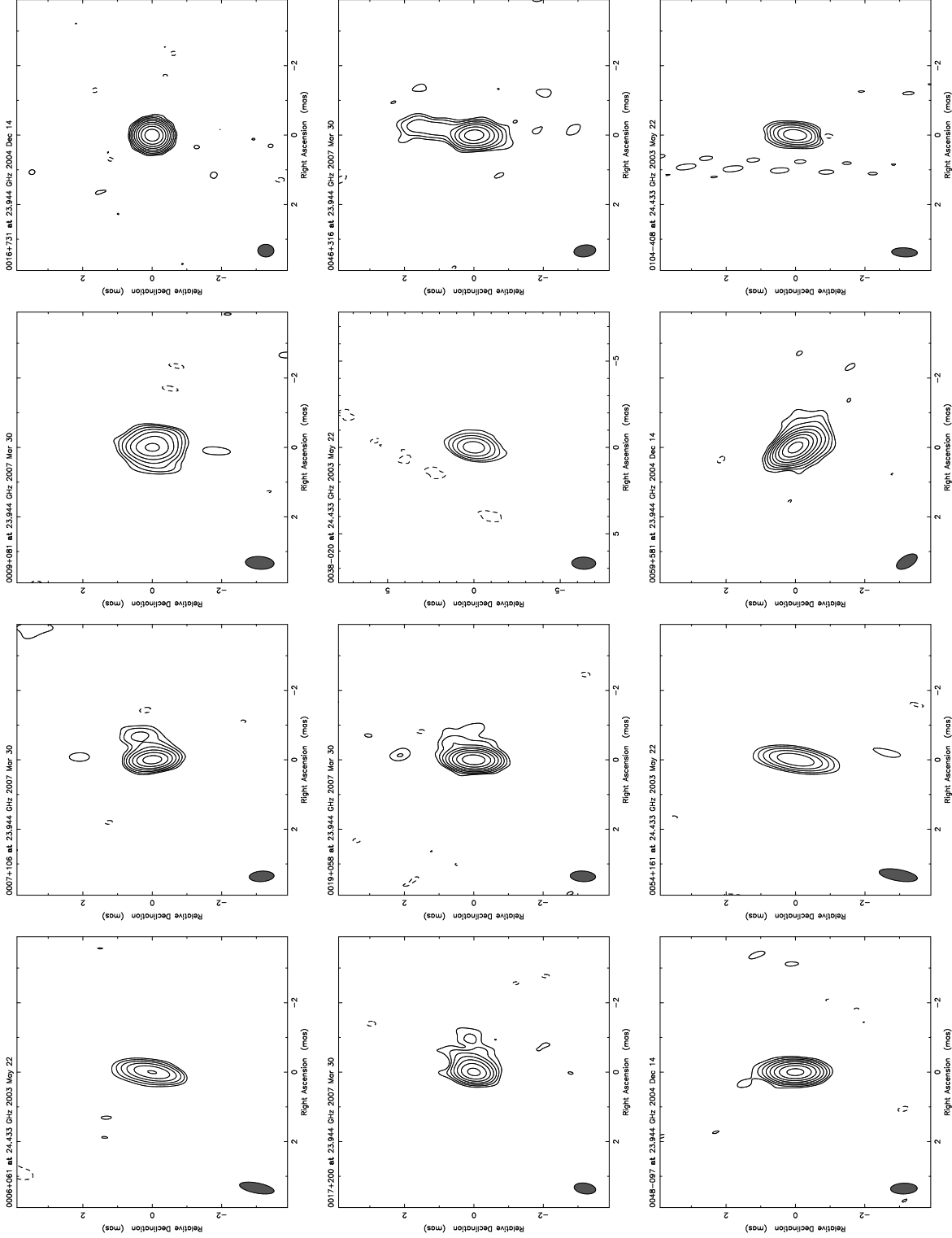
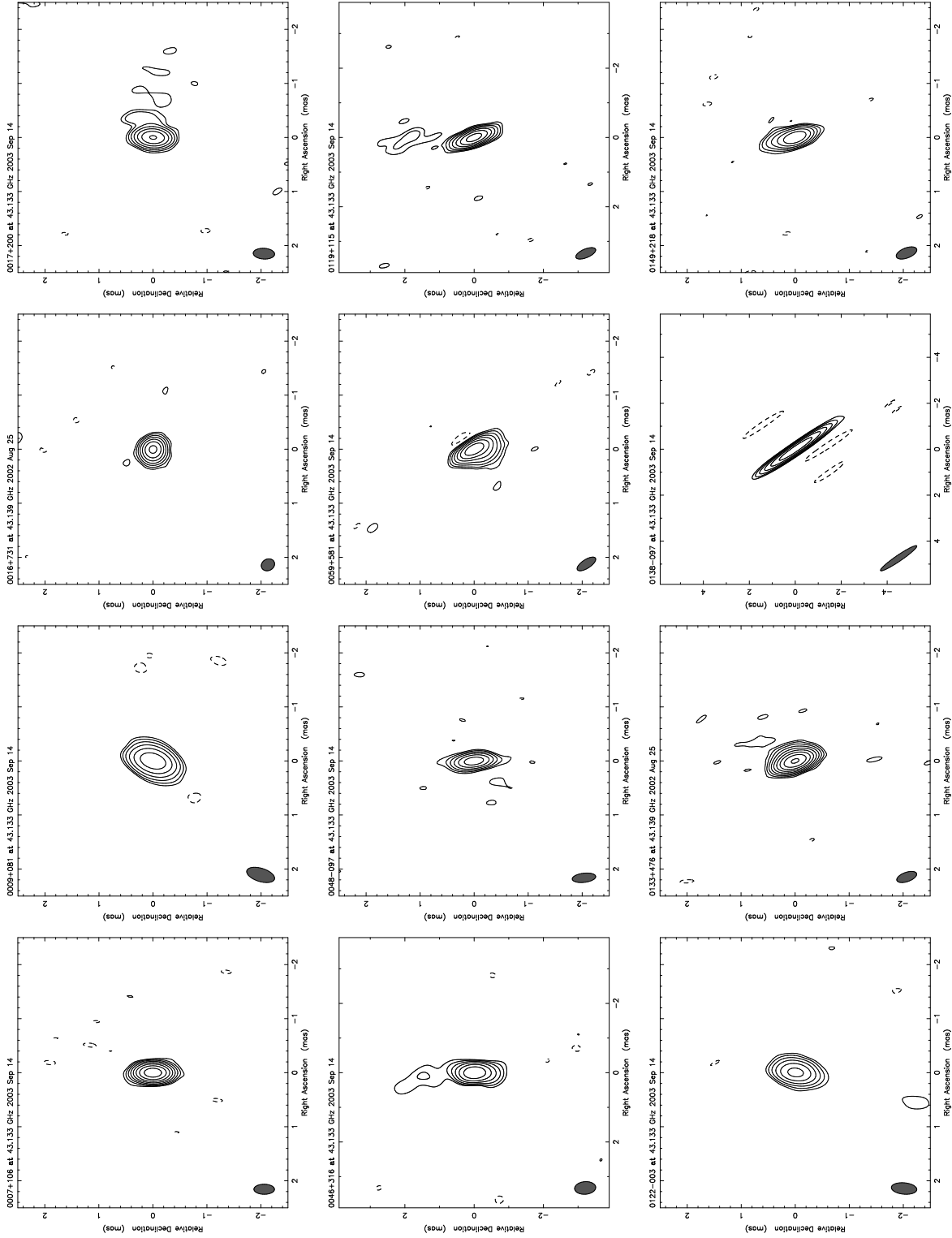
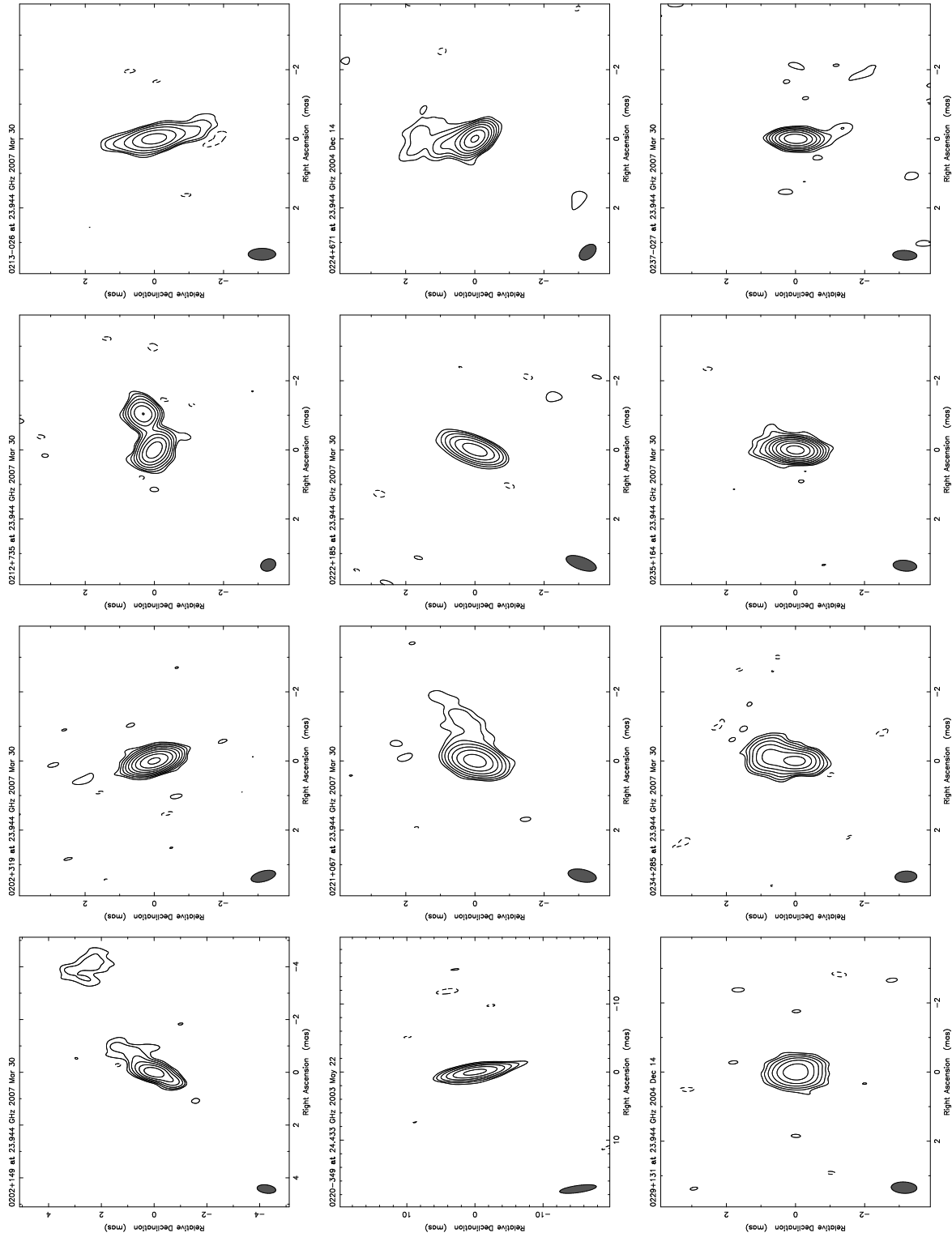
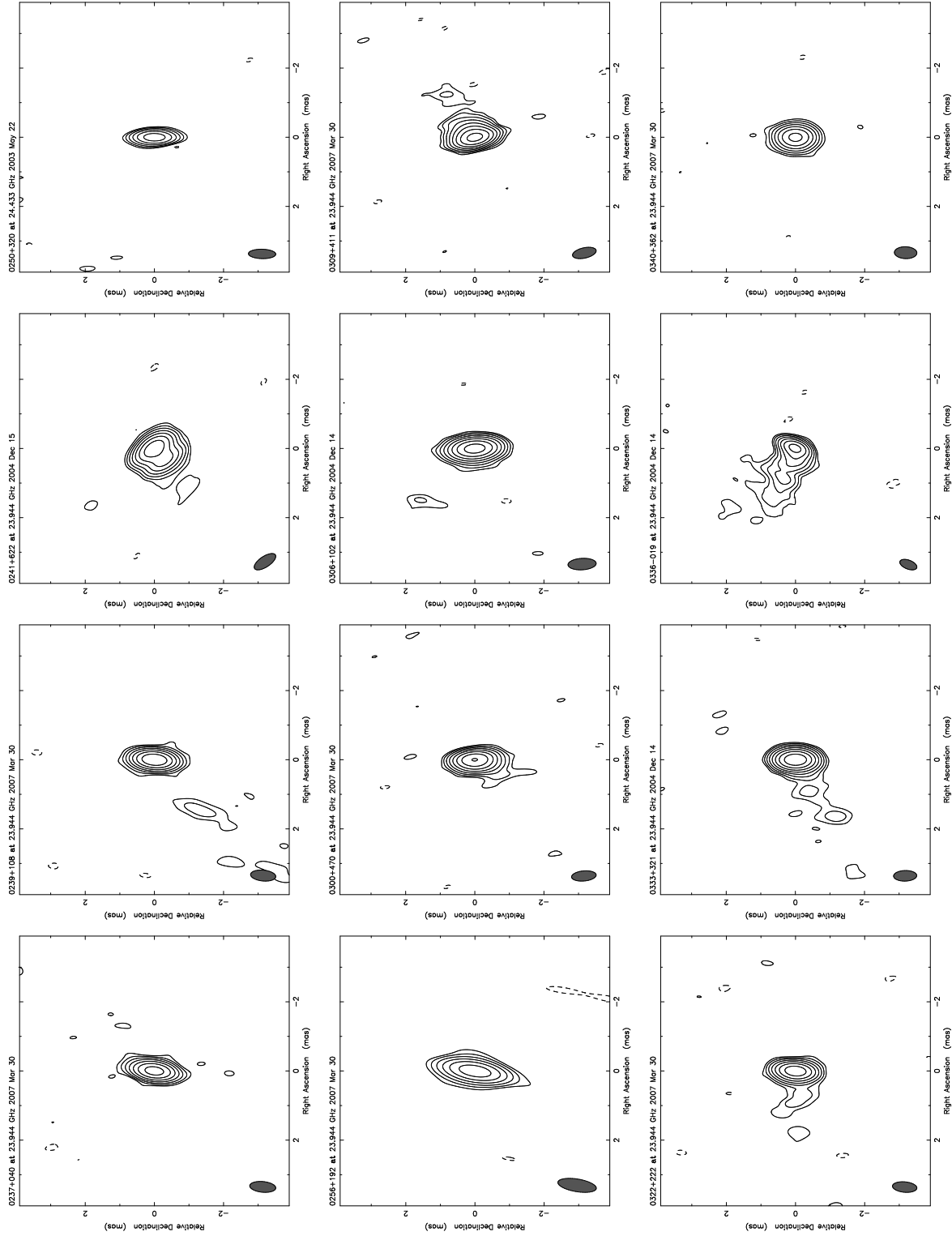
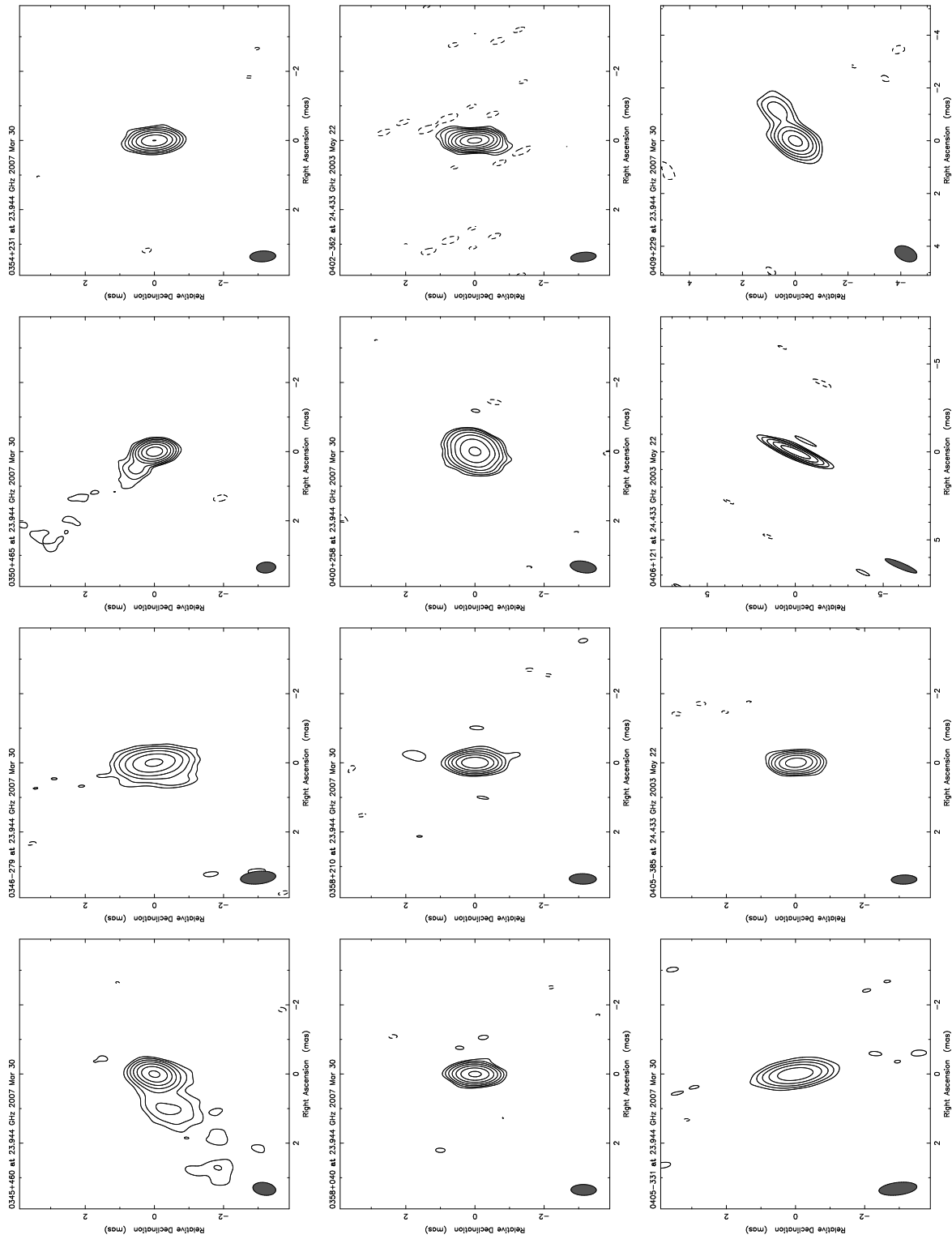


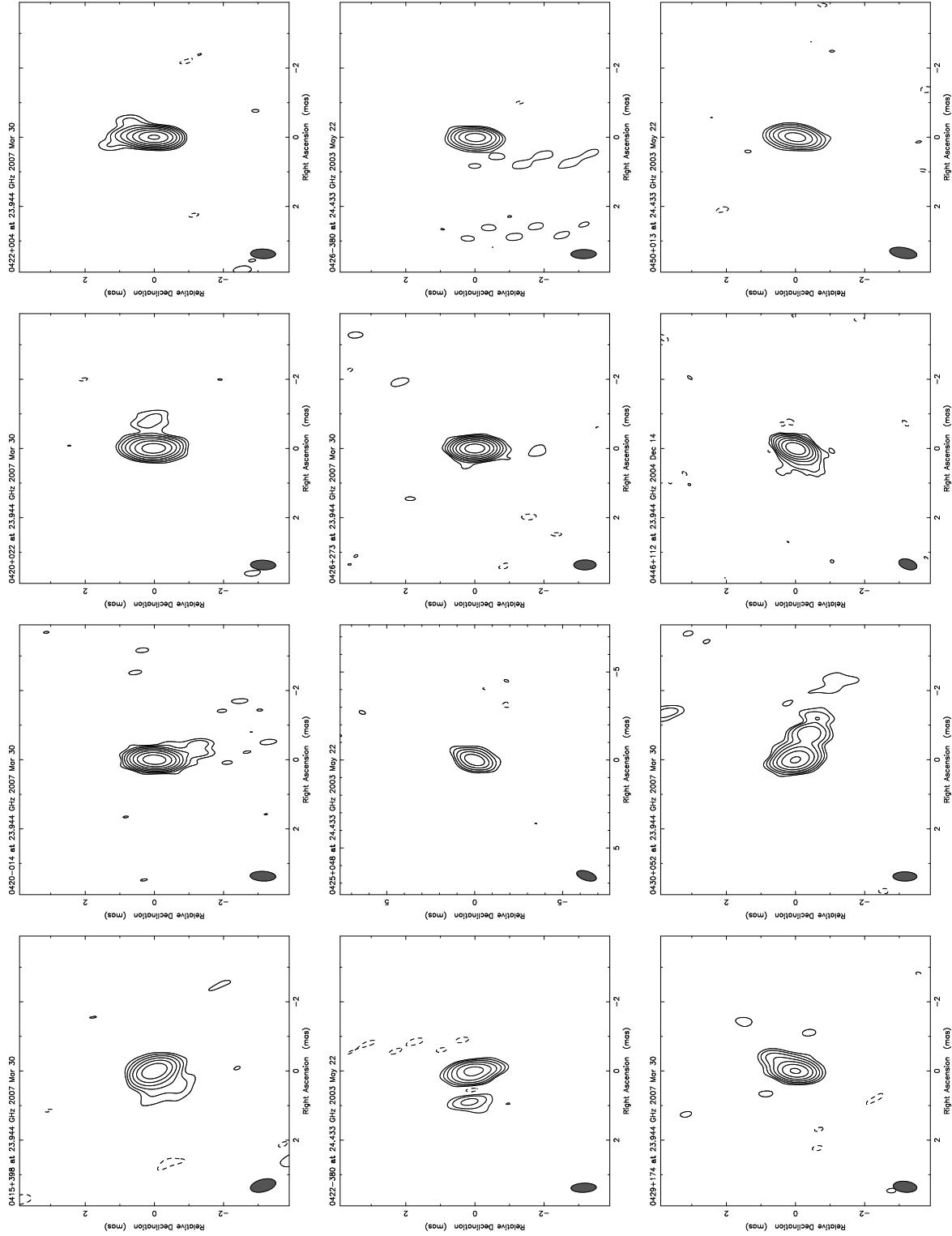
FIG. 1.— Contour plots of 274 extragalactic radio sources at K band. Image parameters are listed in Table 2. The scale of each image is in milliarcseconds. The FWHM Gaussian restoring beam applied to the images is shown as a hatched ellipse in the lower left of each panel. For convenience, the images for each band are labeled only by a single fiducial frequency (~ 23.9 or 24.4 GHz, depending on session) even though they were made using the data from all frequency channels (see § 2).

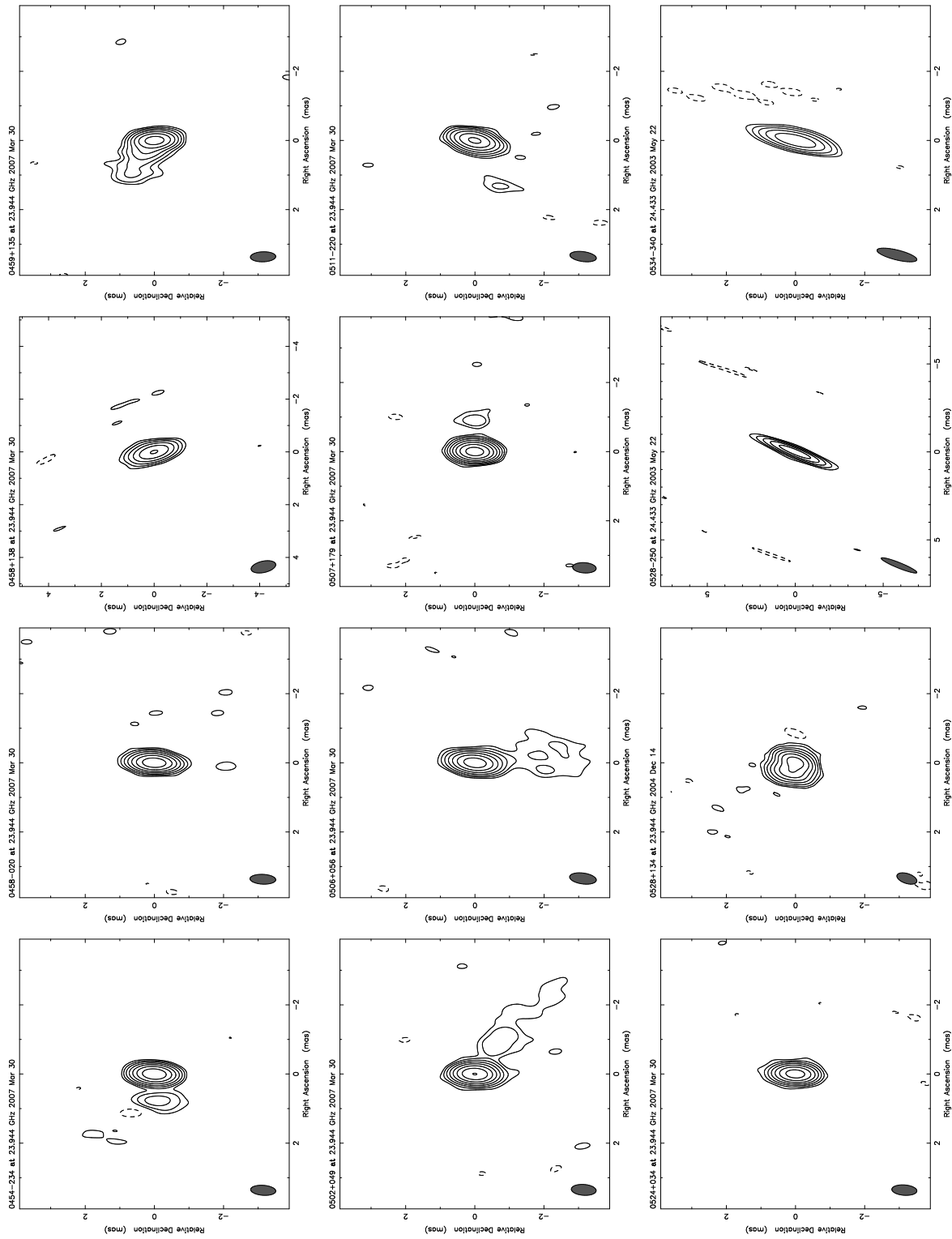
Fig. 1.— *Continued*

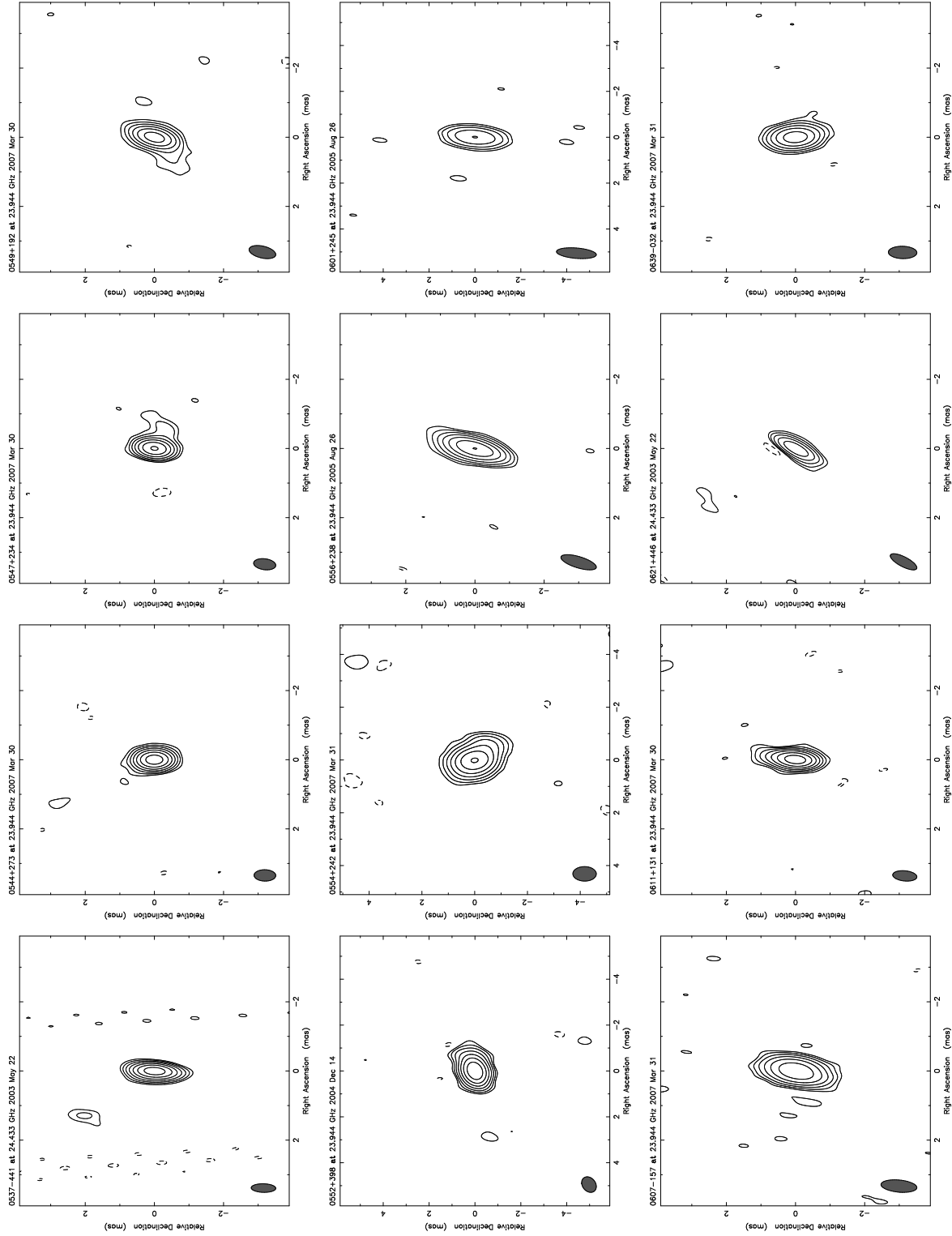
Fig. 1.— *Continued*

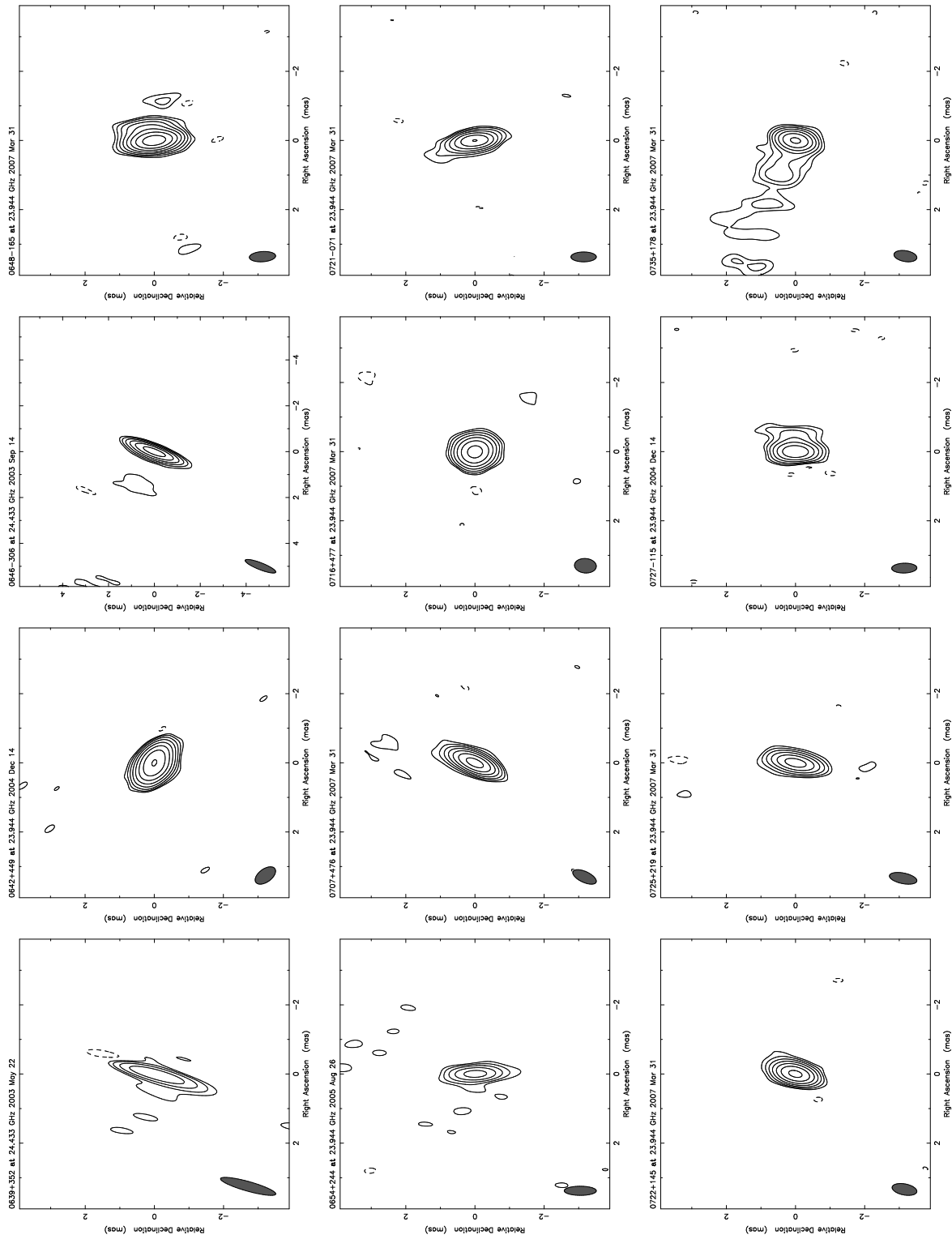
Fig. 1.— *Continued*

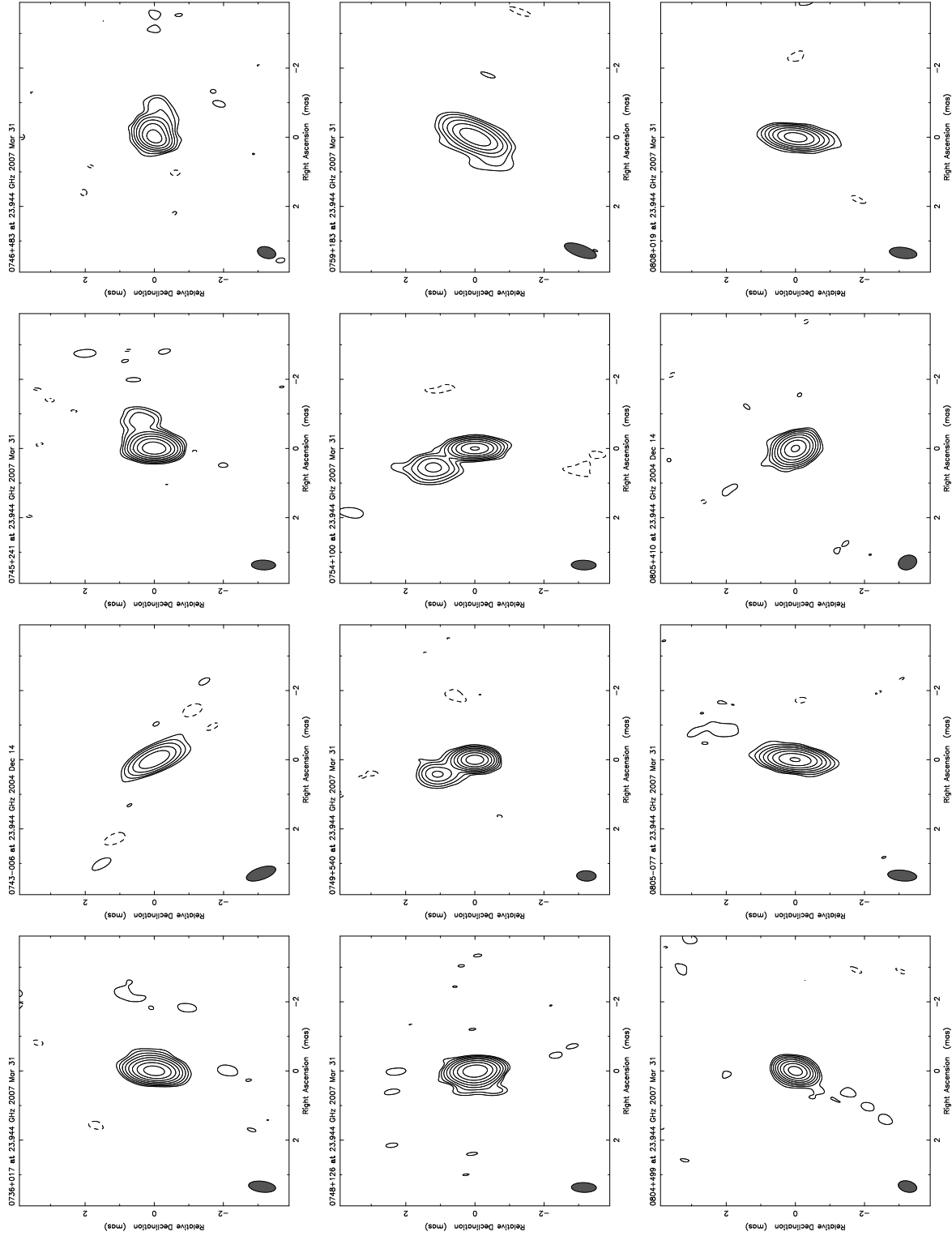
Fig. 1.— *Continued*

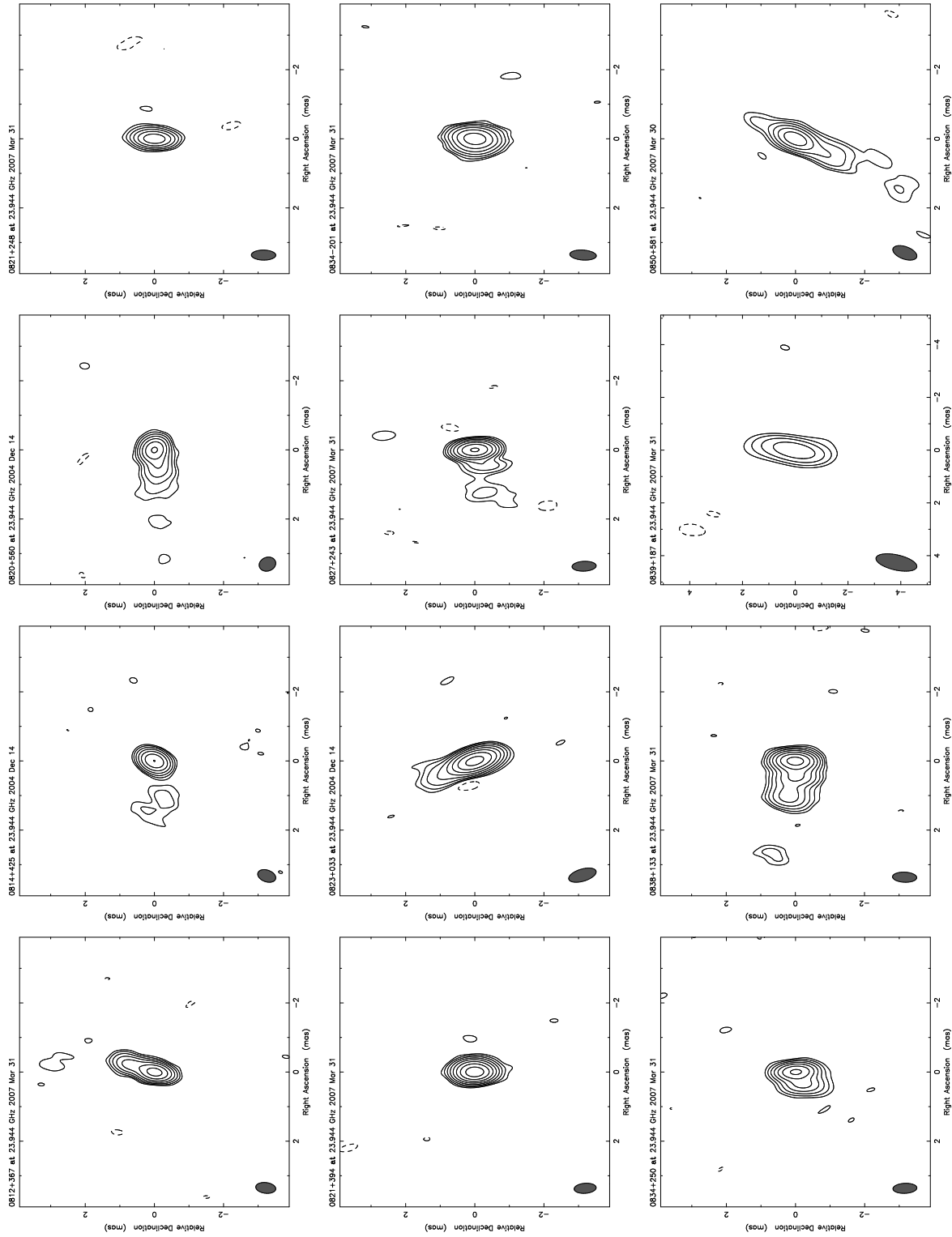
Fig. 1.— *Continued*

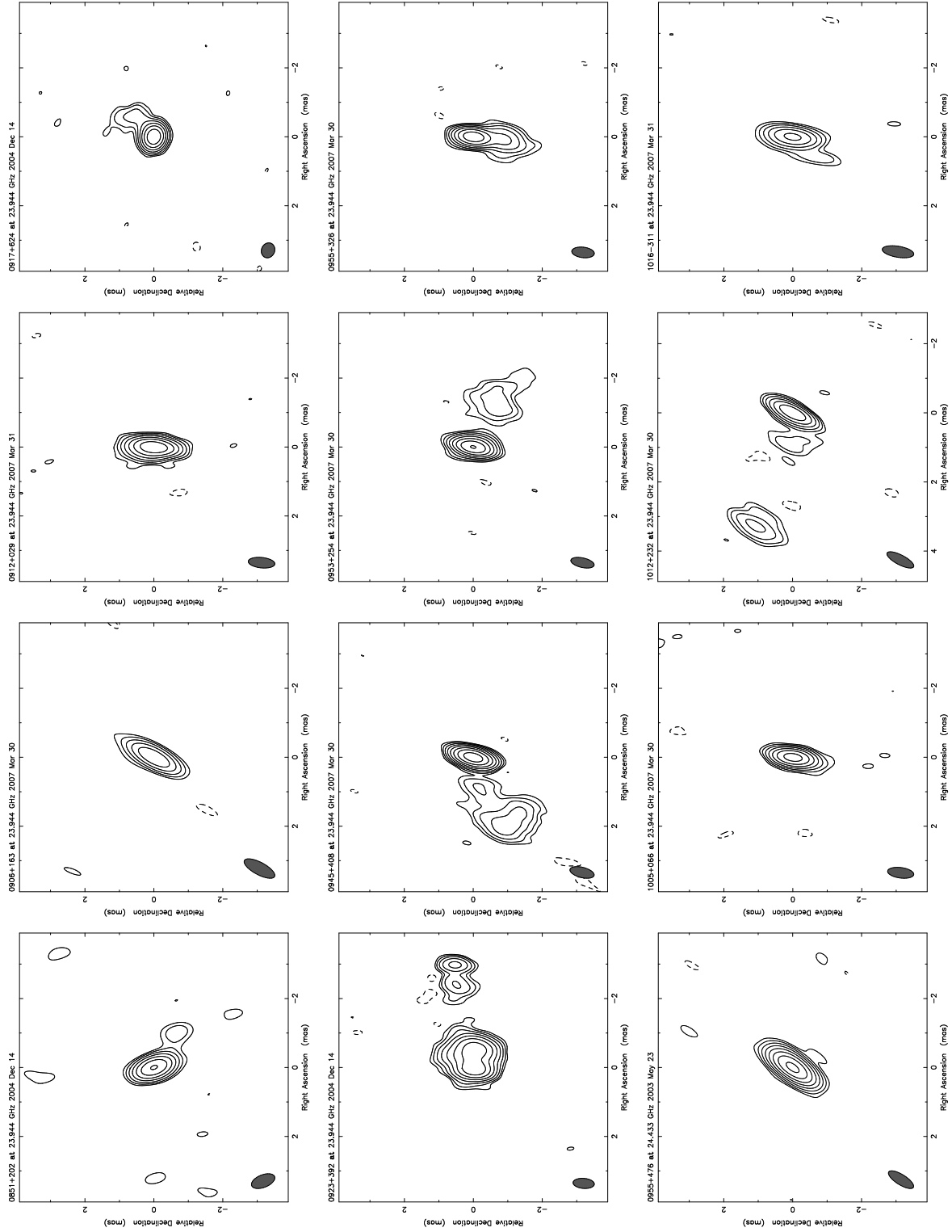
Fig. 1.— *Continued*

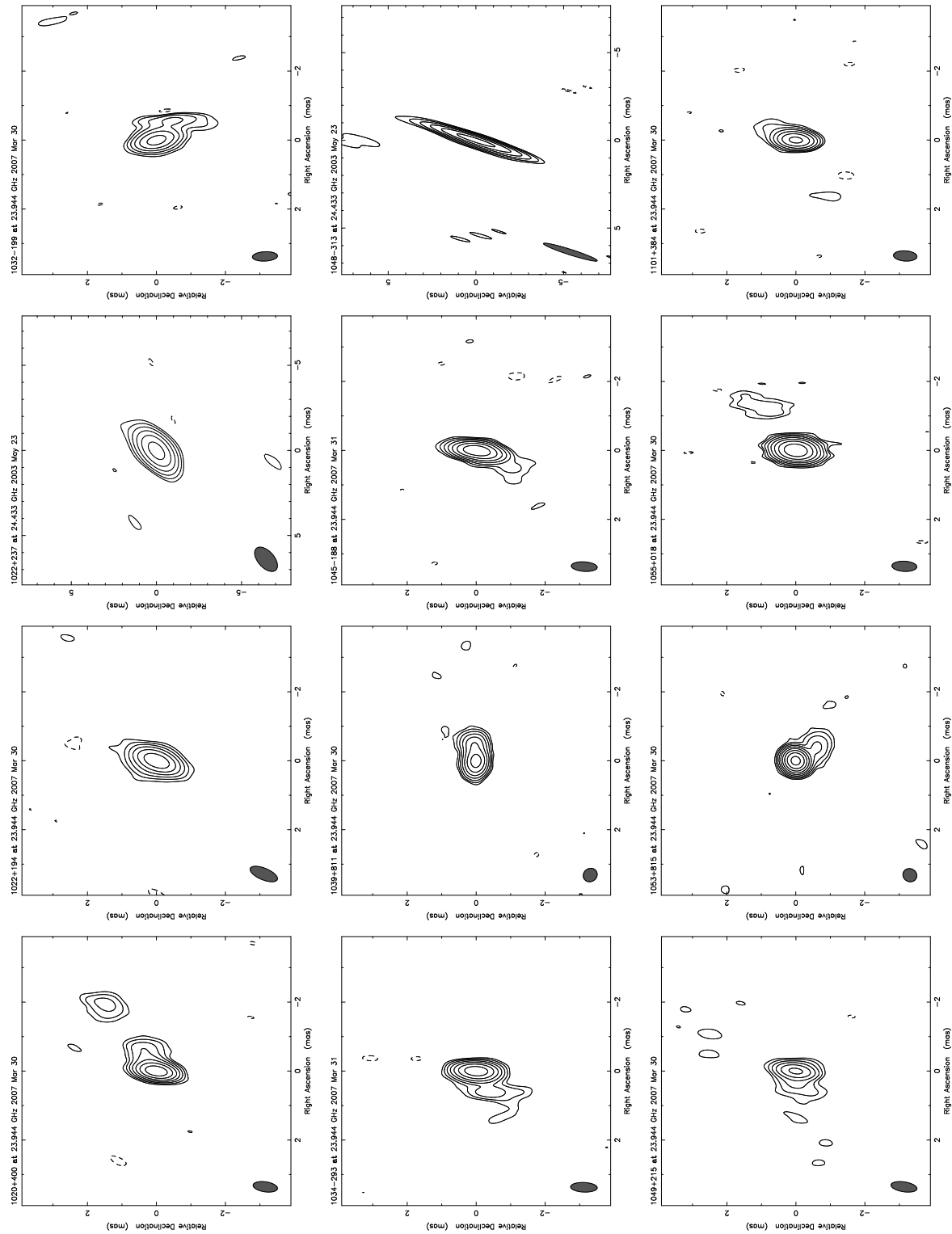
Fig. 1.— *Continued*

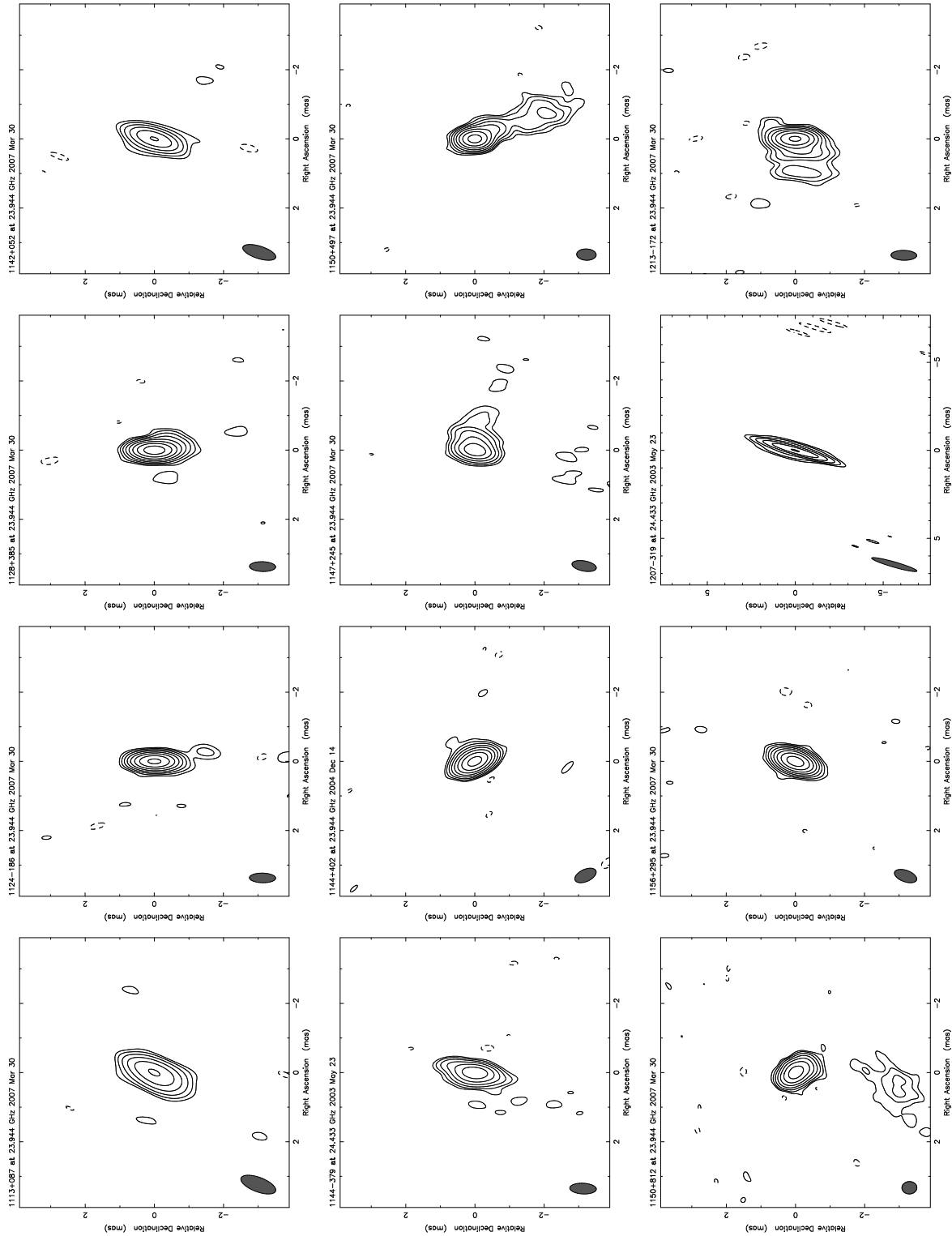
Fig. 1.— *Continued*

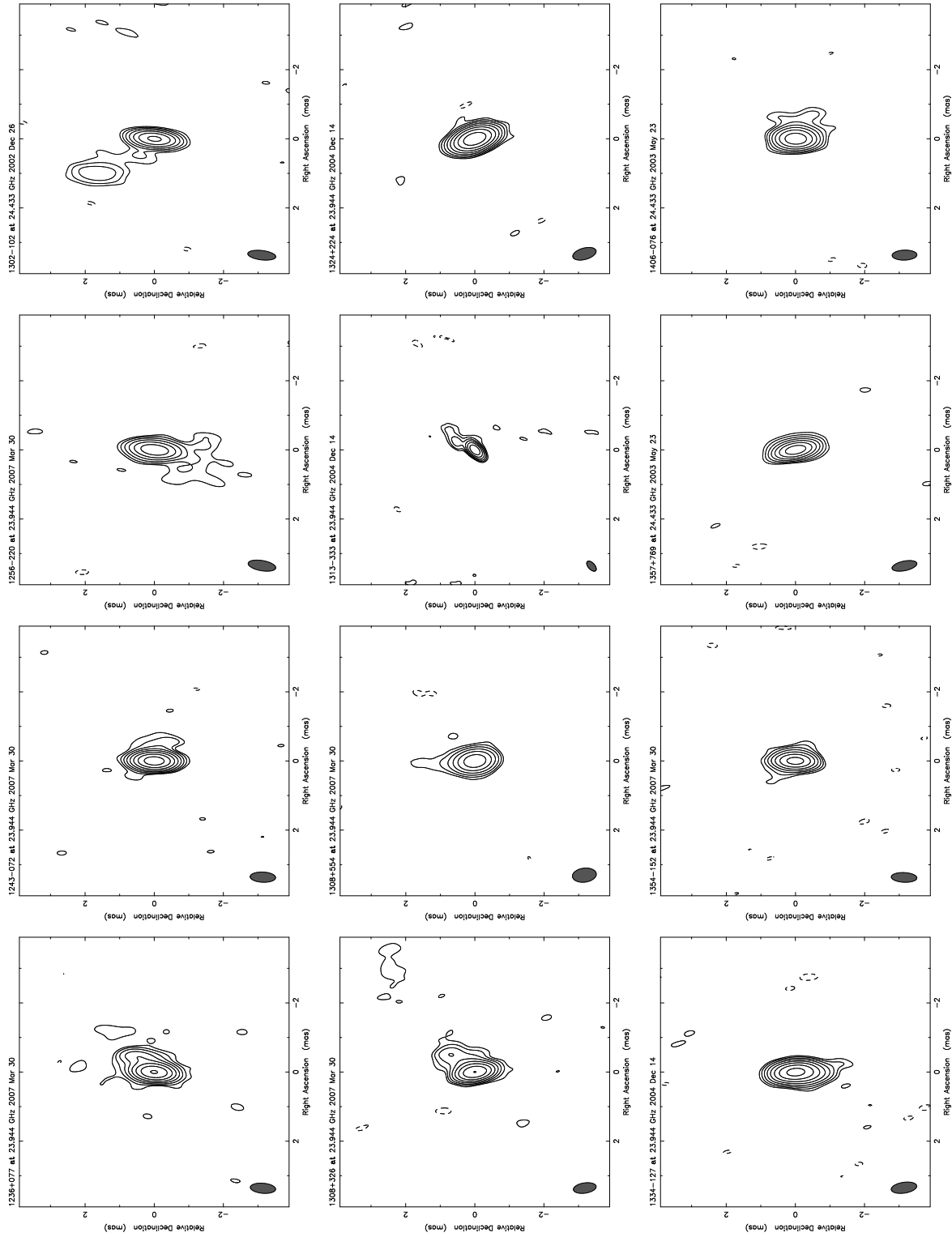
Fig. 1.— *Continued*

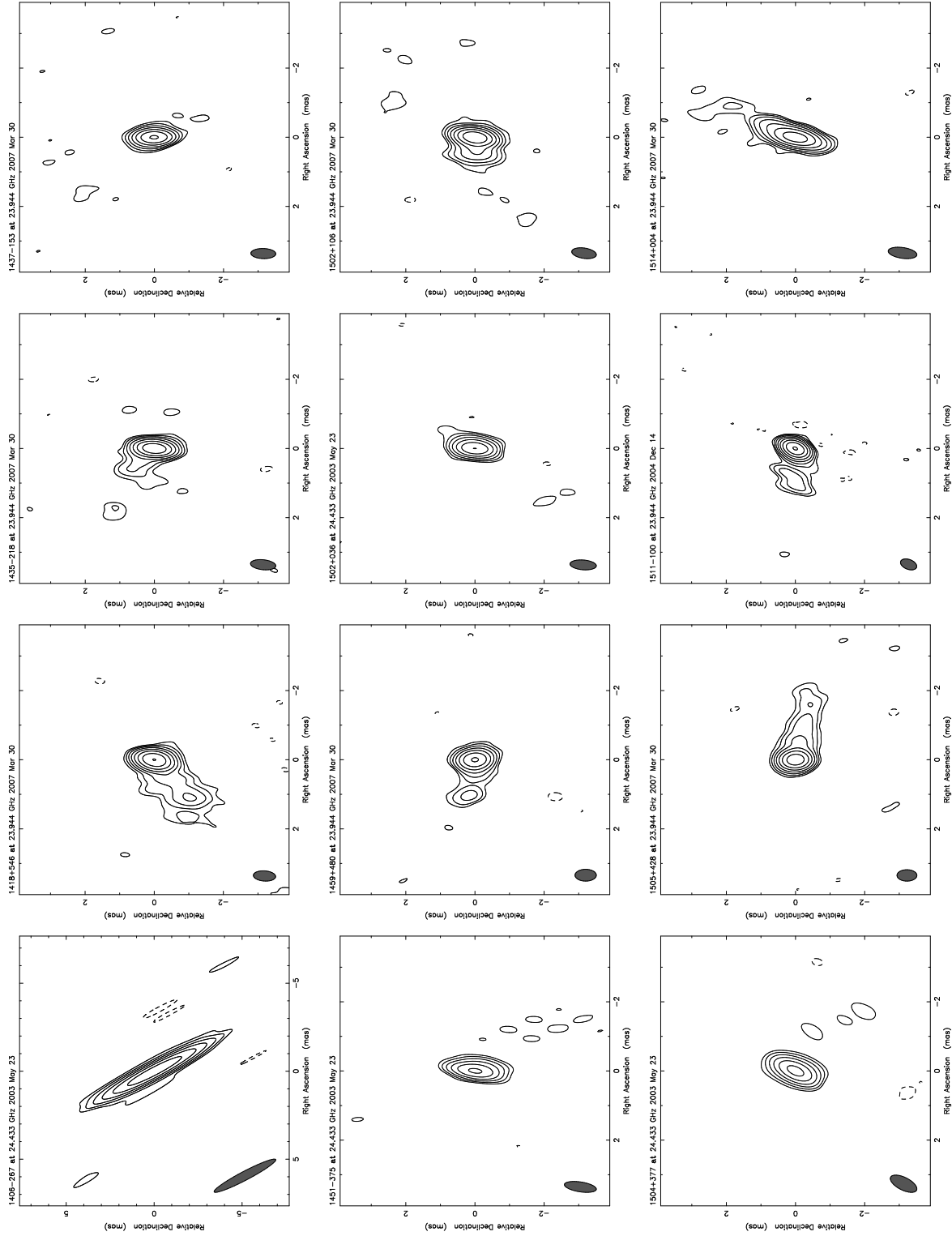
Fig. 1.— *Continued*

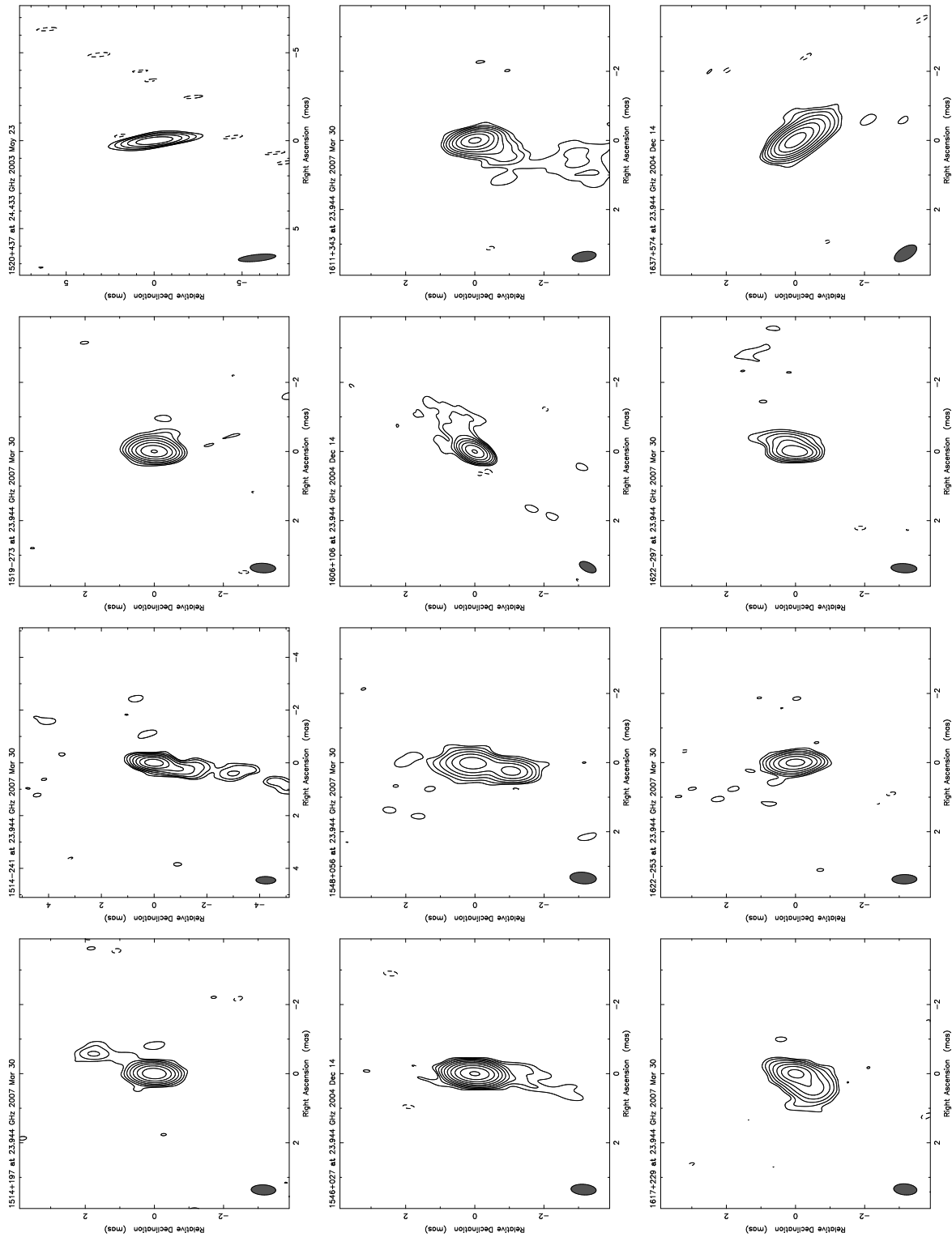
Fig. 1.— *Continued*

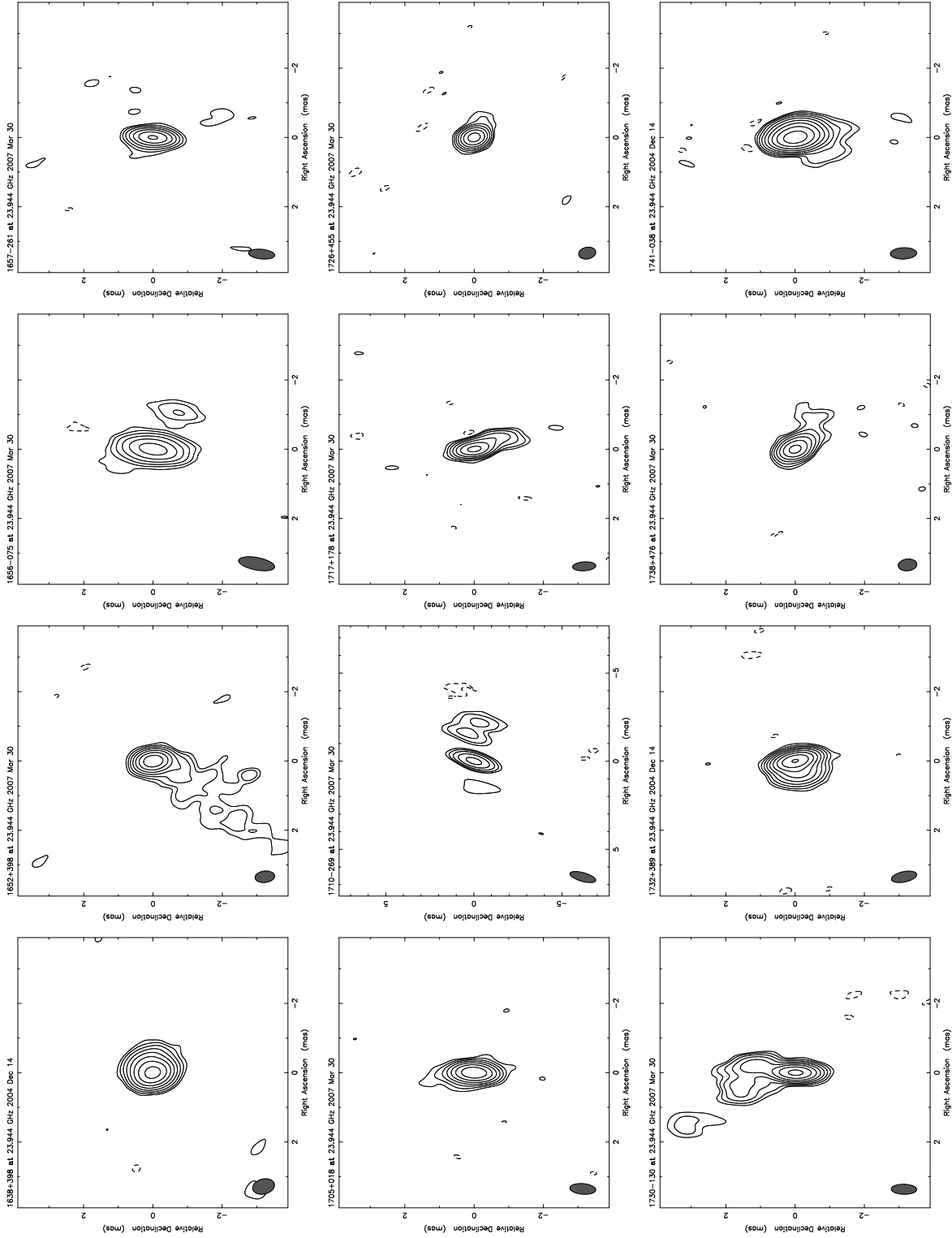
Fig. 1.— *Continued*

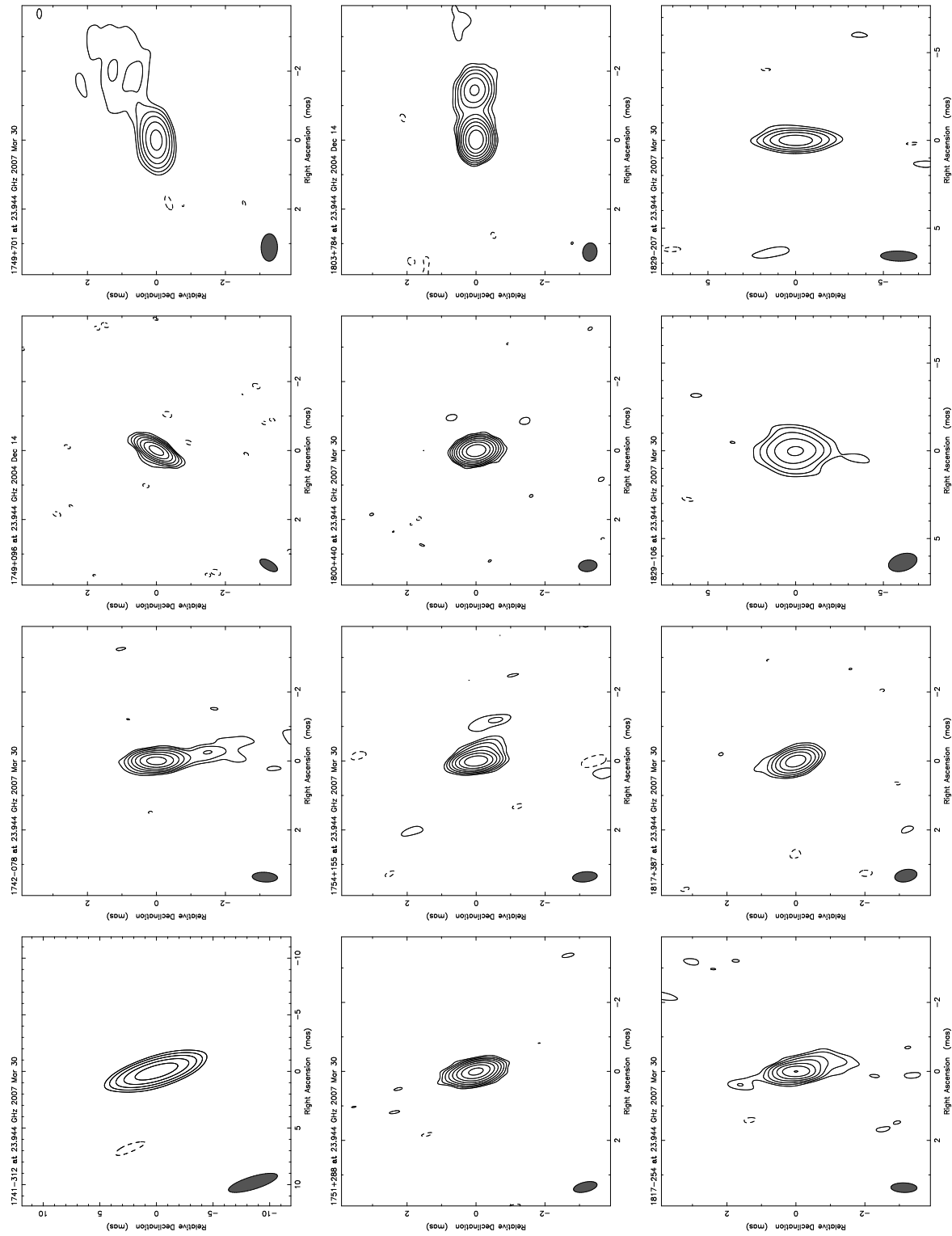
Fig. 1.— *Continued*

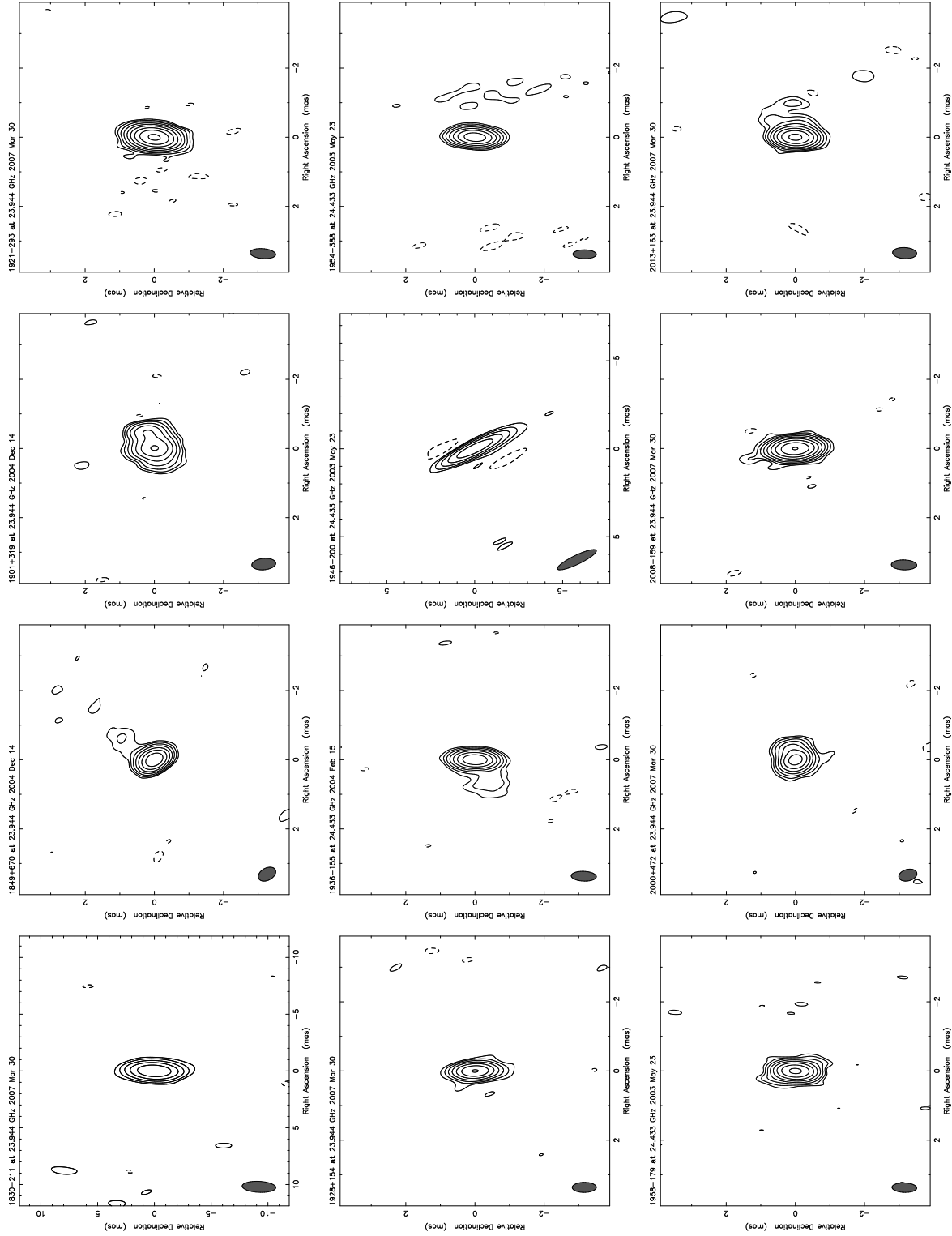
Fig. 1.— *Continued*

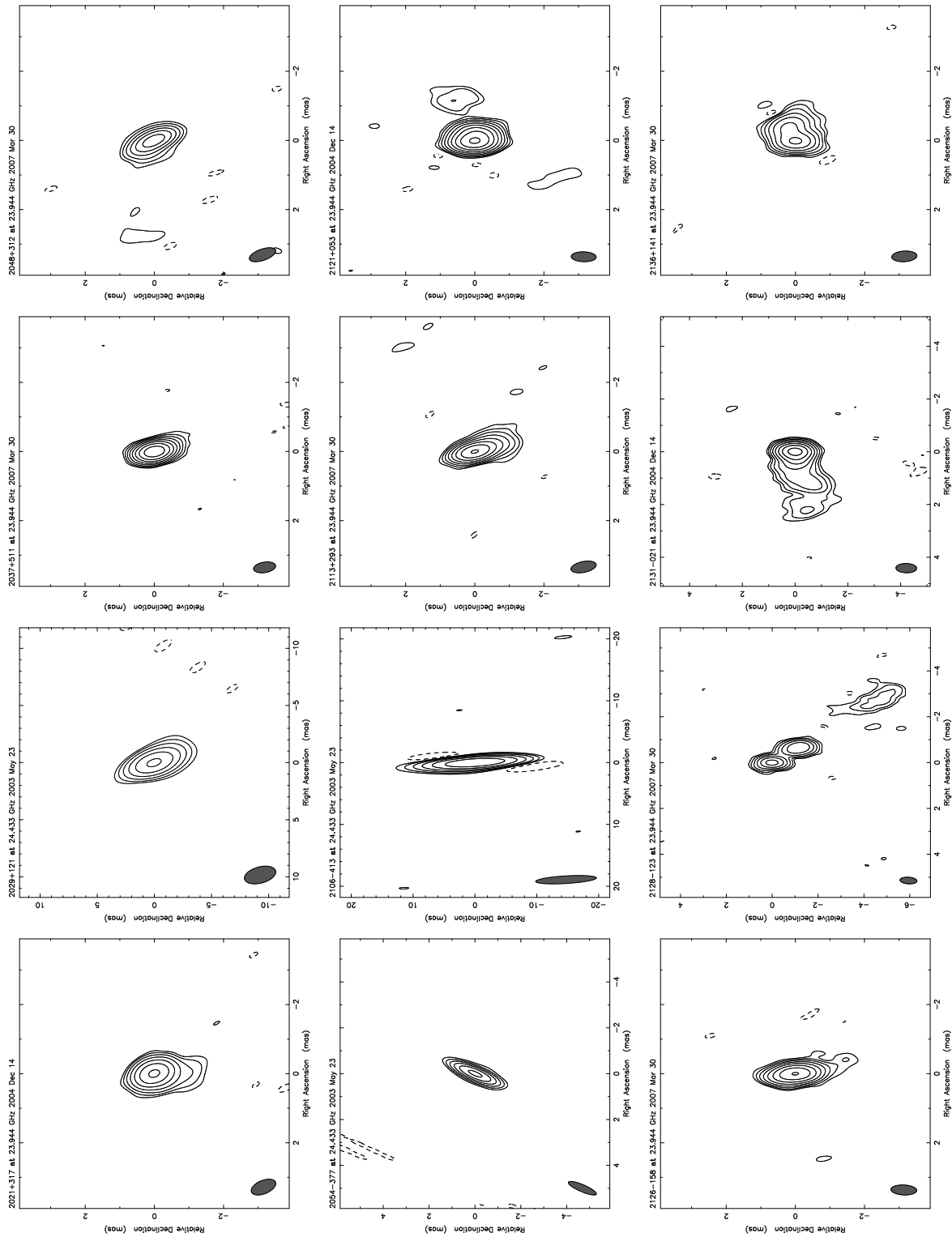
Fig. 1.— *Continued*

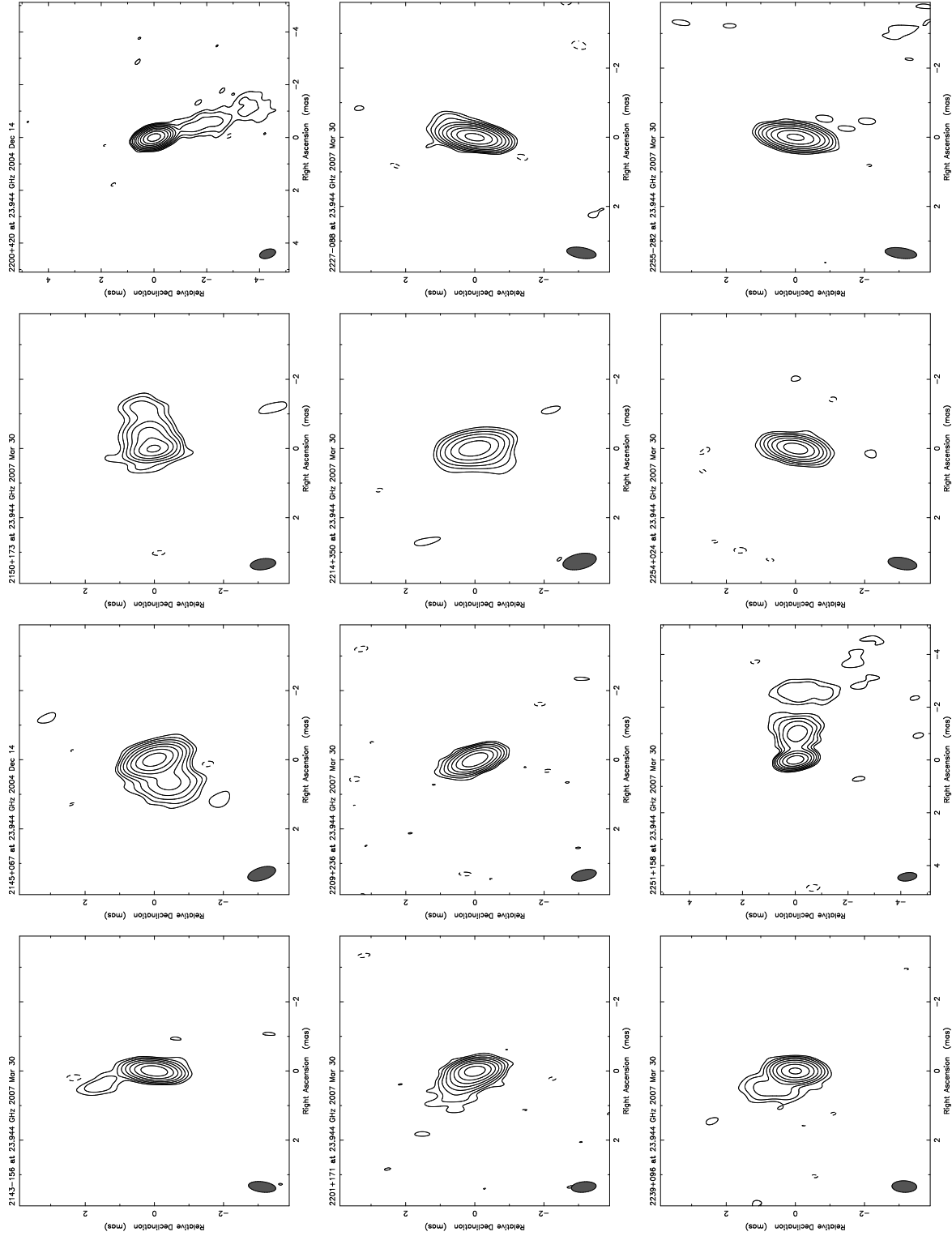
Fig. 1.— *Continued*

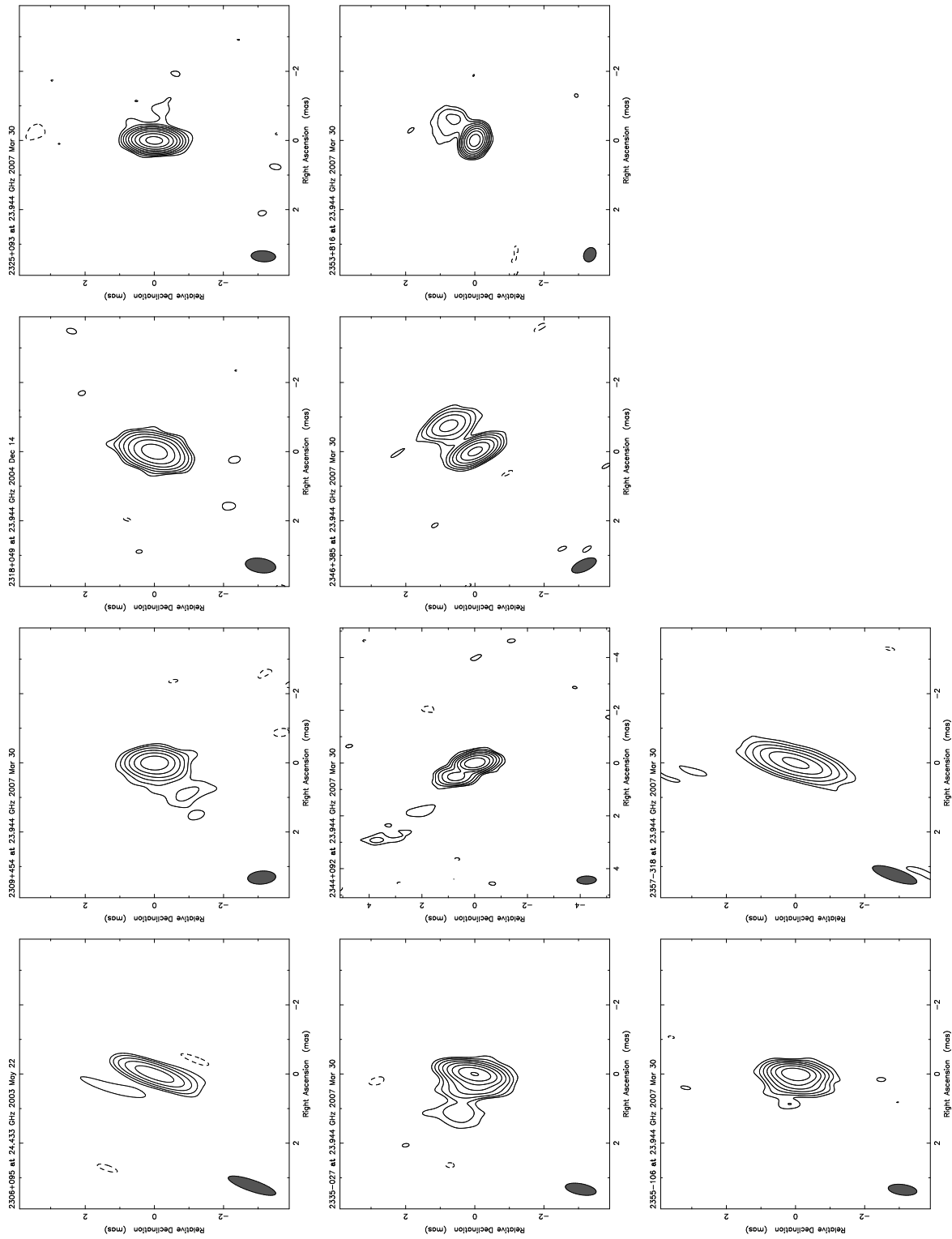
Fig. 1.— *Continued*

Fig. 1.— *Continued*

Fig. 1.— *Continued*

Fig. 1.— *Continued*

Fig. 1.— *Continued*

Fig. 1.— *Continued*

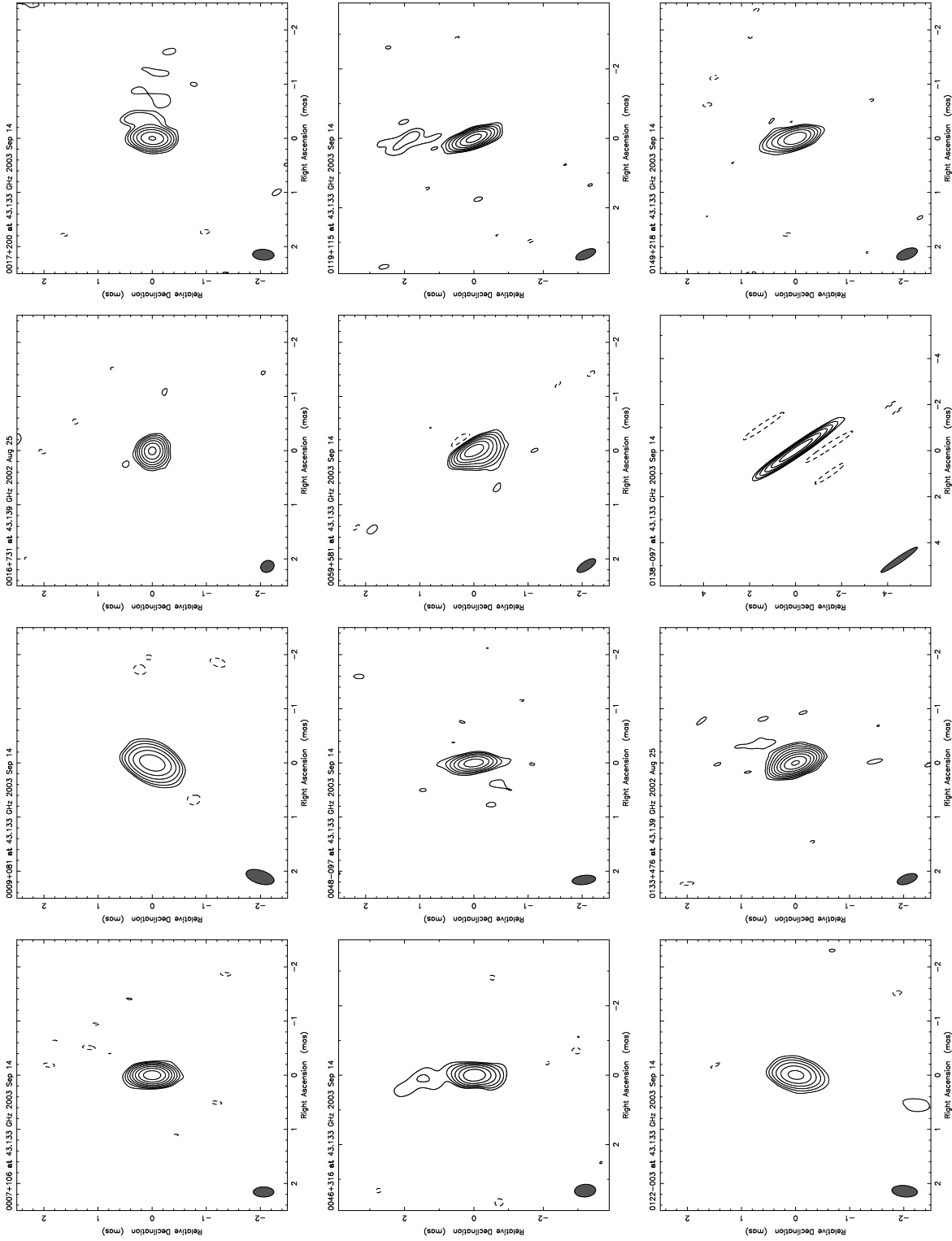
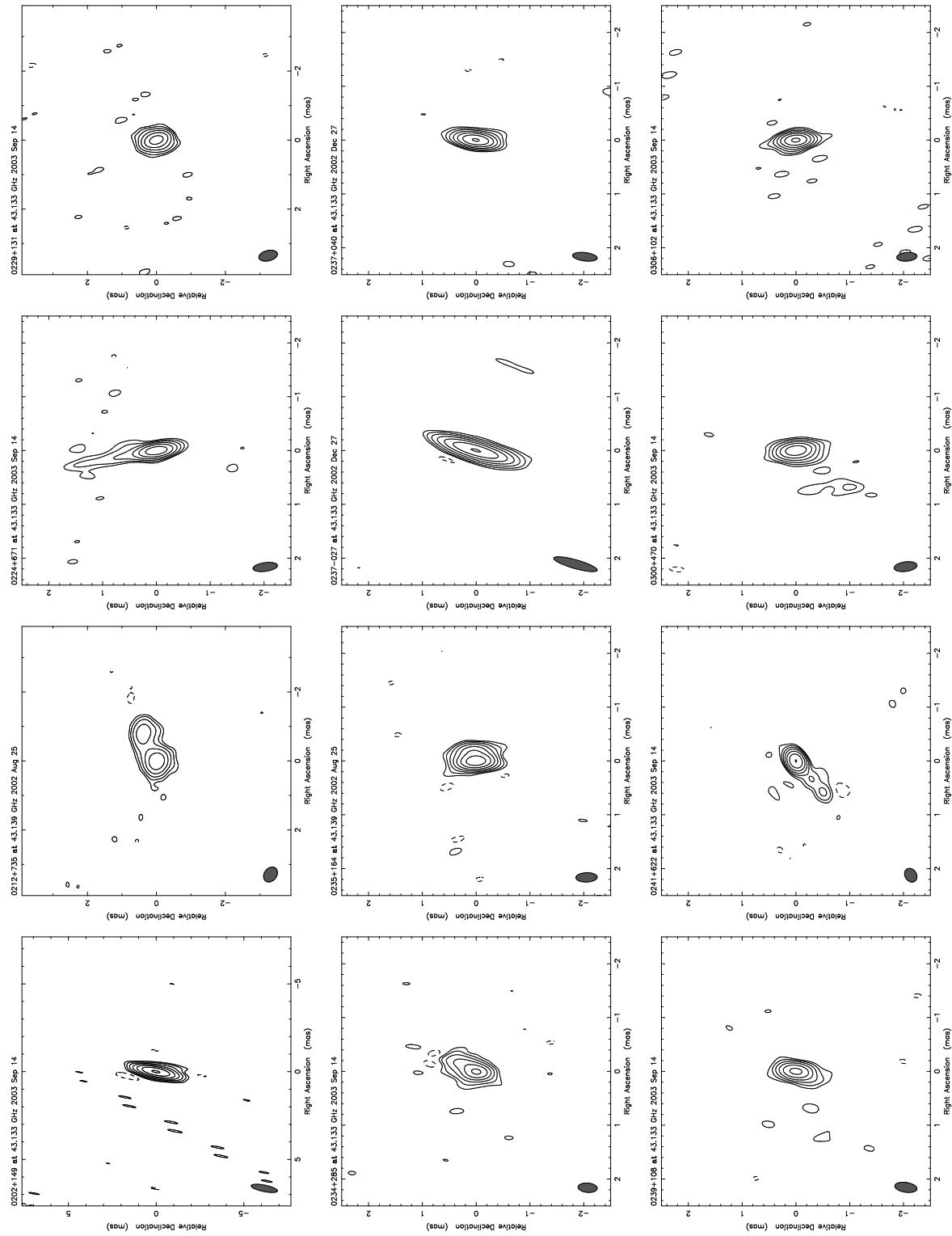
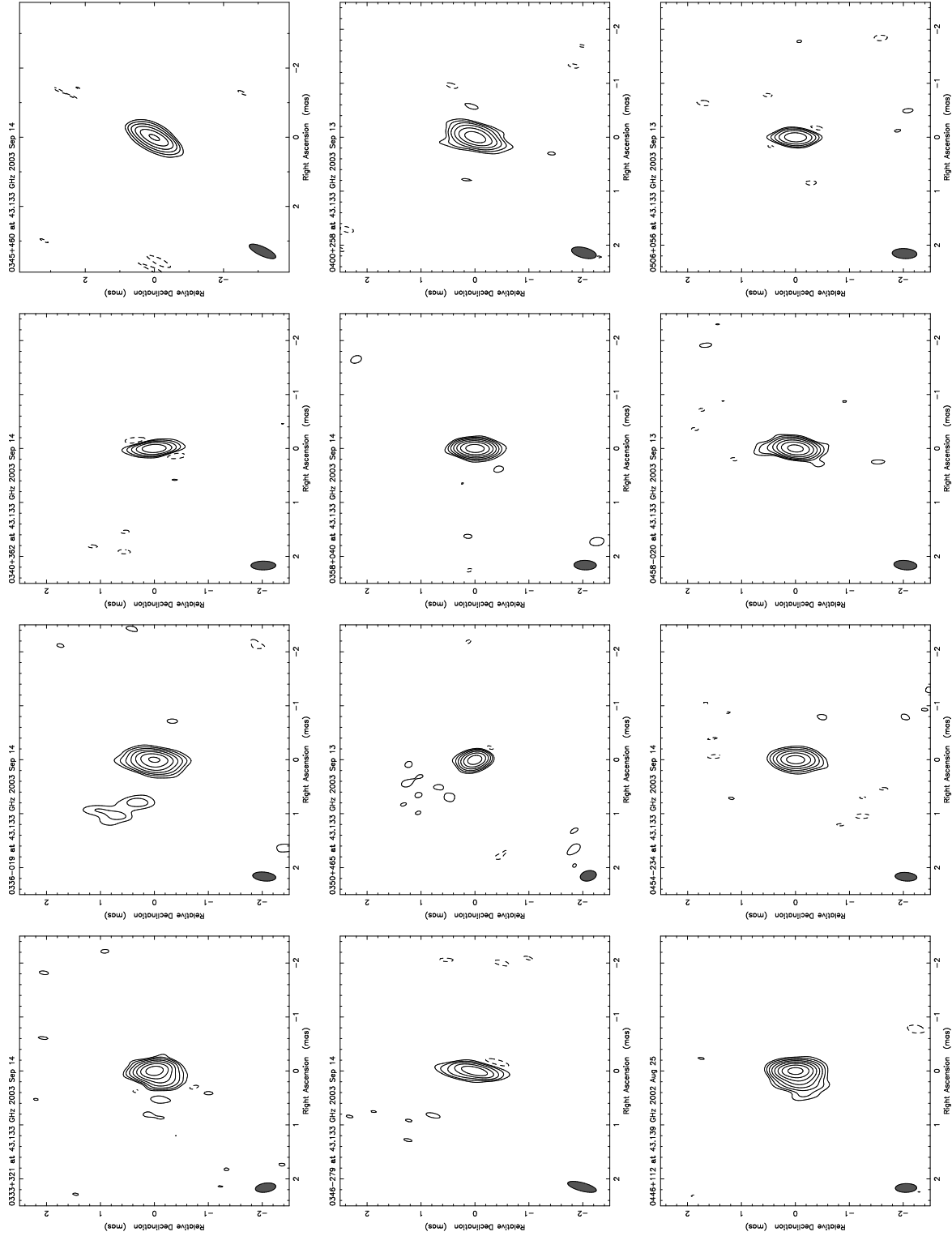
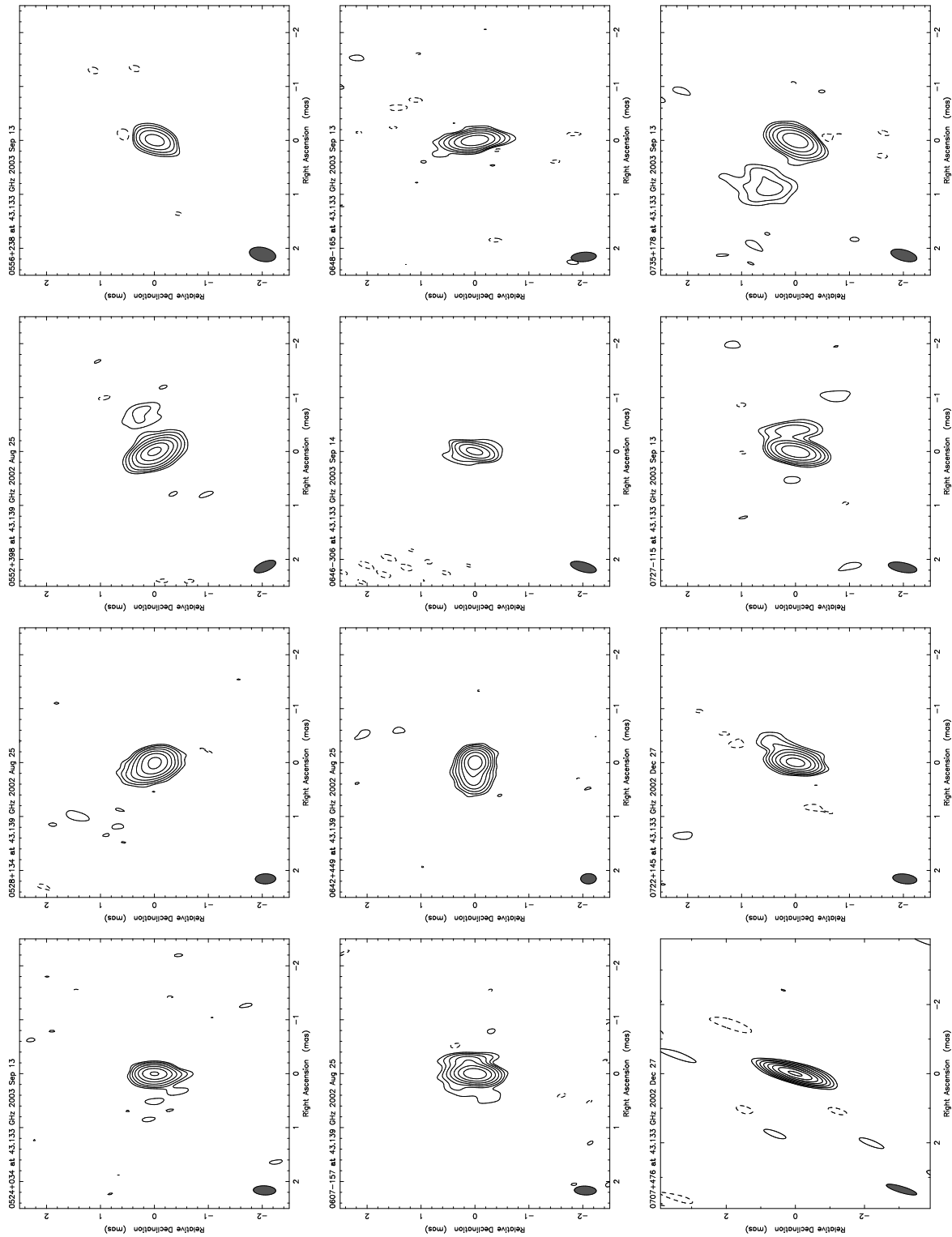
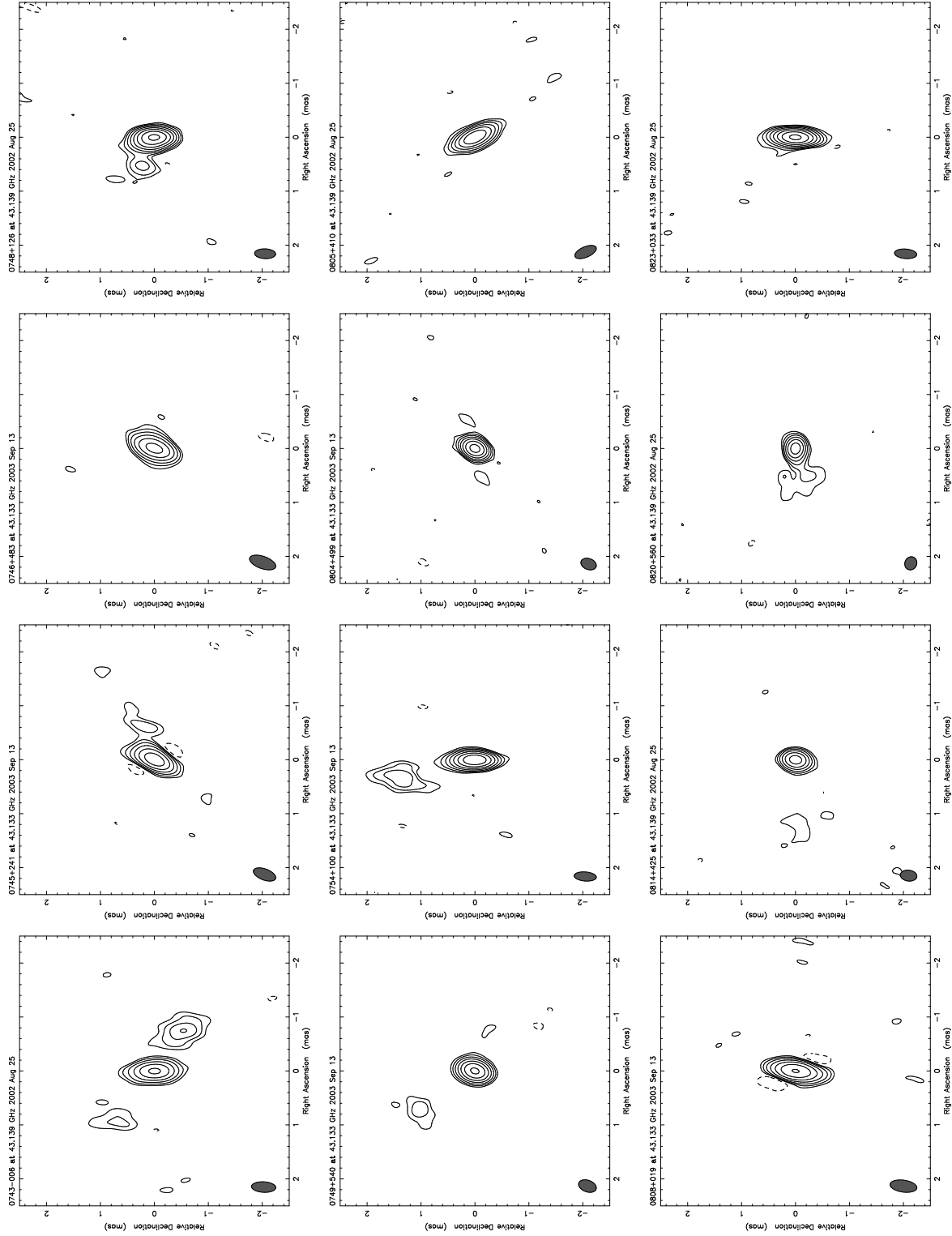


FIG. 2.— Contour plots of 132 extragalactic radio sources at Q band. Image parameters are listed in Table 3. The scale of each image is in milliarcseconds. The FWHM Gaussian restoring beam applied to the images is shown as a hatched ellipse in the lower left of each panel. For convenience, the images for each band are labeled only by a single fiducial frequency (~ 43.1 GHz) even though they were made using the data from all frequency channels (see § 2).

Fig. 2.— *Continued*

Fig. 2.— *Continued*

Fig. 2.— *Continued*

Fig. 2.— *Continued*

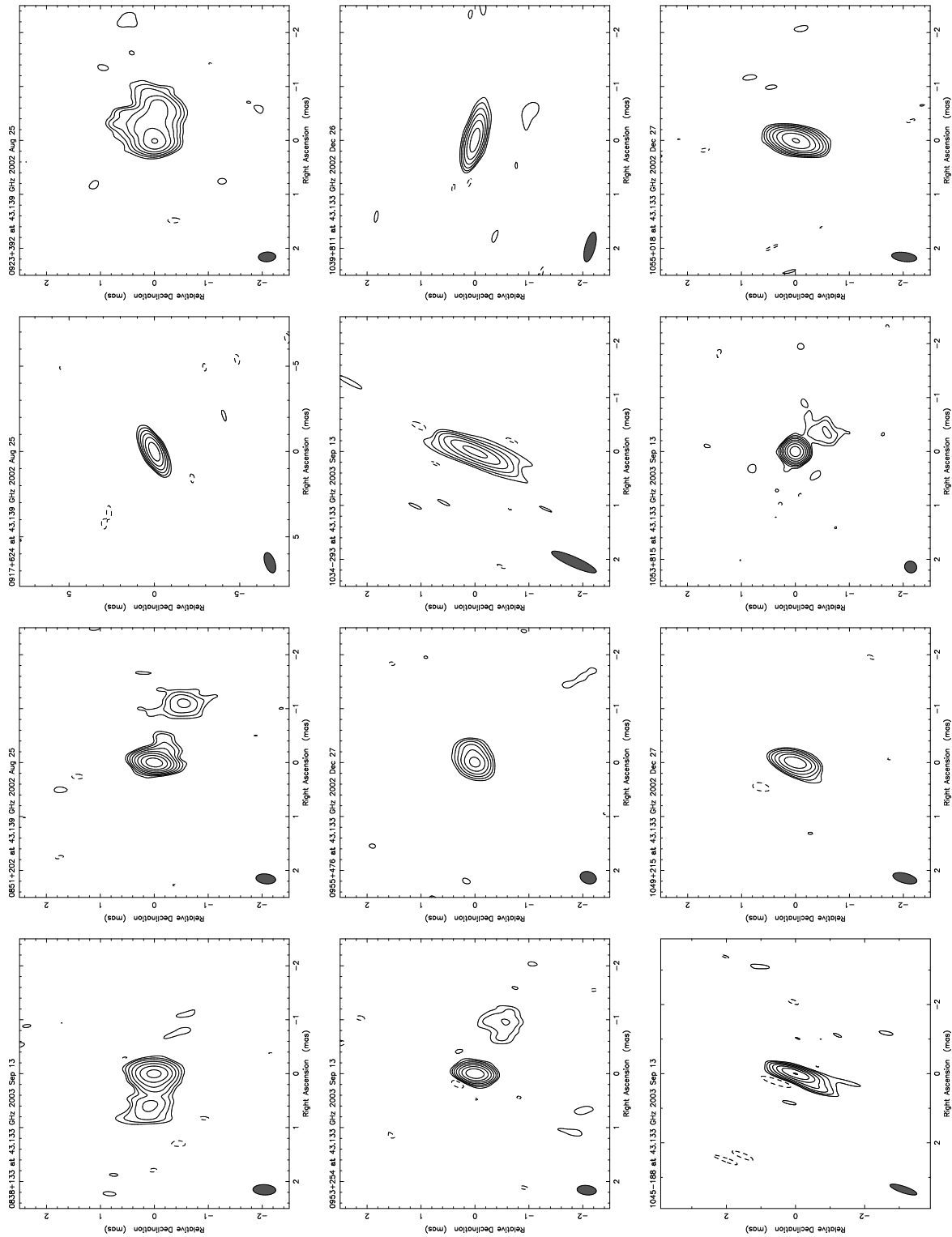
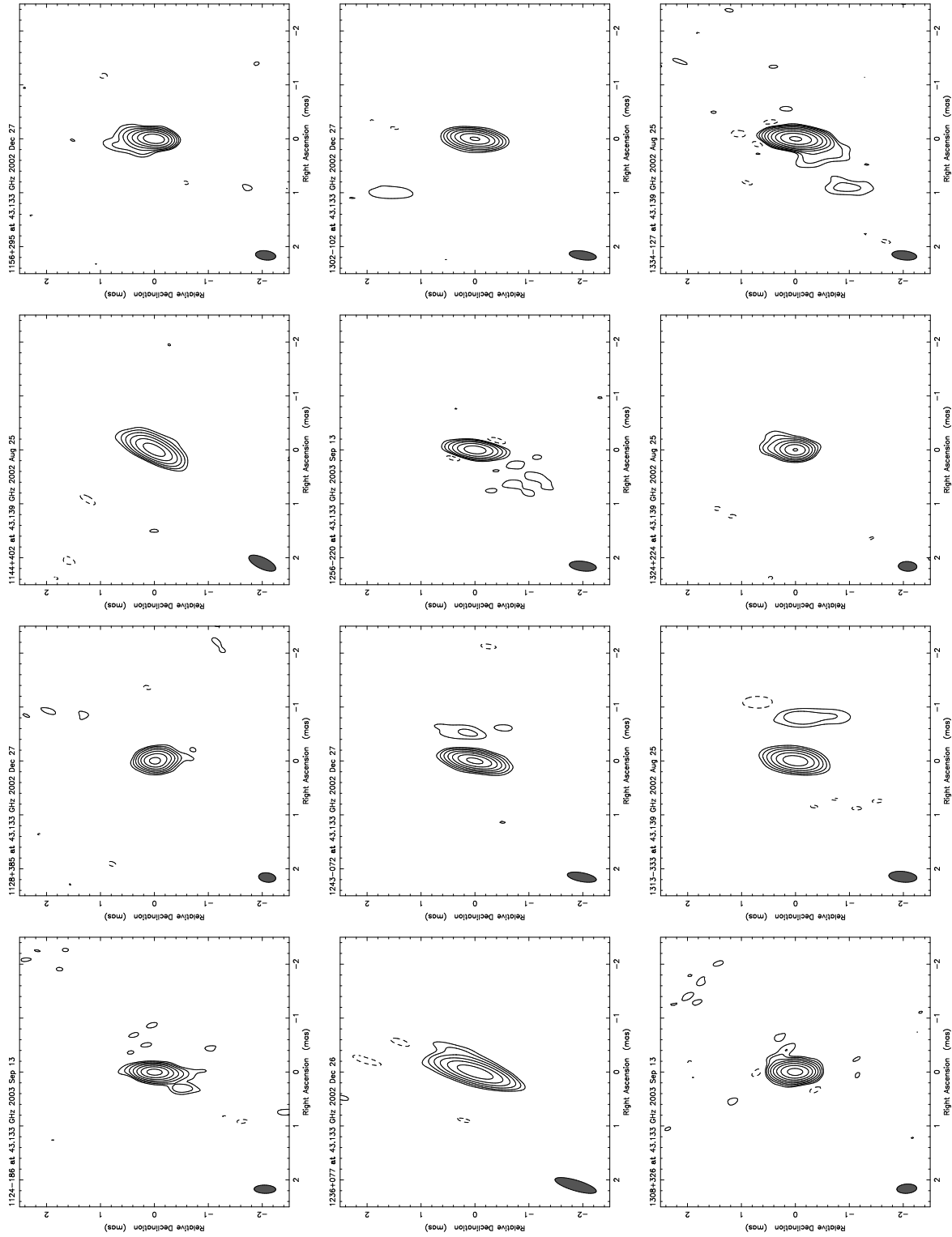


Fig. 2.—Continued

Fig. 2.— *Continued*

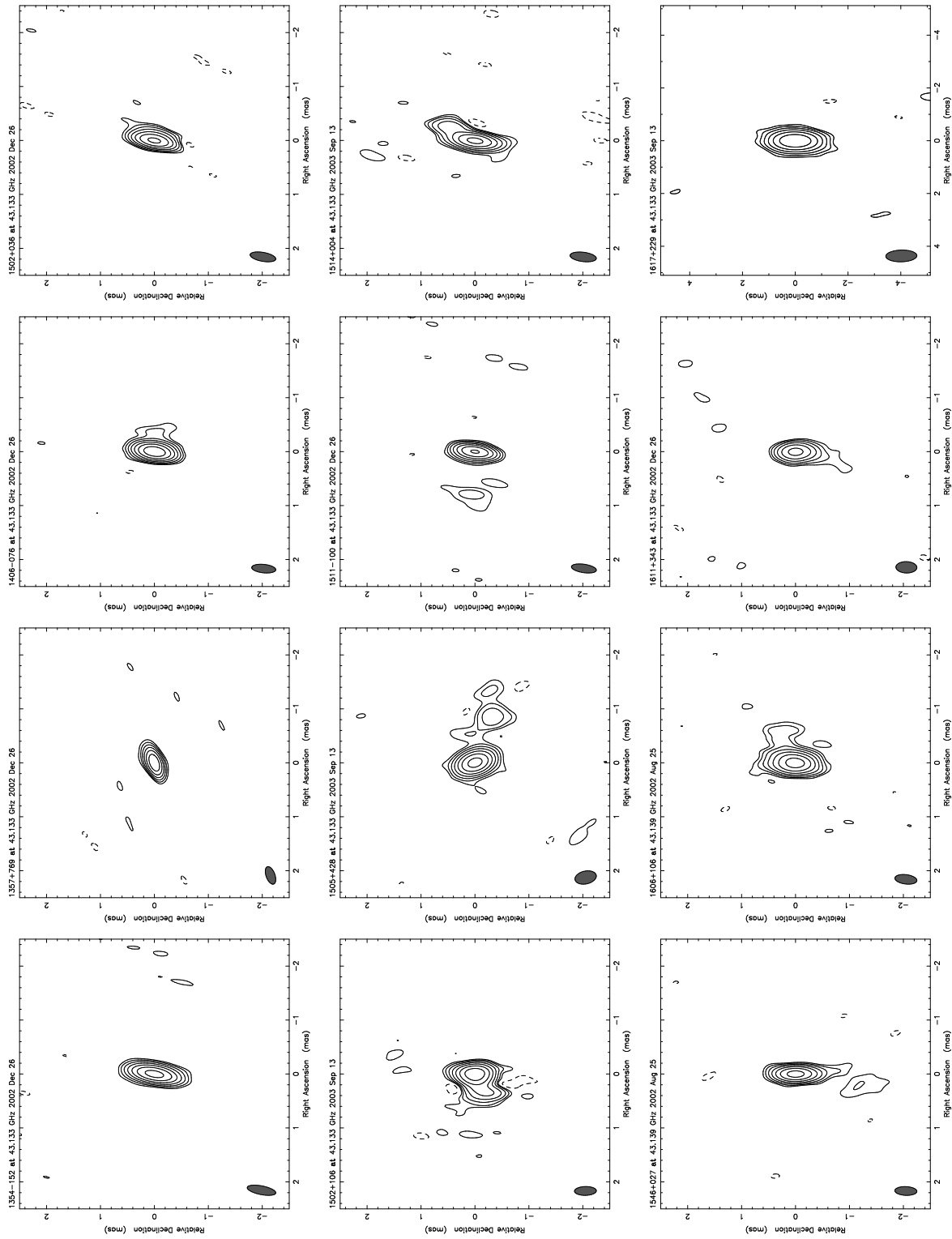
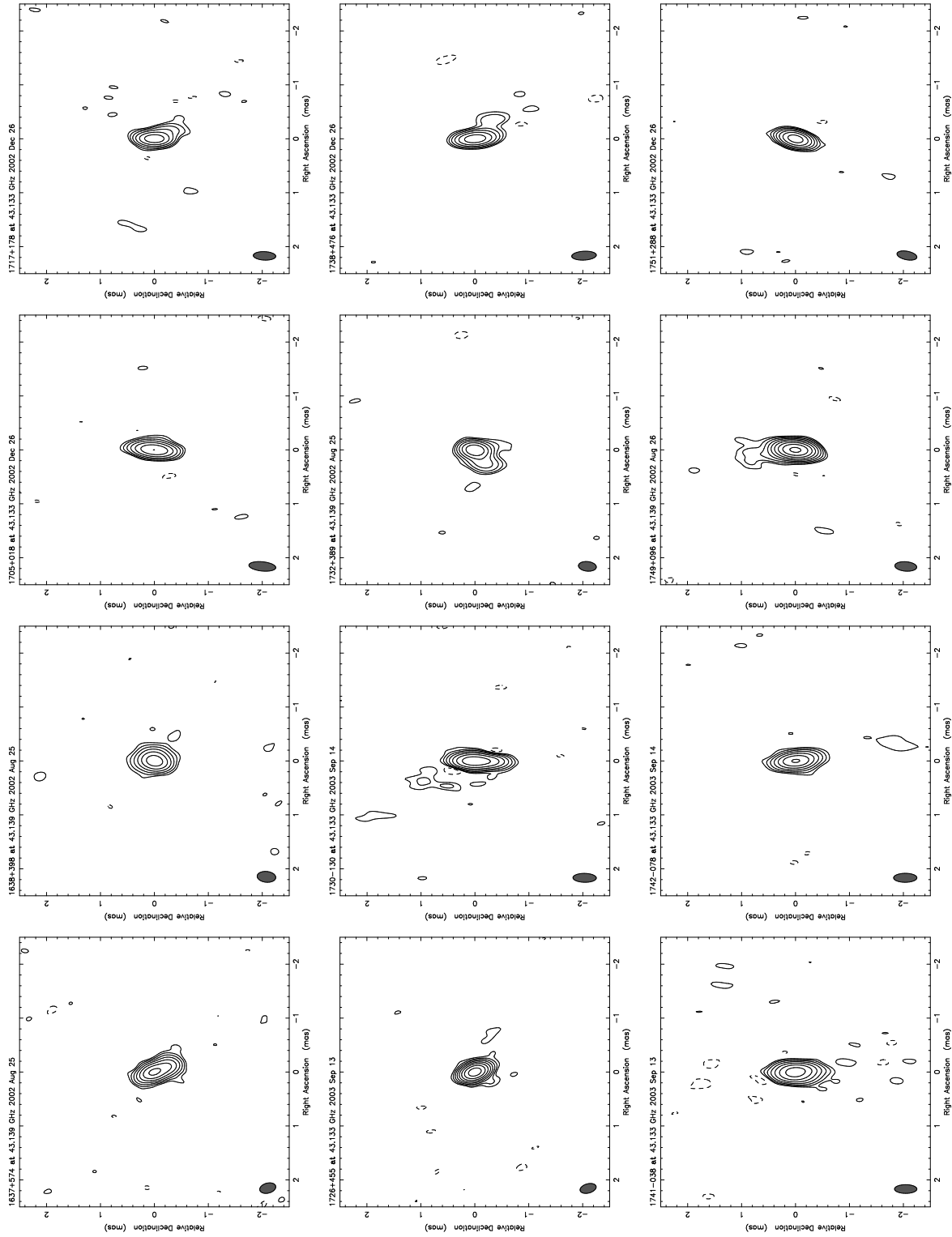


Fig. 2.—Continued

Fig. 2.— *Continued*

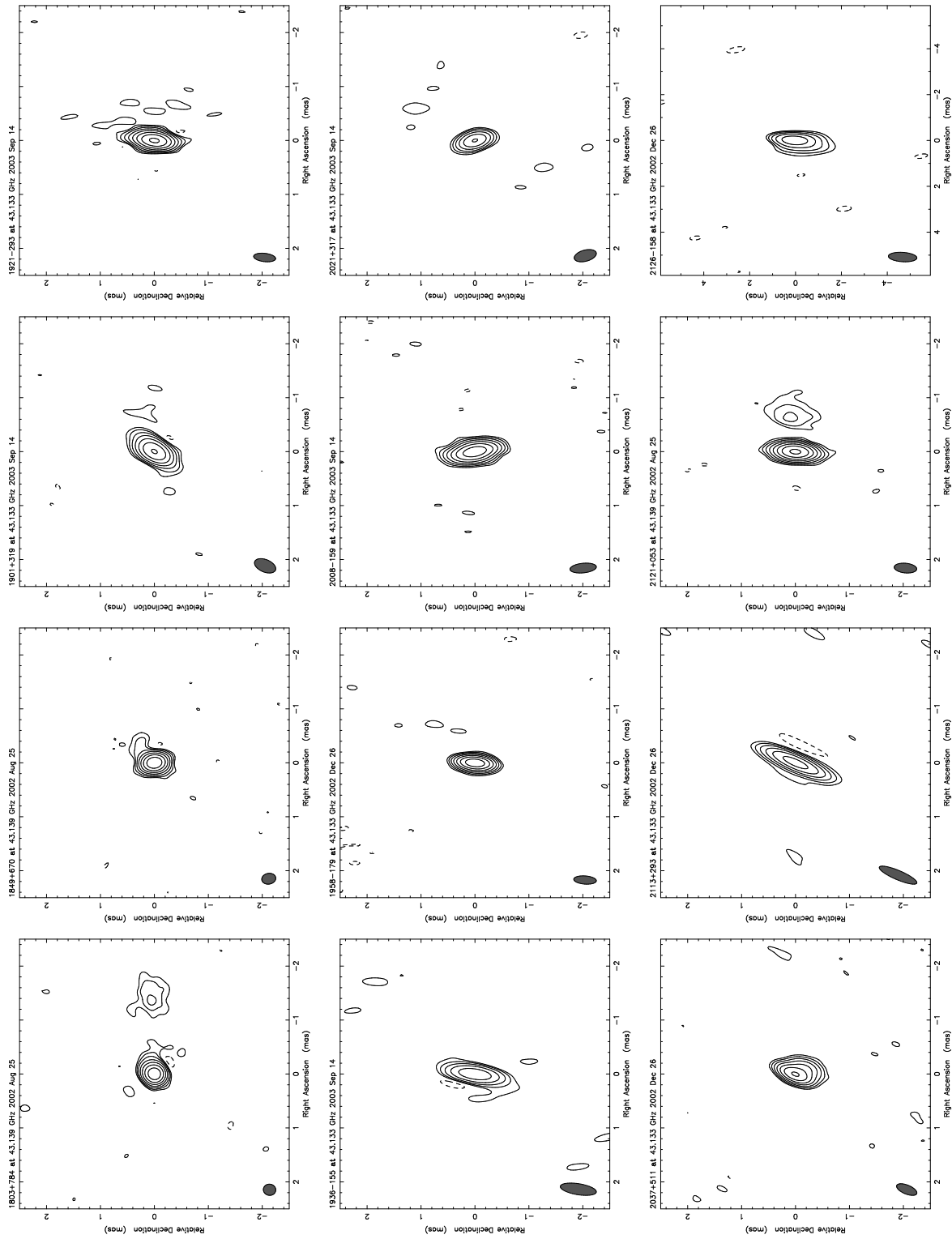


Fig. 2.—Continued

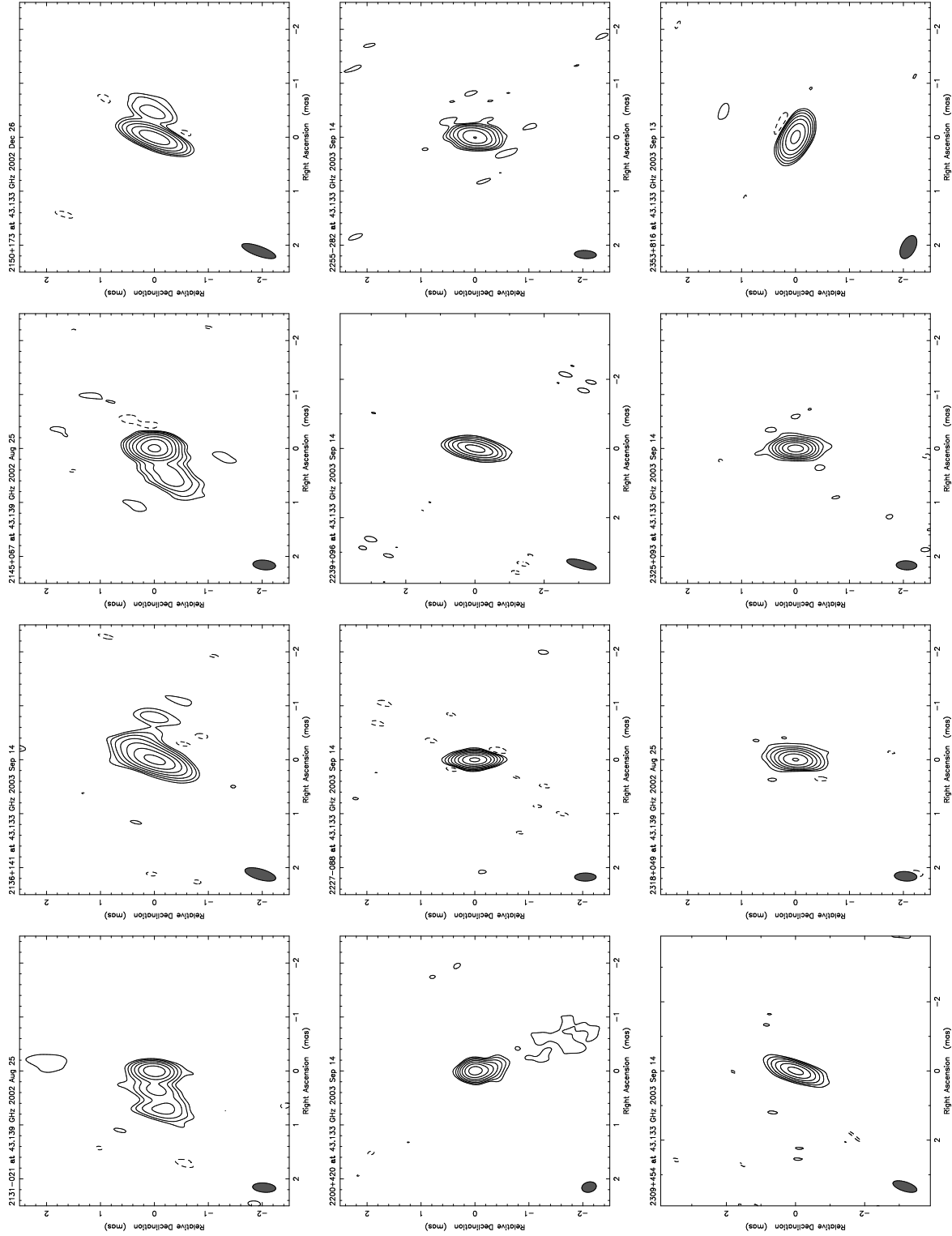


Fig. 2.—Continued

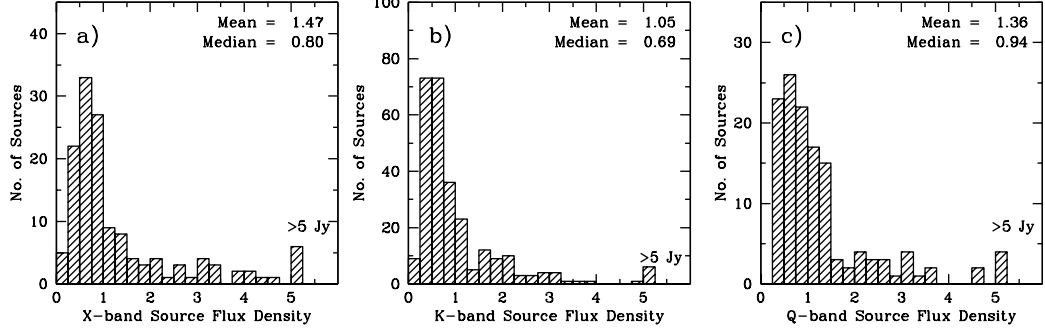


FIG. 3.— Distributions of the mean (averaged over all sessions) source flux density (\bar{S}) at a) X band, b) K band, and b) Q band. There were a total of 138, 274, and 132 sources, respectively, for which the flux density was measured at each of the three bands in our VLBA data set.

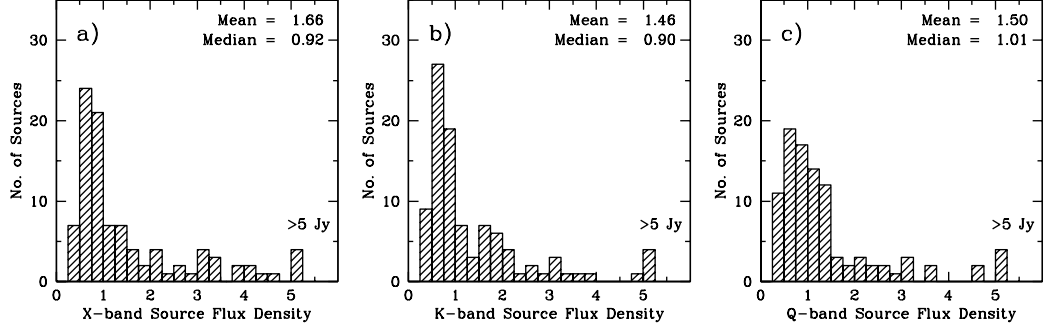


FIG. 4.— Distributions of the mean (averaged over all sessions) source flux density (\bar{S}) at a) X band, b) K band, and b) Q band for the 97 sources common to all three frequencies within our VLBA data set.

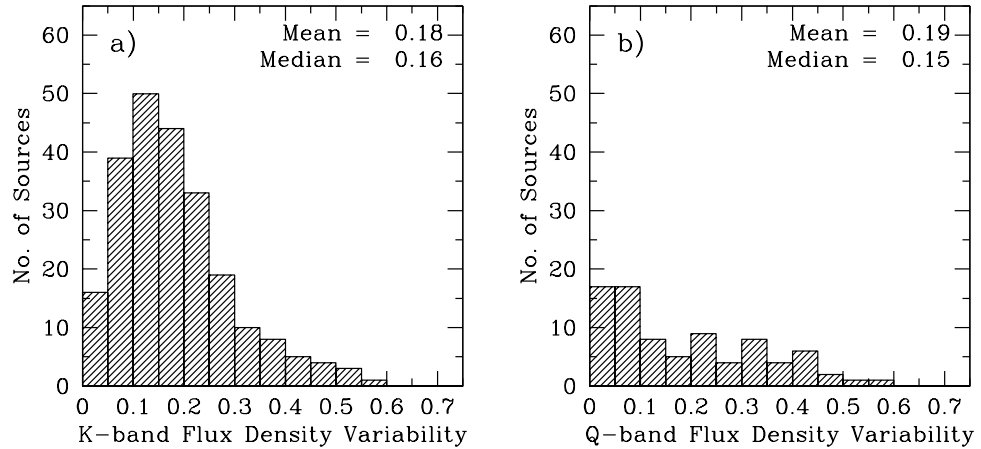


FIG. 5.— Distributions of the source flux density variability index (σ_S/\bar{S}) at a) K band and b) Q band. There are a total of 235 sources observed at K band in more than one session and a total of 82 sources observed at Q band in more than one session.

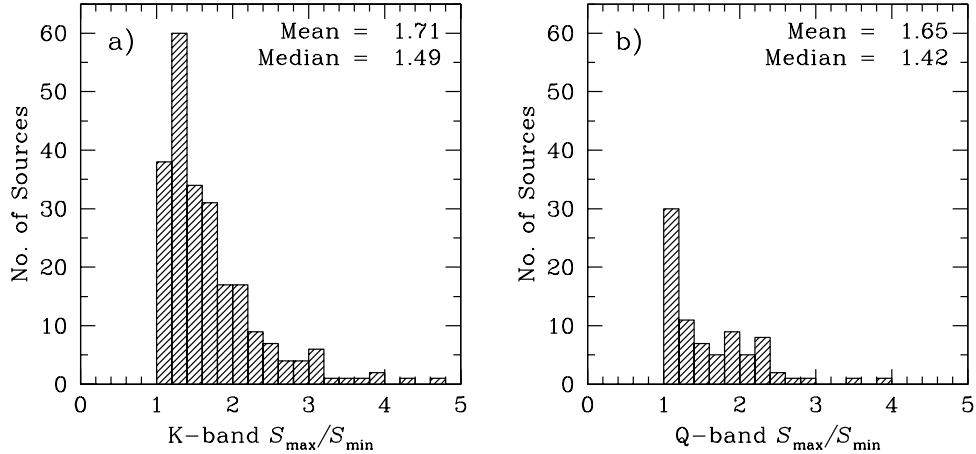


FIG. 6.— Distributions of the ratio of the maximum to minimum source flux density (S_{\max}/S_{\min}) at a) K band and b) Q band. There are a total of 235 sources observed at K band in more than one session and a total of 82 sources observed at Q band in more than one session.

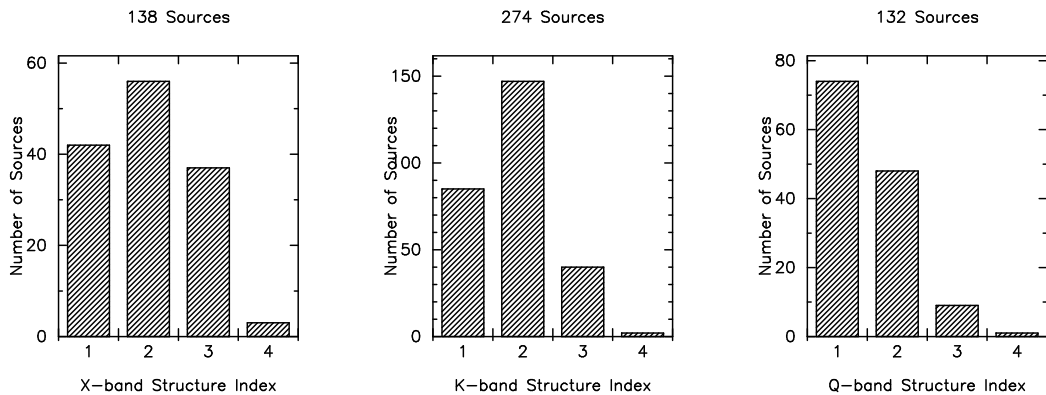


FIG. 7.— Distributions of values for the maximum source structure index (SI) at (a) X band, (b) K band and (c) Q band. There were a total of 138, 274, and 132 sources, respectively, for which the flux density was measured at each of the three bands in our VLBA data set.

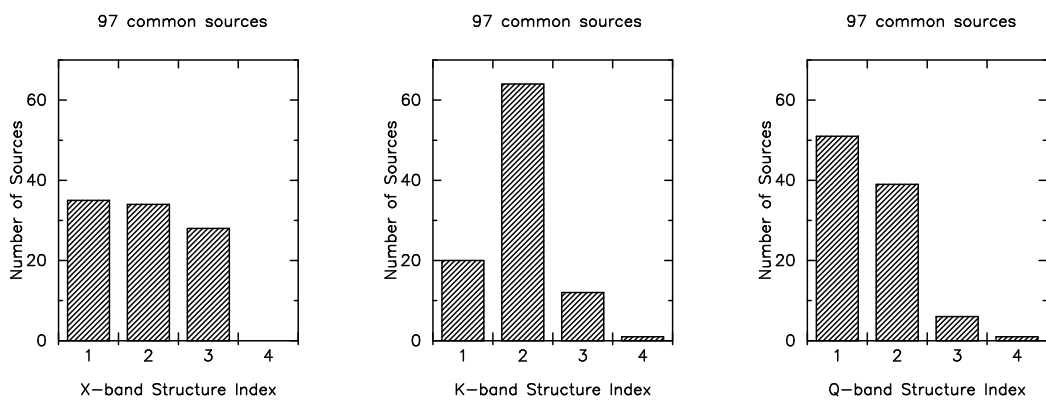


FIG. 8.— Distributions of values for the maximum source structure index (SI) at (a) X band, (b) K band and (c) Q band for the 97 sources common to all three frequencies within our VLBA data set.

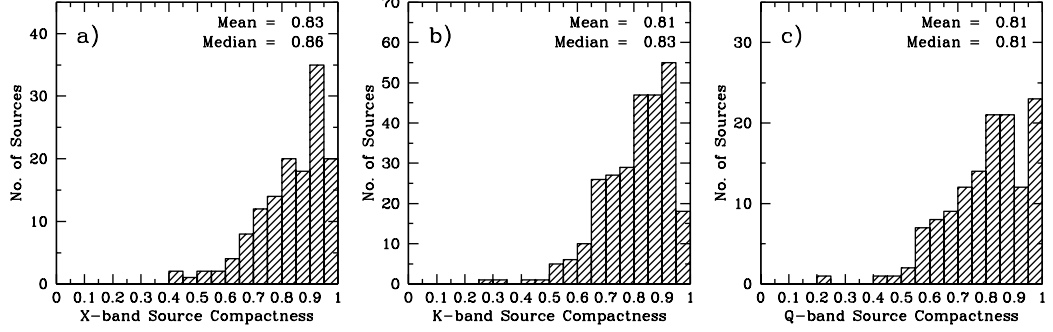


FIG. 9.— Distributions of the mean (averaged over all sessions) source compactness (\bar{C}) at (a) X band, (b) K band, and (c) Q band. There were a total of 138, 274, and 132 sources for which the compactness was determined at each of the three bands, respectively. A maximum compactness, $C = 1.0$, indicates that all of the flux is contained within one synthesized beam.

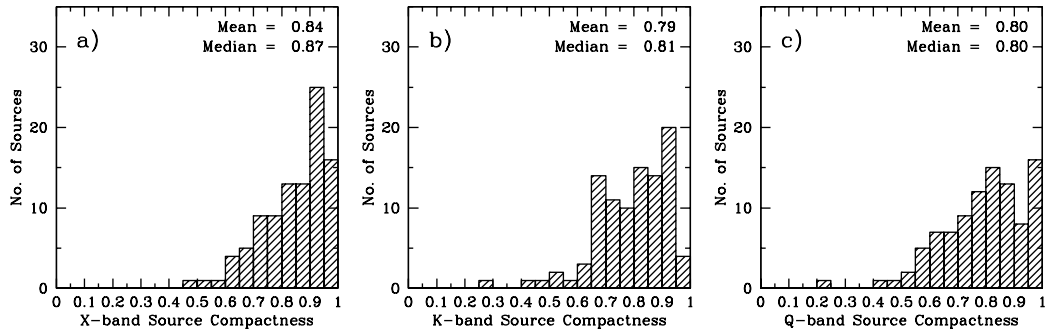


FIG. 10.— Distributions of the mean (averaged over all sessions) source compactness (\bar{C}) at (a) X band, (b) K band, and (c) Q band for the 97 sources common to all three frequencies within our VLBA data set. A maximum compactness, $C = 1.0$, indicates that all of the flux is contained within one synthesized beam.

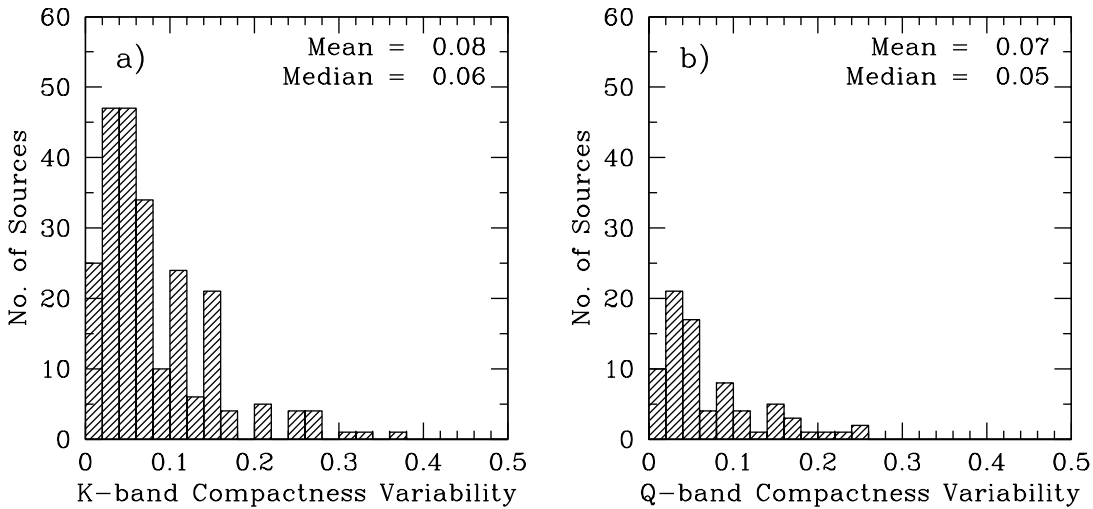


FIG. 11.— Distributions of the source compactness variability index (σ_C/\bar{C}) for sources at (a) K band and (b) Q band. There are a total of 235 sources observed in more than one session at K band, and a total of 82 sources observed in more than one session at Q band. A minimum variability, $\sigma_C/\bar{C} = 0.0$, indicates no variation in the compactness over time.

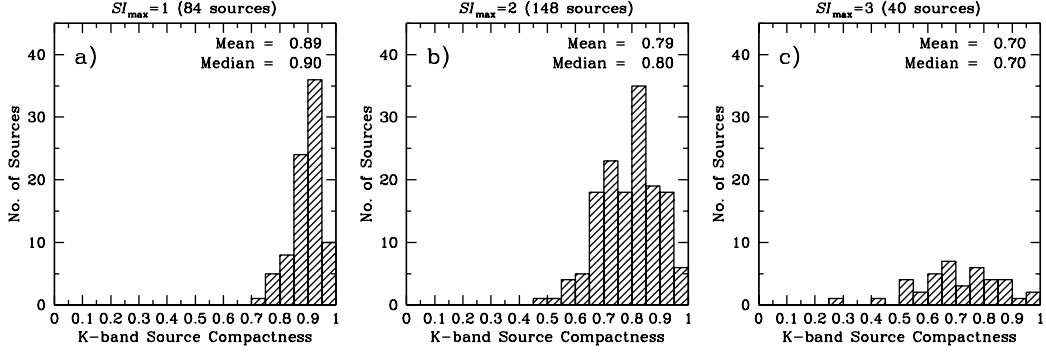


FIG. 12.— Distributions of the mean (averaged over all sessions) source compactness (\bar{C}) separated by maximum structure index (SI_{\max}) for the 274 sources imaged at K band (24 GHz). The three panels represent sources with (a) $SI_{\max} = 1$, (b) $SI_{\max} = 2$, and (c) $SI_{\max} = 3$, respectively. There are two sources with a $SI_{\max} = 4$ that are not shown.

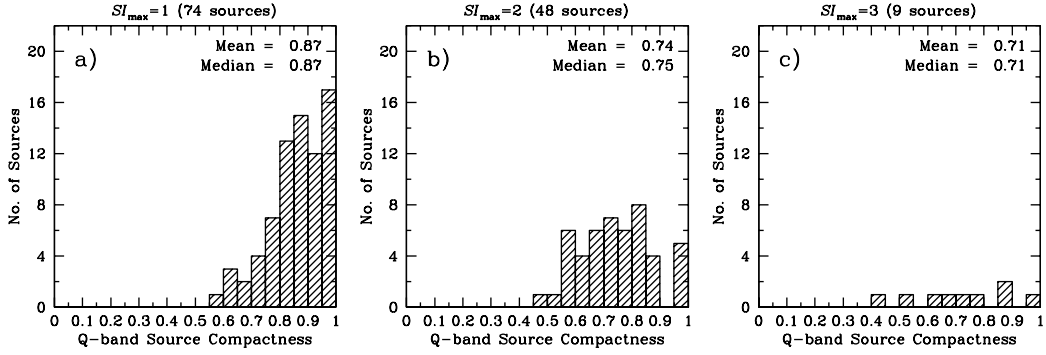


FIG. 13.— Distributions of the mean (averaged over all sessions) source compactness (\bar{C}) separated by maximum structure index (SI_{\max}) for the 132 sources imaged at Q band (43 GHz). The three panels represent sources with (a) $SI_{\max} = 1$, (b) $SI_{\max} = 2$, and (c) $SI_{\max} = 3$, respectively. There is one source with a $SI_{\max} = 4$ that is not shown.

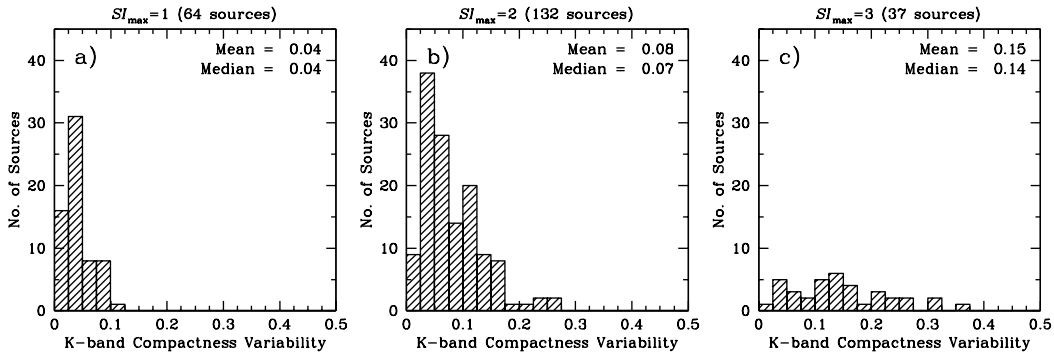


FIG. 14.— Distributions of the compactness variability index (σ_C/\bar{C}) separated by maximum structure index (SI_{\max}) for the 235 sources K-band sources imaged in more than one session. The three panels represent sources with (a) $SI_{\max} = 1$, (b) $SI_{\max} = 2$, and (c) $SI_{\max} = 3$, respectively. There are two sources with a $SI_{\max} = 4$ that are not shown.

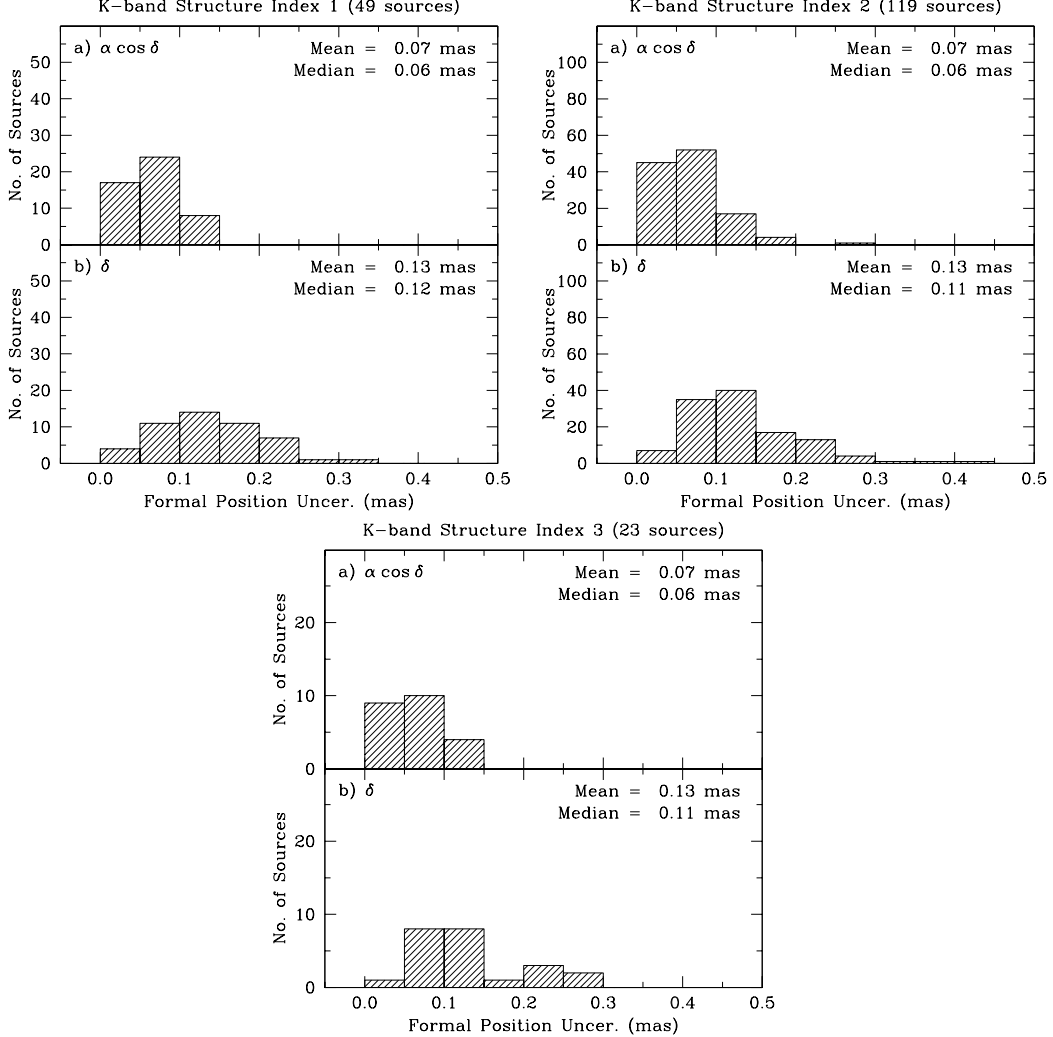


FIG. 15.— Distributions of the formal position uncertainties in $\alpha \cos \delta$ (a) and in δ (b) for the 193 sources with 100 or more delay observations at K band (24 GHz). The three panels represent sources with a maximum source structure index equal to 1, 2 and 3, respectively. There are two sources with a structure index of 4 and with more than 100 delay observations that are not included in the figure.

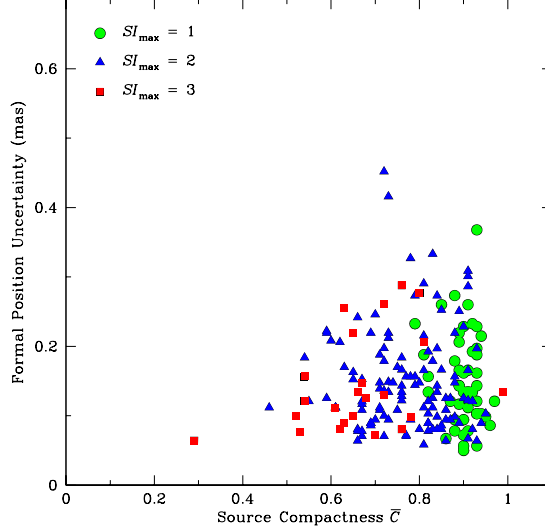


FIG. 16.— Comparison of the formal astrometric position uncertainty versus the mean source compactness (\bar{C}) for K band sources with more than 100 delay measurements. Point color and type represent the maximum structure index for each source over the sessions in which it was observed.

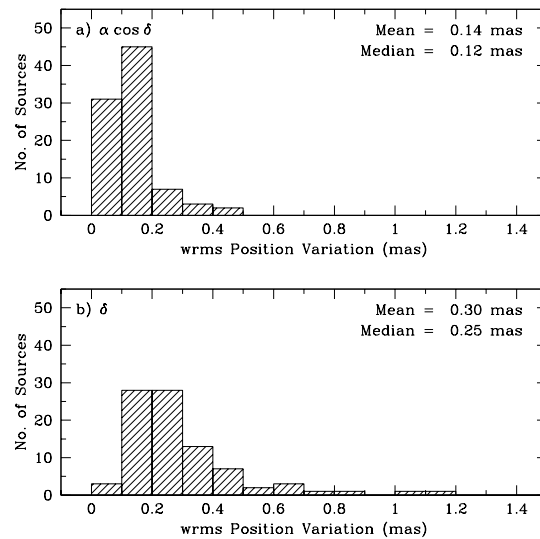


FIG. 17.— Distributions of wrms position stability in (a) $\alpha \cos \delta$ and in (b) δ for the 88 sources observed in five or more sessions at K-band (24 GHz).

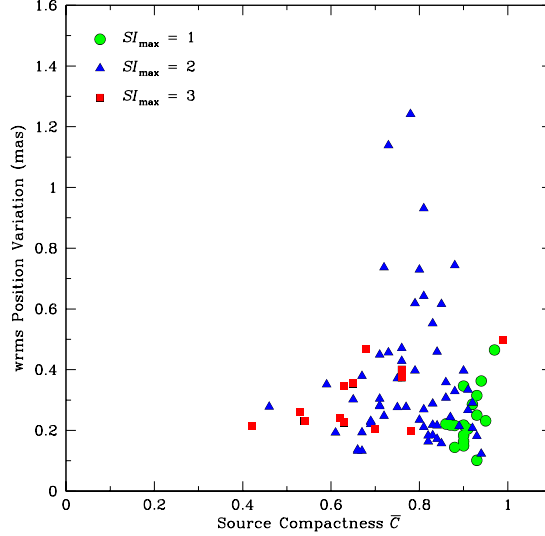


FIG. 18.— Comparison of the wrms position stability versus the mean source compactness (\bar{C}) for sources observed in five or more sessions at K band (24 GHz). Point color and type represent the maximum structure index for each source over the sessions in which it was observed.

TABLE 1
SUMMARY OF VLBA IMAGING AT K AND Q BAND.

Epoch	Band	K-band Sources			Q-band Sources		
		Imaged	Overlap	New	Imaged	Overlap	New
2002-05-15	K ^a /Q ^b	65	...	65	65	...	65
2002-08-25	K ^a /Q ^b	65	65	...	65	65	...
2002-12-26	K ^c /Q ^d	67	24	43	67	24	43
2003-05-22 ^e	K ^c	184	62	122
2003-09-13	K ^c /Q ^d	70	70	...	70	46	24
2004-02-15	K ^c	65	65
2004-12-14	K ^f	101	101
2005-08-26	K ^f	92	67	25
2006-07-09	K ^f	178	163	15
2007-03-30	K ^f	185	181	4

^a $\nu = 24.25, 24.33, 24.51, 24.65$ GHz

^b $\nu = 42.95, 43.03, 43.21, 43.35$ GHz

^c $\nu = 24.21, 24.23, 24.27, 24.34, 24.49, 24.59, 24.66, 24.68$ GHz

^d $\nu = 42.91, 42.93, 42.97, 43.04, 43.19, 43.29, 43.36, 43.38$ GHz

^e K-band only survey of 249 sources.

^f $\nu = 23.72, 23.74, 23.78, 23.85, 24.00, 24.10, 24.17, 24.19$ GHz

TABLE 2
 PARAMETERS OF NATURALLY WEIGHTED IMAGES AT 24 GHz

Source	Observation Session	Beam ^a			Flux Density			Contour Levels ^d (mJy bm ⁻¹)
		<i>a</i> (mas)	<i>b</i> (mas)	ϕ (°)	S_{peak} (Jy bm ⁻¹)	S_{total} ^b (Jy)	S_{rms} ^c (mJy bm ⁻¹)	
0006 + 061	05-22-2003	1.01	0.29	-11	0.24	0.26	2.9	$7.1 \times (1, \dots, 2^5)$
0007 + 106	03-30-2007	0.72	0.30	3	0.42	0.51	1.5	$4.5 \times (1, \dots, 2^6)$
0009 + 081	03-30-2007	0.82	0.37	-4	0.31	0.45	1.4	$4.1 \times (1, \dots, 2^6)$
0016 + 731	12-14-2004	0.46	0.36	-2	1.82	1.98	1.4	$4.1 \times (1, \dots, 2^8)$
0017 + 200	03-30-2007	0.63	0.31	-9	0.43	0.59	1.8	$5.4 \times (1, \dots, 2^6)$
0019 + 058	03-30-2007	0.73	0.30	-3	0.87	0.94	1.3	$3.9 \times (1, \dots, 2^7)$
0038 - 020	05-22-2003	1.39	0.70	-1	0.29	0.35	3.6	$10.9 \times (1, \dots, 2^4)$
0046 + 316	03-30-2007	0.63	0.34	7	0.39	0.53	1.4	$3.9 \times (1, \dots, 2^6)$
0048 - 097	12-14-2004	0.77	0.31	1	0.74	0.78	1.5	$4.4 \times (1, \dots, 2^7)$
0054 + 161	05-22-2003	1.12	0.32	-10	0.25	0.26	2.9	$8.2 \times (1, \dots, 2^4)$
0059 + 581	12-14-2004	0.66	0.33	30	1.31	1.60	1.2	$3.7 \times (1, \dots, 2^8)$
0104 - 408	05-22-2003	0.74	0.26	-3	0.85	1.08	5.0	$15.0 \times (1, \dots, 2^5)$
0109 + 224	03-30-2007	0.64	0.36	-5	0.85	0.95	1.5	$4.4 \times (1, \dots, 2^7)$
0110 + 495	03-30-2007	0.73	0.30	23	1.16	1.35	1.9	$5.5 \times (1, \dots, 2^7)$
0111 + 021	03-30-2007	1.07	0.33	-15	0.33	0.48	1.8	$5.4 \times (1, \dots, 2^5)$
0119 + 041	03-30-2007	0.98	0.36	-13	0.44	0.67	4.2	$12.5 \times (1, \dots, 2^5)$
0119 + 115	12-14-2004	0.71	0.32	-4	0.99	1.26	1.3	$4.0 \times (1, \dots, 2^7)$
0119 + 247	03-30-2007	0.71	0.36	-5	0.26	0.47	1.1	$3.4 \times (1, \dots, 2^6)$
0122 - 003	03-30-2007	0.75	0.30	-1	0.42	0.68	3.1	$9.4 \times (1, \dots, 2^5)$
0123 + 257	03-30-2007	0.82	0.31	-6	0.40	0.46	1.6	$4.7 \times (1, \dots, 2^6)$
0127 + 084	03-30-2007	1.05	0.33	-13	0.26	0.27	1.3	$3.9 \times (1, \dots, 2^6)$
0133 + 476	12-14-2004	0.54	0.33	12	2.82	3.16	2.2	$6.6 \times (1, \dots, 2^8)$
0138 - 097	12-14-2004	0.89	0.34	-8	0.21	0.33	1.2	$3.6 \times (1, \dots, 2^5)$
0149 + 218	03-30-2007	0.67	0.33	-2	0.71	0.81	1.9	$5.6 \times (1, \dots, 2^6)$
0202 + 149	03-30-2007	0.71	0.32	-8	0.40	0.74	2.2	$6.7 \times (1, \dots, 2^5)$
0202 + 319	03-30-2007	0.73	0.30	15	2.65	2.89	2.9	$8.7 \times (1, \dots, 2^8)$
0212 + 735	03-30-2007	0.45	0.35	20	1.12	2.87	3.4	$10.2 \times (1, \dots, 2^6)$
0213 - 026	03-30-2007	0.80	0.34	0	0.28	0.42	2.0	$5.9 \times (1, \dots, 2^5)$
0220 - 349	05-22-2003	5.43	1.04	8	0.48	0.55	3.8	$11.5 \times (1, \dots, 2^5)$
0221 + 067	03-30-2007	0.83	0.36	-11	0.43	0.57	1.4	$4.3 \times (1, \dots, 2^6)$
0222 + 185	03-30-2007	0.92	0.36	-19	0.21	0.21	1.4	$4.2 \times (1, \dots, 2^5)$
0224 + 671	12-14-2004	0.57	0.36	41	0.53	0.70	1.2	$3.7 \times (1, \dots, 2^7)$
0229 + 131	12-14-2004	0.74	0.33	-2	0.53	0.85	3.1	$9.2 \times (1, \dots, 2^5)$
0234 + 285	03-30-2007	0.63	0.32	3	1.07	2.34	3.8	$11.4 \times (1, \dots, 2^6)$
0235 + 164	03-30-2007	0.69	0.31	-5	3.74	3.89	3.4	$10.1 \times (1, \dots, 2^8)$
0237 - 027	03-30-2007	0.70	0.28	-3	0.61	0.63	1.9	$5.2 \times (1, \dots, 2^6)$
0237 + 040	03-30-2007	0.76	0.31	-5	0.53	0.59	1.9	$5.8 \times (1, \dots, 2^6)$
0239 + 108	03-30-2007	0.73	0.31	-6	0.53	0.61	1.4	$4.3 \times (1, \dots, 2^6)$
0241 + 622	12-14-2004	0.72	0.31	33	0.57	1.05	1.7	$5.2 \times (1, \dots, 2^6)$
0250 + 320	05-22-2003	0.79	0.27	-1	0.23	0.21	1.5	$4.6 \times (1, \dots, 2^5)$
0256 + 192	03-30-2007	1.13	0.37	-9	0.26	0.29	1.7	$5.1 \times (1, \dots, 2^5)$
0300 + 470	03-30-2007	0.71	0.29	5	0.55	0.70	1.4	$4.2 \times (1, \dots, 2^7)$
0306 + 102	12-14-2004	0.82	0.33	3	1.09	1.25	2.0	$5.9 \times (1, \dots, 2^7)$
0309 + 411	03-30-2007	0.70	0.30	13	0.78	1.01	1.5	$4.6 \times (1, \dots, 2^7)$
0322 + 222	03-30-2007	0.71	0.30	-5	0.42	0.49	1.3	$3.9 \times (1, \dots, 2^6)$
0333 + 321	12-14-2004	0.67	0.31	1	1.63	2.01	2.4	$7.0 \times (1, \dots, 2^7)$
0336 - 019	12-14-2004	0.52	0.26	-21	0.67	1.49	2.6	$7.9 \times (1, \dots, 2^6)$
0340 + 362	03-30-2007	0.65	0.34	-2	0.28	0.34	1.2	$3.4 \times (1, \dots, 2^6)$
0345 + 460	03-30-2007	0.67	0.37	-9	0.21	0.30	1.0	$2.9 \times (1, \dots, 2^6)$
0346 - 279	03-30-2007	1.02	0.37	5	0.49	0.71	4.4	$13.3 \times (1, \dots, 2^5)$
0350 + 465	03-30-2007	0.56	0.31	4	0.34	0.40	1.1	$3.4 \times (1, \dots, 2^6)$
0354 + 231	03-30-2007	0.75	0.31	3	0.22	0.23	1.1	$3.4 \times (1, \dots, 2^6)$
0358 + 040	03-30-2007	0.73	0.32	-1	0.45	0.44	2.0	$5.9 \times (1, \dots, 2^6)$
0358 + 210	03-30-2007	0.78	0.30	-1	0.21	0.23	1.2	$3.4 \times (1, \dots, 2^5)$
0400 + 258	03-30-2007	0.76	0.33	-9	0.42	0.77	1.9	$5.7 \times (1, \dots, 2^6)$
0402 - 362	05-22-2003	0.74	0.27	5	2.02	2.14	4.0	$12.7 \times (1, \dots, 2^7)$
0405 - 331	03-30-2007	1.10	0.36	7	0.61	0.65	9.2	$21.2 \times (1, \dots, 2^4)$
0405 - 385	05-22-2003	0.74	0.27	1	0.54	0.69	4.0	$10.8 \times (1, \dots, 2^5)$
0406 + 121	05-22-2003	1.95	0.34	-23	0.23	0.27	2.8	$8.3 \times (1, \dots, 2^4)$
0409 + 229	03-30-2007	0.88	0.54	-24	0.19	0.25	1.6	$4.7 \times (1, \dots, 2^5)$
0415 + 398	03-30-2007	0.75	0.36	14	0.25	0.32	1.3	$3.9 \times (1, \dots, 2^5)$
0420 - 014	03-30-2007	0.74	0.28	-2	4.24	4.72	6.4	$19.1 \times (1, \dots, 2^7)$
0420 + 022	03-30-2007	0.73	0.28	-2	0.66	0.91	2.1	$6.3 \times (1, \dots, 2^6)$
0422 + 004	03-30-2007	0.72	0.28	-2	0.85	0.98	1.9	$5.8 \times (1, \dots, 2^7)$
0422 - 380	05-22-2003	0.73	0.27	2	0.64	1.04	4.7	$14.2 \times (1, \dots, 2^5)$
0425 + 048	05-22-2003	1.16	0.52	-17	0.24	0.30	2.5	$7.6 \times (1, \dots, 2^4)$
0426 + 273	03-30-2007	0.65	0.29	0	0.74	0.79	1.1	$3.4 \times (1, \dots, 2^7)$

TABLE 2 — *Continued*

Source	Observation Session	Beam ^a			Flux Density			Contour Levels ^d (mJy bm ⁻¹)
		<i>a</i> (mas)	<i>b</i> (mas)	ϕ (°)	S_{peak} (Jy bm ⁻¹)	$S_{\text{total}}^{\text{b}}$ (Jy)	$S_{\text{rms}}^{\text{c}}$ (mJy bm ⁻¹)	
0426 – 380	05-22-2003	0.73	0.26	1	0.61	0.72	4.3	$12.4 \times (1, \dots, 2^5)$
0429 + 174	03-30-2007	0.69	0.32	–6	0.26	0.30	1.2	$3.5 \times (1, \dots, 2^6)$
0430 + 052	03-30-2007	0.69	0.27	0	1.17	2.50	5.5	$16.5 \times (1, \dots, 2^6)$
0446 + 112	12-14-2004	0.54	0.29	–17	1.12	1.39	2.9	$8.8 \times (1, \dots, 2^6)$
0450 + 013	05-22-2003	0.80	0.31	–9	0.25	0.27	2.0	$5.3 \times (1, \dots, 2^5)$
0454 – 234	03-30-2007	0.73	0.29	–4	2.41	2.91	6.9	$20.6 \times (1, \dots, 2^6)$
0458 – 020	03-30-2007	0.75	0.28	–3	0.66	0.76	2.0	$6.0 \times (1, \dots, 2^6)$
0458 + 138	03-30-2007	0.95	0.43	12	0.22	0.26	2.3	$6.6 \times (1, \dots, 2^5)$
0459 + 135	03-30-2007	0.73	0.29	2	0.43	0.60	1.5	$4.6 \times (1, \dots, 2^6)$
0502 + 049	03-30-2007	0.72	0.31	–4	0.62	0.73	1.6	$4.8 \times (1, \dots, 2^7)$
0506 + 056	03-30-2007	0.78	0.31	–8	0.52	0.65	1.7	$5.1 \times (1, \dots, 2^6)$
0507 + 179	03-30-2007	0.68	0.30	–4	0.76	0.86	1.3	$4.0 \times (1, \dots, 2^7)$
0511 – 220	03-30-2007	0.77	0.29	–8	0.58	0.74	2.6	$7.9 \times (1, \dots, 2^6)$
0524 + 034	03-30-2007	0.73	0.30	–4	0.43	0.45	1.5	$4.6 \times (1, \dots, 2^6)$
0528 + 134	12-14-2004	0.60	0.29	–18	0.96	1.91	3.3	$9.8 \times (1, \dots, 2^6)$
0528 – 250	05-22-2003	2.18	0.31	–22	0.26	0.32	3.3	$10.0 \times (1, \dots, 2^4)$
0534 – 340	05-22-2003	1.19	0.29	–14	0.31	0.37	3.4	$10.2 \times (1, \dots, 2^4)$
0537 – 441	05-22-2003	0.71	0.25	–1	2.15	2.73	7.3	$21.8 \times (1, \dots, 2^6)$
0544 + 273	03-30-2007	0.63	0.33	–1	0.30	0.32	1.0	$3.1 \times (1, \dots, 2^6)$
0547 + 234	03-30-2007	0.64	0.32	–7	0.22	0.25	1.1	$3.2 \times (1, \dots, 2^6)$
0549 + 192	03-30-2007	0.79	0.34	–13	0.18	0.21	1.3	$3.8 \times (1, \dots, 2^5)$
0552 + 398	12-14-2004	0.74	0.57	–52	1.49	1.99	4.0	$12.0 \times (1, \dots, 2^6)$
0554 + 242	03-30-2007	0.89	0.55	–1	0.26	0.40	1.3	$3.9 \times (1, \dots, 2^6)$
0556 + 238	08-26-2005	1.07	0.33	–17	0.32	0.38	1.6	$4.9 \times (1, \dots, 2^6)$
0601 + 245	08-26-2005	1.74	0.45	–5	0.40	0.50	8.3	$24.8 \times (1, \dots, 2^4)$
0607 – 157	03-30-2007	1.04	0.35	–5	1.29	1.76	7.4	$22.1 \times (1, \dots, 2^5)$
0611 + 131	03-30-2007	0.70	0.30	–6	0.31	0.37	1.1	$3.2 \times (1, \dots, 2^6)$
0621 + 446	05-22-2003	0.85	0.28	–27	0.20	0.22	2.4	$7.2 \times (1, \dots, 2^4)$
0639 – 032	03-30-2007	0.83	0.36	–1	0.30	0.36	2.1	$6.0 \times (1, \dots, 2^5)$
0639 + 352	05-22-2003	1.66	0.28	–16	0.22	0.25	4.7	$14.1 \times (1, \dots, 2^3)$
0642 + 449	12-14-2004	0.68	0.38	36	1.57	2.44	3.9	$11.8 \times (1, \dots, 2^7)$
0646 – 306	09-13-2003	1.43	0.30	–21	0.38	0.47	2.8	$8.4 \times (1, \dots, 2^5)$
0648 – 165	03-30-2007	0.76	0.30	4	1.45	2.04	2.4	$7.2 \times (1, \dots, 2^7)$
0654 + 244	08-26-2005	0.93	0.27	0	0.26	0.31	3.9	$11.7 \times (1, \dots, 2^4)$
0707 + 476	03-30-2007	0.74	0.31	–25	0.43	0.52	1.7	$5.0 \times (1, \dots, 2^6)$
0716 + 477	03-30-2007	0.63	0.42	–4	0.31	0.41	1.2	$3.6 \times (1, \dots, 2^6)$
0721 – 071	03-30-2007	0.73	0.28	0	0.48	0.61	2.5	$7.4 \times (1, \dots, 2^6)$
0722 + 145	03-30-2007	0.73	0.32	–11	0.51	0.58	2.2	$6.5 \times (1, \dots, 2^6)$
0725 + 219	03-30-2007	0.81	0.31	–11	0.20	0.25	1.5	$4.5 \times (1, \dots, 2^5)$
0727 – 115	12-14-2004	0.73	0.28	1	2.23	3.32	12.0	$36.0 \times (1, \dots, 2^5)$
0735 + 178	03-30-2007	0.67	0.31	–10	0.36	0.61	1.6	$4.9 \times (1, \dots, 2^6)$
0736 + 017	03-30-2007	0.79	0.32	–7	1.78	2.08	3.1	$9.2 \times (1, \dots, 2^7)$
0743 – 006	12-14-2004	0.89	0.35	19	0.68	0.83	7.1	$21.4 \times (1, \dots, 2^4)$
0745 + 241	03-30-2007	0.70	0.28	–2	0.88	1.19	1.2	$3.6 \times (1, \dots, 2^7)$
0746 + 483	03-30-2007	0.54	0.33	–16	0.39	0.59	1.3	$3.8 \times (1, \dots, 2^6)$
0748 + 126	03-30-2007	0.72	0.28	–2	2.40	3.27	3.3	$10.0 \times (1, \dots, 2^7)$
0749 + 540	03-30-2007	0.56	0.30	–2	0.68	0.82	1.0	$3.1 \times (1, \dots, 2^7)$
0754 + 100	03-30-2007	0.72	0.28	–1	0.91	1.24	2.2	$6.6 \times (1, \dots, 2^7)$
0759 + 183	03-30-2007	0.97	0.34	–19	0.24	0.32	1.4	$4.1 \times (1, \dots, 2^5)$
0804 + 499	03-30-2007	0.54	0.32	–14	0.57	0.64	1.0	$3.0 \times (1, \dots, 2^7)$
0805 – 077	03-30-2007	0.84	0.31	–5	0.95	1.09	2.3	$6.9 \times (1, \dots, 2^7)$
0805 + 410	12-14-2004	0.54	0.41	18	0.59	0.66	1.4	$4.1 \times (1, \dots, 2^7)$
0808 + 019	03-30-2007	0.80	0.32	–7	0.51	0.55	1.7	$5.1 \times (1, \dots, 2^6)$
0812 + 367	03-30-2007	0.58	0.31	–7	0.33	0.48	1.2	$3.7 \times (1, \dots, 2^6)$
0814 + 425	12-14-2004	0.54	0.34	–20	0.38	0.48	2.0	$6.0 \times (1, \dots, 2^6)$
0820 + 560	12-14-2004	0.49	0.40	20	0.31	0.46	1.5	$4.4 \times (1, \dots, 2^6)$
0821 + 248	03-30-2007	0.71	0.29	–1	0.23	0.25	1.4	$4.2 \times (1, \dots, 2^5)$
0821 + 394	03-30-2007	0.64	0.29	4	0.82	1.01	1.4	$4.1 \times (1, \dots, 2^7)$
0823 + 033	12-14-2004	0.82	0.35	17	1.24	1.36	2.4	$7.3 \times (1, \dots, 2^7)$
0827 + 243	03-30-2007	0.70	0.29	3	0.53	0.62	1.3	$3.8 \times (1, \dots, 2^7)$
0834 – 201	03-30-2007	0.77	0.29	–4	0.97	1.52	3.3	$9.9 \times (1, \dots, 2^6)$
0834 + 250	03-30-2007	0.69	0.29	3	0.31	0.45	1.5	$4.2 \times (1, \dots, 2^6)$
0838 + 133	03-30-2007	0.70	0.29	–2	0.56	0.97	1.1	$3.2 \times (1, \dots, 2^7)$
0839 + 187	03-30-2007	1.59	0.58	–13	0.18	0.22	4.2	$12.5 \times (1, \dots, 2^3)$
0850 + 581	03-30-2007	0.73	0.36	–20	0.19	0.29	1.1	$3.4 \times (1, \dots, 2^5)$
0851 + 202	12-14-2004	0.71	0.36	22	2.07	2.44	11.0	$30.7 \times (1, \dots, 2^6)$
0906 + 163	03-30-2007	0.99	0.36	–28	0.21	0.23	2.2	$6.7 \times (1, \dots, 2^4)$
0912 + 029	03-30-2007	0.77	0.30	–6	0.82	1.06	2.3	$6.9 \times (1, \dots, 2^6)$

TABLE 2 — *Continued*

Source	Observation Session	Beam ^a			Flux Density			Contour Levels ^d (mJy bm ⁻¹)
		<i>a</i> (mas)	<i>b</i> (mas)	ϕ (°)	S_{peak} (Jy bm ⁻¹)	S_{total} ^b (Jy)	S_{rms} ^c (mJy bm ⁻¹)	
0917 + 624	12-14-2004	0.44	0.38	66	0.49	0.58	1.3	$4.0 \times (1, \dots, 2^6)$
0923 + 392	12-14-2004	0.62	0.29	-5	1.71	6.25	4.5	$13.4 \times (1, \dots, 2^6)$
0945 + 408	03-30-2007	0.72	0.30	-14	1.02	1.32	1.7	$5.2 \times (1, \dots, 2^7)$
0953 + 254	03-30-2007	0.69	0.28	-13	0.72	1.00	1.8	$5.5 \times (1, \dots, 2^7)$
0955 + 326	03-30-2007	0.66	0.31	-7	0.50	0.70	1.5	$4.5 \times (1, \dots, 2^6)$
0955 + 476	05-22-2003	0.84	0.30	-32	0.81	1.10	1.8	$5.3 \times (1, \dots, 2^7)$
1005 + 066	03-30-2007	0.76	0.30	-8	0.61	0.66	2.3	$6.8 \times (1, \dots, 2^6)$
1012 + 232	03-30-2007	0.86	0.28	-27	0.46	0.72	2.5	$7.6 \times (1, \dots, 2^5)$
1016 - 311	03-30-2007	0.92	0.32	-9	0.41	0.51	3.5	$10.6 \times (1, \dots, 2^5)$
1020 + 400	03-30-2007	0.71	0.29	-8	0.39	0.51	1.2	$3.5 \times (1, \dots, 2^6)$
1022 + 194	03-30-2007	0.85	0.34	-22	0.25	0.33	1.5	$4.6 \times (1, \dots, 2^5)$
1022 + 237	05-22-2003	1.71	0.96	-48	0.29	0.32	2.3	$6.4 \times (1, \dots, 2^5)$
1032 - 199	03-30-2007	0.73	0.27	3	0.58	1.14	4.5	$13.4 \times (1, \dots, 2^5)$
1034 - 293	03-30-2007	0.77	0.28	-2	1.66	2.10	5.1	$15.4 \times (1, \dots, 2^6)$
1039 + 811	03-30-2007	0.42	0.38	35	0.48	0.81	1.7	$5.2 \times (1, \dots, 2^6)$
1045 - 188	03-30-2007	0.75	0.28	-4	0.84	1.10	2.4	$7.2 \times (1, \dots, 2^6)$
1048 - 313	05-22-2003	3.22	0.31	-18	0.36	0.47	2.7	$8.2 \times (1, \dots, 2^5)$
1049 + 215	03-30-2007	0.76	0.29	-9	0.37	0.49	3.2	$9.6 \times (1, \dots, 2^5)$
1053 + 815	03-30-2007	0.41	0.37	-28	0.79	0.86	0.8	$2.3 \times (1, \dots, 2^8)$
1055 + 018	03-30-2007	0.72	0.30	-3	4.54	6.23	6.6	$19.9 \times (1, \dots, 2^7)$
1101 + 384	03-30-2007	0.68	0.30	-4	0.34	0.39	1.4	$4.3 \times (1, \dots, 2^6)$
1113 + 087	03-30-2007	1.07	0.42	-21	0.25	0.34	2.5	$7.5 \times (1, \dots, 2^5)$
1124 - 186	03-30-2007	0.76	0.28	-1	1.20	1.35	2.7	$8.0 \times (1, \dots, 2^7)$
1128 + 385	03-30-2007	0.75	0.28	-2	0.86	1.05	1.5	$4.4 \times (1, \dots, 2^7)$
1142 + 052	03-30-2007	1.00	0.36	-18	0.20	0.23	2.0	$6.1 \times (1, \dots, 2^5)$
1144 - 379	05-22-2003	0.77	0.31	-3	0.76	1.05	4.5	$13.5 \times (1, \dots, 2^5)$
1144 + 402	12-14-2004	0.66	0.35	25	0.95	1.04	1.9	$5.6 \times (1, \dots, 2^7)$
1147 + 245	03-30-2007	0.71	0.30	-10	0.38	0.63	2.5	$7.0 \times (1, \dots, 2^5)$
1150 + 497	03-30-2007	0.56	0.33	-2	0.89	1.26	1.8	$5.1 \times (1, \dots, 2^7)$
1150 + 812	03-30-2007	0.43	0.36	2	0.62	1.21	2.2	$6.5 \times (1, \dots, 2^6)$
1156 + 295	03-30-2007	0.67	0.33	-20	0.97	1.03	1.7	$5.2 \times (1, \dots, 2^7)$
1207 - 319	05-22-2003	2.67	0.30	-16	0.34	0.40	3.4	$10.3 \times (1, \dots, 2^5)$
1213 - 172	03-30-2007	0.74	0.29	-1	1.03	1.49	2.3	$7.0 \times (1, \dots, 2^7)$
1236 + 077	03-30-2007	0.73	0.29	-5	0.84	1.05	2.1	$6.2 \times (1, \dots, 2^7)$
1243 - 072	03-30-2007	0.74	0.30	-2	0.89	0.94	1.5	$4.5 \times (1, \dots, 2^7)$
1256 - 220	03-30-2007	0.81	0.30	-10	0.37	0.52	2.1	$6.4 \times (1, \dots, 2^5)$
1302 - 102	12-26-2002	0.81	0.27	-7	0.38	0.52	1.8	$5.1 \times (1, \dots, 2^6)$
1308 + 326	03-30-2007	0.66	0.30	9	0.79	0.98	2.0	$6.1 \times (1, \dots, 2^7)$
1308 + 554	03-30-2007	0.69	0.41	7	0.18	0.20	1.1	$3.3 \times (1, \dots, 2^5)$
1313 - 333	12-14-2004	0.36	0.19	-48	0.79	1.10	4.5	$13.5 \times (1, \dots, 2^5)$
1324 + 224	12-14-2004	0.70	0.33	15	0.92	1.10	1.4	$4.1 \times (1, \dots, 2^7)$
1334 - 127	12-14-2004	0.74	0.31	9	4.87	6.26	9.6	$28.8 \times (1, \dots, 2^7)$
1354 - 152	03-30-2007	0.74	0.28	-3	0.42	0.49	1.6	$4.9 \times (1, \dots, 2^6)$
1357 + 769	05-22-2003	0.73	0.28	12	0.58	0.66	1.9	$5.8 \times (1, \dots, 2^6)$
1406 - 076	05-22-2003	0.71	0.29	2	0.76	1.04	2.4	$7.2 \times (1, \dots, 2^6)$
1406 - 267	05-22-2003	3.95	0.50	28	0.59	0.64	3.7	$11.0 \times (1, \dots, 2^5)$
1418 + 546	03-30-2007	0.64	0.30	-4	0.63	0.98	1.6	$4.9 \times (1, \dots, 2^7)$
1435 - 218	03-30-2007	0.73	0.29	-6	0.75	0.88	2.2	$6.5 \times (1, \dots, 2^6)$
1437 - 153	03-30-2007	0.72	0.29	-2	0.42	0.46	2.0	$6.1 \times (1, \dots, 2^6)$
1451 - 375	05-22-2003	0.93	0.29	-9	0.51	0.61	5.3	$14.3 \times (1, \dots, 2^5)$
1459 + 480	03-30-2007	0.62	0.34	0	0.26	0.34	1.3	$3.9 \times (1, \dots, 2^6)$
1502 + 036	05-22-2003	0.76	0.28	-5	0.38	0.46	2.2	$6.0 \times (1, \dots, 2^6)$
1502 + 106	03-30-2007	0.72	0.30	-8	1.02	1.34	2.8	$8.3 \times (1, \dots, 2^6)$
1504 + 377	05-22-2003	0.84	0.37	-27	0.29	0.38	2.3	$7.0 \times (1, \dots, 2^5)$
1505 + 428	03-30-2007	0.58	0.33	0	0.35	0.49	1.1	$3.3 \times (1, \dots, 2^6)$
1511 - 100	12-14-2004	0.49	0.28	-21	0.94	1.24	2.3	$7.0 \times (1, \dots, 2^7)$
1514 + 004	03-30-2007	0.84	0.31	-8	0.62	0.86	2.1	$6.4 \times (1, \dots, 2^6)$
1514 + 197	03-30-2007	0.71	0.29	-2	0.62	0.71	1.7	$5.1 \times (1, \dots, 2^6)$
1514 - 241	03-30-2007	0.75	0.28	-1	1.61	2.74	5.1	$15.2 \times (1, \dots, 2^6)$
1519 - 273	03-30-2007	0.73	0.28	-2	1.02	1.24	2.6	$7.7 \times (1, \dots, 2^7)$
1520 + 437	05-22-2003	2.14	0.39	6	0.24	0.25	2.7	$8.1 \times (1, \dots, 2^4)$
1546 + 027	12-14-2004	0.73	0.31	-4	3.10	3.49	1.8	$5.5 \times (1, \dots, 2^9)$
1548 + 056	03-30-2007	0.77	0.34	-5	1.01	2.36	6.5	$19.6 \times (1, \dots, 2^5)$
1606 + 106	12-14-2004	0.52	0.26	-26	1.05	1.28	2.6	$7.7 \times (1, \dots, 2^7)$
1611 + 343	03-30-2007	0.70	0.28	9	2.02	2.91	4.4	$13.3 \times (1, \dots, 2^7)$
1617 + 229	03-30-2007	0.67	0.32	-4	0.32	0.55	1.2	$3.7 \times (1, \dots, 2^6)$
1622 - 253	03-30-2007	0.72	0.27	1	1.32	1.65	5.0	$15.1 \times (1, \dots, 2^6)$
1622 - 297	03-30-2007	0.75	0.27	-3	1.28	1.76	6.8	$20.5 \times (1, \dots, 2^5)$

TABLE 2 — *Continued*

Source	Observation Session	Beam ^a			Flux Density			Contour Levels ^d (mJy bm ⁻¹)
		<i>a</i> (mas)	<i>b</i> (mas)	ϕ (°)	S_{peak} (Jy bm ⁻¹)	$S_{\text{total}}^{\text{b}}$ (Jy)	$S_{\text{rms}}^{\text{c}}$ (mJy bm ⁻¹)	
1637 + 574	12-14-2004	0.73	0.35	32	0.72	0.96	1.2	$3.6 \times (1, \dots, 2^7)$
1638 + 398	12-14-2004	0.64	0.43	15	0.69	0.91	1.4	$3.9 \times (1, \dots, 2^7)$
1652 + 398	03-30-2007	0.57	0.33	6	0.44	0.71	1.3	$3.8 \times (1, \dots, 2^6)$
1656 - 075	03-30-2007	1.06	0.36	-11	0.26	0.37	1.8	$5.5 \times (1, \dots, 2^5)$
1657 - 261	03-30-2007	0.76	0.28	-6	0.42	0.50	2.0	$6.0 \times (1, \dots, 2^6)$
1705 + 018	03-30-2007	0.75	0.31	-5	0.58	0.66	1.6	$4.9 \times (1, \dots, 2^6)$
1710 - 269	03-30-2007	1.51	0.49	-16	0.41	0.81	7.6	$20.4 \times (1, \dots, 2^4)$
1717 + 178	03-30-2007	0.67	0.26	3	0.49	0.70	2.1	$6.2 \times (1, \dots, 2^6)$
1726 + 455	03-30-2007	0.50	0.34	11	0.37	0.38	1.3	$4.0 \times (1, \dots, 2^6)$
1730 - 130	03-30-2007	0.73	0.29	-1	1.40	2.31	3.0	$9.0 \times (1, \dots, 2^7)$
1732 + 389	12-14-2004	0.74	0.30	12	0.87	1.11	1.1	$3.2 \times (1, \dots, 2^8)$
1738 + 476	03-30-2007	0.54	0.34	6	0.40	0.58	1.6	$4.9 \times (1, \dots, 2^6)$
1741 - 038	12-14-2004	0.76	0.33	2	3.70	5.60	3.1	$9.2 \times (1, \dots, 2^8)$
1741 - 312	03-30-2007	4.51	1.13	17	0.56	0.66	6.9	$20.8 \times (1, \dots, 2^4)$
1742 - 078	03-30-2007	0.73	0.28	-3	0.50	0.66	1.8	$5.4 \times (1, \dots, 2^6)$
1749 + 096	12-14-2004	0.58	0.26	-31	2.77	3.37	10.0	$29.9 \times (1, \dots, 2^6)$
1749 + 701	03-30-2007	0.80	0.47	89	0.24	0.35	1.8	$5.4 \times (1, \dots, 2^5)$
1751 + 288	03-30-2007	0.70	0.28	13	1.68	1.97	3.4	$10.2 \times (1, \dots, 2^7)$
1754 + 155	03-30-2007	0.72	0.29	6	0.39	0.44	1.1	$3.3 \times (1, \dots, 2^6)$
1800 + 440	03-30-2007	0.54	0.33	6	1.52	1.72	2.0	$6.1 \times (1, \dots, 2^7)$
1803 + 784	12-14-2004	0.53	0.41	82	0.89	1.22	1.2	$3.6 \times (1, \dots, 2^7)$
1817 - 254	03-30-2007	0.76	0.28	-1	0.49	0.67	2.5	$7.6 \times (1, \dots, 2^6)$
1817 + 387	03-30-2007	0.65	0.35	11	0.20	0.22	1.2	$3.7 \times (1, \dots, 2^5)$
1829 - 106	03-30-2007	1.67	0.97	17	0.37	0.62	6.8	$20.3 \times (1, \dots, 2^4)$
1829 - 207	03-30-2007	2.07	0.58	-1	0.33	0.41	4.5	$12.2 \times (1, \dots, 2^4)$
1830 - 211	03-30-2007	2.96	0.97	-3	2.82	3.11	33.6	$90.8 \times (1, \dots, 2^4)$
1849 + 670	12-14-2004	0.54	0.35	28	0.41	0.45	1.1	$3.4 \times (1, \dots, 2^6)$
1901 + 319	12-14-2004	0.69	0.33	5	0.31	0.65	1.5	$4.6 \times (1, \dots, 2^6)$
1921 - 293	03-30-2007	0.74	0.29	-5	7.10	9.43	8.0	$24.1 \times (1, \dots, 2^8)$
1928 + 154	03-30-2007	0.70	0.29	1	0.32	0.36	1.6	$4.7 \times (1, \dots, 2^6)$
1936 - 155	02-15-2004	0.73	0.28	-2	0.51	0.58	1.4	$4.2 \times (1, \dots, 2^6)$
1946 - 200	05-22-2003	2.44	0.52	26	0.38	0.36	4.5	$13.5 \times (1, \dots, 2^4)$
1954 - 388	05-22-2003	0.68	0.25	-1	1.70	2.21	5.2	$16.5 \times (1, \dots, 2^6)$
1958 - 179	05-22-2003	0.71	0.27	-2	1.28	1.54	3.1	$8.5 \times (1, \dots, 2^7)$
2000 + 472	03-30-2007	0.53	0.33	14	0.36	0.52	1.3	$3.9 \times (1, \dots, 2^6)$
2008 - 159	03-30-2007	0.73	0.29	-2	1.85	2.34	2.3	$7.0 \times (1, \dots, 2^8)$
2013 + 163	03-30-2007	0.70	0.32	-3	0.46	0.51	1.0	$2.9 \times (1, \dots, 2^7)$
2021 + 317	12-14-2004	0.75	0.39	22	0.39	0.59	1.8	$5.5 \times (1, \dots, 2^6)$
2029 + 121	05-22-2003	2.81	1.43	15	0.33	0.38	3.0	$9.0 \times (1, \dots, 2^5)$
2037 + 511	03-30-2007	0.64	0.30	9	2.60	2.98	3.9	$11.7 \times (1, \dots, 2^7)$
2048 + 312	03-30-2007	0.80	0.33	19	0.22	0.29	1.5	$4.5 \times (1, \dots, 2^5)$
2054 - 377	05-22-2003	1.32	0.31	-23	0.43	0.50	4.4	$11.5 \times (1, \dots, 2^5)$
2106 - 413	05-22-2003	9.82	1.24	3	0.88	0.82	4.5	$14.0 \times (1, \dots, 2^5)$
2113 + 293	03-30-2007	0.74	0.31	11	0.64	0.79	1.6	$4.8 \times (1, \dots, 2^7)$
2121 + 053	12-14-2004	0.72	0.29	-2	1.61	2.60	1.9	$5.6 \times (1, \dots, 2^8)$
2126 - 158	03-30-2007	0.75	0.29	-3	0.62	0.84	1.6	$4.7 \times (1, \dots, 2^7)$
2128 - 123	03-30-2007	0.74	0.29	-4	0.53	1.88	4.1	$12.2 \times (1, \dots, 2^5)$
2131 - 021	12-14-2004	0.79	0.36	-1	1.35	2.23	2.6	$7.8 \times (1, \dots, 2^7)$
2136 + 141	03-30-2007	0.73	0.31	3	0.74	1.55	3.3	$10.0 \times (1, \dots, 2^6)$
2143 - 156	03-30-2007	0.79	0.30	-7	0.40	0.43	1.1	$3.3 \times (1, \dots, 2^6)$
2145 + 067	12-14-2004	0.83	0.37	17	6.03	8.64	9.9	$29.8 \times (1, \dots, 2^7)$
2150 + 173	03-30-2007	0.74	0.32	8	0.31	0.60	1.4	$4.1 \times (1, \dots, 2^6)$
2200 + 420	12-14-2004	0.63	0.34	17	3.37	3.98	2.9	$8.8 \times (1, \dots, 2^8)$
2201 + 171	03-30-2007	0.72	0.30	6	0.97	1.22	1.6	$4.8 \times (1, \dots, 2^7)$
2209 + 236	03-30-2007	0.73	0.31	13	0.66	0.82	1.8	$5.5 \times (1, \dots, 2^6)$
2214 + 350	03-30-2007	0.98	0.45	12	0.25	0.29	1.5	$4.4 \times (1, \dots, 2^5)$
2227 - 088	03-30-2007	0.86	0.31	-9	2.24	2.36	2.2	$6.6 \times (1, \dots, 2^8)$
2239 + 096	03-30-2007	0.72	0.34	-2	0.58	0.67	1.3	$3.9 \times (1, \dots, 2^7)$
2251 + 158	03-30-2007	0.73	0.31	8	2.15	4.30	7.0	$19.5 \times (1, \dots, 2^6)$
2254 + 024	03-30-2007	0.84	0.34	-10	0.37	0.39	1.2	$3.6 \times (1, \dots, 2^6)$
2255 - 282	03-30-2007	0.92	0.30	-7	1.58	1.82	3.6	$10.2 \times (1, \dots, 2^7)$
2306 + 095	05-22-2003	1.45	0.33	-19	0.26	0.27	3.3	$9.8 \times (1, \dots, 2^4)$
2309 + 454	03-30-2007	0.81	0.38	5	0.19	0.26	1.1	$3.3 \times (1, \dots, 2^5)$
2318 + 049	12-14-2004	0.89	0.42	-8	0.45	0.57	1.5	$4.4 \times (1, \dots, 2^6)$
2325 + 093	03-30-2007	0.71	0.32	-3	1.33	1.36	1.3	$3.8 \times (1, \dots, 2^8)$
2335 - 027	03-30-2007	0.90	0.32	-10	0.57	0.74	1.4	$4.3 \times (1, \dots, 2^7)$
2344 + 092	03-30-2007	0.74	0.31	2	0.56	0.88	1.5	$4.4 \times (1, \dots, 2^6)$
2346 + 385	03-30-2007	0.77	0.33	25	0.37	0.55	1.5	$4.6 \times (1, \dots, 2^6)$

TABLE 2 — *Continued*

Source	Observation Session	Beam ^a			Flux Density			Contour Levels ^d (mJy bm ⁻¹)
		<i>a</i> (mas)	<i>b</i> (mas)	ϕ (°)	S_{peak} (Jy bm ⁻¹)	S_{total} ^b (Jy)	S_{rms} ^c (mJy bm ⁻¹)	
2353 + 816	03-30-2007	0.43	0.34	61	0.84	0.90	1.3	$4.0 \times (1, \dots, 2^7)$
2355 – 106	03-30-2007	0.83	0.31	–7	0.58	0.75	1.5	$4.6 \times (1, \dots, 2^6)$
2357 – 318	03-30-2007	1.35	0.35	–18	0.50	0.62	4.1	$12.3 \times (1, \dots, 2^5)$

^a The restoring beam is an elliptical Gaussian with FWHM major axis *a* and minor axis *b*, with major axis in position angle ϕ (measured north through east).

^b The total image flux defined by the sum of the CLEAN components. In some cases this may be slightly less than the peak flux density due to the presence of components with negative amplitude in the CLEAN model.

^c The root mean square (rms) of the residuals of the final hybrid image.

^d Contours levels are represented by the geometric series $1, \dots, 2^n$, e.g. for $n = 5$ the contour levels would be $\pm 1, 2, 4, 8, 16, 32$.

TABLE 3
PARAMETERS OF NATURALLY WEIGHTED IMAGES AT 43 GHz

Source	Observation Epoch	Beam ^a			Flux Density			Contour Levels ^d (mJy bm ⁻¹)
		<i>a</i> (mas)	<i>b</i> (mas)	ϕ (°)	S_{peak} (Jy bm ⁻¹)	$S_{\text{total}}^{\text{b}}$ (Jy)	$S_{\text{rms}}^{\text{c}}$ (mJy bm ⁻¹)	
0007 + 106	09-13-2003	0.38	0.19	0	3.54	3.66	5.6	$16.8 \times (1, \dots, 2^7)$
0009 + 081	09-13-2003	0.54	0.25	-17	0.72	0.92	4.3	$12.9 \times (1, \dots, 2^5)$
0016 + 731	08-25-2002	0.25	0.21	27	0.61	0.77	2.6	$7.7 \times (1, \dots, 2^6)$
0017 + 200	09-13-2003	0.40	0.20	-3	0.95	1.13	4.6	$13.8 \times (1, \dots, 2^6)$
0046 + 316	09-13-2003	0.61	0.36	4	0.74	0.80	4.3	$11.9 \times (1, \dots, 2^5)$
0048 - 097	09-13-2003	0.44	0.17	7	1.13	1.14	7.4	$22.2 \times (1, \dots, 2^5)$
0059 + 581	09-13-2003	0.40	0.16	33	2.89	4.09	8.7	$26.2 \times (1, \dots, 2^6)$
0119 + 115	09-13-2003	0.61	0.25	23	1.23	1.45	4.5	$13.4 \times (1, \dots, 2^6)$
0122 - 003	09-13-2003	0.47	0.21	-5	0.74	1.03	6.0	$17.9 \times (1, \dots, 2^5)$
0133 + 476	08-25-2002	0.39	0.17	19	2.84	3.39	3.3	$10.0 \times (1, \dots, 2^8)$
0138 - 097	09-13-2003	1.90	0.27	34	0.69	0.64	4.2	$12.6 \times (1, \dots, 2^5)$
0149 + 218	09-13-2003	0.40	0.19	21	1.65	1.91	8.6	$25.7 \times (1, \dots, 2^5)$
0202 + 149	09-13-2003	1.52	0.37	-11	0.94	1.01	4.3	$13.9 \times (1, \dots, 2^6)$
0212 + 735	08-25-2002	0.47	0.36	53	0.37	0.81	4.2	$12.5 \times (1, \dots, 2^4)$
0224 + 671	09-13-2003	0.46	0.16	8	0.97	1.26	6.7	$18.1 \times (1, \dots, 2^5)$
0229 + 131	09-13-2003	0.55	0.30	13	0.79	0.95	6.0	$17.3 \times (1, \dots, 2^5)$
0234 + 285	09-13-2003	0.36	0.17	-5	1.59	2.62	14.2	$42.5 \times (1, \dots, 2^5)$
0235 + 164	08-25-2002	0.40	0.17	2	0.85	1.23	2.6	$7.9 \times (1, \dots, 2^6)$
0237 - 027	12-26-2002	0.84	0.16	-16	0.38	0.43	2.0	$5.7 \times (1, \dots, 2^6)$
0237 + 040	12-26-2002	0.46	0.16	-7	0.46	0.52	2.3	$6.8 \times (1, \dots, 2^6)$
0239 + 108	09-13-2003	0.42	0.18	-9	0.78	0.90	6.5	$19.5 \times (1, \dots, 2^5)$
0241 + 622	09-13-2003	0.27	0.21	-57	1.01	1.12	5.2	$15.6 \times (1, \dots, 2^6)$
0300 + 470	09-13-2003	0.43	0.18	8	0.90	1.20	5.4	$16.3 \times (1, \dots, 2^5)$
0306 + 102	09-13-2003	0.38	0.16	5	1.66	1.82	7.6	$22.8 \times (1, \dots, 2^6)$
0333 + 321	09-13-2003	0.38	0.17	8	2.26	3.23	7.3	$21.9 \times (1, \dots, 2^6)$
0336 - 019	09-13-2003	0.43	0.16	-6	1.56	2.55	7.0	$21.0 \times (1, \dots, 2^6)$
0340 + 362	09-13-2003	0.46	0.16	0	0.46	0.41	5.2	$15.6 \times (1, \dots, 2^4)$
0345 + 460	09-13-2003	0.84	0.26	-25	0.49	0.58	4.5	$13.6 \times (1, \dots, 2^5)$
0346 - 279	09-13-2003	0.55	0.16	-15	0.71	0.72	8.2	$24.7 \times (1, \dots, 2^4)$
0350 + 465	09-13-2003	0.30	0.19	13	0.80	0.80	5.1	$15.2 \times (1, \dots, 2^5)$
0358 + 040	09-13-2003	0.41	0.18	-1	1.11	1.09	3.6	$10.8 \times (1, \dots, 2^6)$
0400 + 258	09-13-2003	0.47	0.19	-14	0.81	1.01	5.2	$15.6 \times (1, \dots, 2^5)$
0446 + 112	08-25-2002	0.40	0.16	1	1.10	1.47	2.1	$6.2 \times (1, \dots, 2^7)$
0454 - 234	09-13-2003	0.40	0.16	-4	1.43	2.09	9.6	$28.9 \times (1, \dots, 2^5)$
0458 - 020	09-13-2003	0.43	0.17	-5	1.42	1.59	5.4	$16.1 \times (1, \dots, 2^6)$
0506 + 056	09-13-2003	0.46	0.19	-3	0.58	0.49	6.9	$20.6 \times (1, \dots, 2^4)$
0524 + 034	09-13-2003	0.42	0.17	-2	0.99	1.16	5.0	$14.0 \times (1, \dots, 2^6)$
0528 + 134	08-25-2002	0.38	0.19	1	0.79	1.51	3.2	$9.6 \times (1, \dots, 2^6)$
0552 + 398	08-25-2002	0.43	0.18	23	0.90	1.47	3.8	$11.3 \times (1, \dots, 2^6)$
0556 + 238	09-13-2003	0.50	0.26	-12	0.43	0.39	6.0	$18.1 \times (1, \dots, 2^4)$
0607 - 157	08-25-2002	0.41	0.17	-2	1.82	2.70	5.0	$15.0 \times (1, \dots, 2^6)$
0642 + 449	08-25-2002	0.29	0.19	1	0.97	1.83	3.0	$9.0 \times (1, \dots, 2^6)$
0646 - 306	09-13-2003	0.49	0.18	-15	0.64	0.75	10.1	$30.2 \times (1, \dots, 2^4)$
0648 - 165	09-13-2003	0.47	0.18	4	2.09	2.73	11.6	$34.8 \times (1, \dots, 2^5)$
0707 + 476	12-26-2002	0.91	0.18	-17	0.25	0.26	0.5	$1.7 \times (1, \dots, 2^7)$
0722 + 145	12-26-2002	0.45	0.18	-7	0.48	0.60	1.7	$5.0 \times (1, \dots, 2^6)$
0727 - 115	09-13-2003	0.54	0.18	-11	2.22	3.01	12.3	$37.0 \times (1, \dots, 2^5)$
0735 + 178	09-13-2003	0.50	0.20	-15	0.71	1.05	3.8	$11.5 \times (1, \dots, 2^5)$
0743 - 006	08-25-2002	0.45	0.20	-3	0.32	0.59	2.9	$8.6 \times (1, \dots, 2^5)$
0745 + 241	09-13-2003	0.44	0.21	-21	0.79	0.97	5.0	$15.0 \times (1, \dots, 2^5)$
0746 + 483	09-13-2003	0.51	0.23	-19	0.55	0.60	4.3	$12.9 \times (1, \dots, 2^5)$
0748 + 126	08-25-2002	0.39	0.18	-2	1.26	1.67	2.7	$8.2 \times (1, \dots, 2^7)$
0749 + 540	09-13-2003	0.34	0.22	-20	0.69	0.83	3.1	$9.4 \times (1, \dots, 2^6)$
0754 + 100	09-13-2003	0.41	0.17	-4	1.71	2.22	4.7	$14.0 \times (1, \dots, 2^6)$
0804 + 499	09-13-2003	0.30	0.20	-20	0.78	0.80	3.0	$9.1 \times (1, \dots, 2^6)$
0805 + 410	08-25-2002	0.42	0.19	23	0.38	0.45	2.2	$6.3 \times (1, \dots, 2^5)$
0808 + 019	09-13-2003	0.50	0.22	-8	0.69	0.70	3.5	$10.4 \times (1, \dots, 2^6)$
0814 + 425	08-25-2002	0.31	0.20	-7	0.36	0.39	2.6	$7.8 \times (1, \dots, 2^5)$
0820 + 560	08-25-2002	0.25	0.22	66	0.44	0.56	3.0	$9.0 \times (1, \dots, 2^5)$
0823 + 033	08-25-2002	0.41	0.18	-5	1.08	1.17	2.4	$7.1 \times (1, \dots, 2^7)$
0838 + 133	09-13-2003	0.42	0.19	-2	1.30	2.22	5.2	$15.7 \times (1, \dots, 2^6)$
0851 + 202	08-25-2002	0.36	0.18	-7	2.33	2.90	3.8	$11.3 \times (1, \dots, 2^7)$
0917 + 624	08-25-2002	1.24	0.58	-70	0.34	0.39	2.1	$6.4 \times (1, \dots, 2^5)$
0923 + 392	08-25-2002	0.32	0.18	3	0.83	3.90	4.1	$12.2 \times (1, \dots, 2^6)$
0953 + 254	09-13-2003	0.36	0.18	-6	1.32	1.47	3.7	$11.0 \times (1, \dots, 2^6)$
0955 + 476	12-26-2002	0.31	0.22	-19	0.50	0.80	4.0	$11.9 \times (1, \dots, 2^5)$
1034 - 293	09-13-2003	0.90	0.18	-24	1.18	1.29	9.9	$29.6 \times (1, \dots, 2^5)$

TABLE 3 — *Continued*

Source	Observation Epoch	Beam ^a			Flux Density			Contour Levels ^d (mJy bm ⁻¹)
		<i>a</i> (mas)	<i>b</i> (mas)	ϕ (°)	S_{peak} (Jy bm ⁻¹)	$S_{\text{total}}^{\text{b}}$ (Jy)	$S_{\text{rms}}^{\text{c}}$ (mJy bm ⁻¹)	
1039 + 811	12-26-2002	0.57	0.18	75	0.45	0.48	3.4	$9.1 \times (1, \dots, 2^5)$
1045 - 188	09-13-2003	0.82	0.19	-18	0.82	1.02	4.2	$12.7 \times (1, \dots, 2^6)$
1049 + 215	12-26-2002	0.46	0.18	-15	0.37	0.42	2.2	$6.6 \times (1, \dots, 2^5)$
1053 + 815	09-13-2003	0.23	0.21	-33	1.43	1.55	2.2	$6.7 \times (1, \dots, 2^7)$
1055 + 018	12-26-2002	0.47	0.17	-7	1.54	2.37	4.1	$11.5 \times (1, \dots, 2^7)$
1124 - 186	09-13-2003	0.40	0.15	-1	1.47	1.76	5.5	$16.6 \times (1, \dots, 2^6)$
1128 + 385	12-26-2002	0.32	0.17	-8	0.65	0.91	2.7	$8.0 \times (1, \dots, 2^6)$
1144 + 402	08-25-2002	0.54	0.21	-25	0.33	0.39	2.3	$6.8 \times (1, \dots, 2^5)$
1156 + 295	12-26-2002	0.38	0.17	-7	1.18	1.43	3.2	$9.6 \times (1, \dots, 2^6)$
1236 + 077	12-26-2002	0.80	0.20	-16	0.39	0.46	2.5	$7.4 \times (1, \dots, 2^5)$
1243 - 072	12-26-2002	0.55	0.16	-11	0.41	0.47	1.7	$5.2 \times (1, \dots, 2^6)$
1256 - 220	09-13-2003	0.50	0.18	-7	1.05	1.00	7.1	$21.2 \times (1, \dots, 2^5)$
1302 - 102	12-26-2002	0.51	0.16	-8	0.44	0.52	2.1	$6.3 \times (1, \dots, 2^6)$
1308 + 326	09-13-2003	0.37	0.17	4	2.94	3.82	5.6	$16.8 \times (1, \dots, 2^7)$
1313 - 333	08-25-2002	0.52	0.20	-5	0.64	0.79	4.0	$12.0 \times (1, \dots, 2^5)$
1324 + 224	08-25-2002	0.34	0.18	-3	0.39	0.48	1.9	$5.8 \times (1, \dots, 2^6)$
1334 - 127	08-25-2002	0.46	0.17	-6	3.87	5.05	4.4	$13.2 \times (1, \dots, 2^8)$
1354 - 152	12-26-2002	0.54	0.16	-11	0.54	0.68	2.3	$6.4 \times (1, \dots, 2^6)$
1357 + 769	12-26-2002	0.34	0.16	-70	0.63	0.67	3.5	$10.5 \times (1, \dots, 2^5)$
1406 - 076	12-26-2002	0.45	0.16	-6	0.74	0.97	2.2	$6.6 \times (1, \dots, 2^6)$
1502 + 036	12-26-2002	0.48	0.17	-10	0.39	0.43	1.7	$5.1 \times (1, \dots, 2^6)$
1502 + 106	09-13-2003	0.40	0.16	1	1.27	2.30	3.8	$11.3 \times (1, \dots, 2^6)$
1505 + 428	09-13-2003	0.40	0.24	12	0.70	0.90	2.7	$8.2 \times (1, \dots, 2^6)$
1511 - 100	12-26-2002	0.47	0.16	-8	0.51	0.61	2.6	$7.4 \times (1, \dots, 2^6)$
1514 + 004	09-13-2003	0.49	0.17	-7	0.86	1.17	3.6	$10.8 \times (1, \dots, 2^6)$
1546 + 027	08-25-2002	0.41	0.16	-2	0.95	1.32	3.6	$10.8 \times (1, \dots, 2^6)$
1606 + 106	08-25-2002	0.41	0.17	-7	0.76	1.36	2.7	$8.1 \times (1, \dots, 2^6)$
1611 + 343	12-26-2002	0.39	0.21	-2	1.09	1.37	9.4	$26.4 \times (1, \dots, 2^5)$
1617 + 229	09-13-2003	1.18	0.45	1	0.61	0.68	3.2	$9.6 \times (1, \dots, 2^5)$
1637 + 574	08-25-2002	0.30	0.19	15	0.81	1.37	3.4	$10.3 \times (1, \dots, 2^6)$
1638 + 398	08-25-2002	0.35	0.20	-6	0.43	0.57	2.8	$8.3 \times (1, \dots, 2^5)$
1705 + 018	12-26-2002	0.50	0.17	-6	0.41	0.41	2.3	$6.3 \times (1, \dots, 2^6)$
1717 + 178	12-26-2002	0.42	0.16	-2	0.37	0.45	2.5	$6.9 \times (1, \dots, 2^5)$
1726 + 455	09-13-2003	0.31	0.17	15	1.67	1.78	2.8	$8.4 \times (1, \dots, 2^7)$
1730 - 130	09-13-2003	0.43	0.17	-1	3.89	5.59	11.7	$35.0 \times (1, \dots, 2^6)$
1732 + 389	08-25-2002	0.33	0.18	-6	0.47	0.68	2.5	$7.6 \times (1, \dots, 2^5)$
1738 + 476	12-26-2002	0.46	0.16	3	0.34	0.39	2.1	$6.4 \times (1, \dots, 2^5)$
1741 - 038	09-13-2003	0.41	0.16	0	5.51	8.49	18.9	$56.6 \times (1, \dots, 2^6)$
1742 - 078	09-13-2003	0.43	0.17	0	0.82	1.03	4.0	$11.9 \times (1, \dots, 2^6)$
1749 + 096	08-25-2002	0.41	0.17	-4	2.92	3.25	3.2	$9.6 \times (1, \dots, 2^8)$
1751 + 288	12-26-2002	0.37	0.16	-11	1.35	1.50	4.7	$14.2 \times (1, \dots, 2^6)$
1803 + 784	08-25-2002	0.23	0.21	-8	1.03	1.52	3.0	$9.0 \times (1, \dots, 2^6)$
1849 + 670	08-25-2002	0.26	0.20	10	1.05	1.32	2.9	$8.7 \times (1, \dots, 2^6)$
1901 + 319	09-13-2003	0.42	0.23	-22	0.88	1.01	4.6	$13.0 \times (1, \dots, 2^6)$
1921 - 293	09-13-2003	0.41	0.15	-7	14.04	18.40	33.2	$96.2 \times (1, \dots, 2^7)$
1936 - 155	09-13-2003	0.68	0.20	-9	0.86	0.81	10.3	$30.8 \times (1, \dots, 2^4)$
1958 - 179	12-26-2002	0.42	0.15	-4	0.87	0.94	2.7	$8.1 \times (1, \dots, 2^6)$
2008 - 159	09-13-2003	0.49	0.18	6	1.75	2.26	5.7	$17.0 \times (1, \dots, 2^6)$
2021 + 317	09-13-2003	0.42	0.21	15	0.71	0.67	7.1	$21.4 \times (1, \dots, 2^5)$
2037 + 511	12-26-2002	0.40	0.17	-22	0.76	1.08	3.7	$10.8 \times (1, \dots, 2^6)$
2113 + 293	12-26-2002	0.75	0.17	-23	0.28	0.31	2.2	$6.5 \times (1, \dots, 2^5)$
2121 + 053	08-25-2002	0.42	0.18	-5	1.44	1.72	3.3	$9.8 \times (1, \dots, 2^7)$
2126 - 158	12-26-2002	1.24	0.41	-4	0.42	0.50	5.6	$15.6 \times (1, \dots, 2^4)$
2131 - 021	08-25-2002	0.43	0.17	-5	0.59	1.16	3.4	$10.1 \times (1, \dots, 2^5)$
2136 + 141	09-13-2003	0.59	0.20	-16	1.16	1.82	4.6	$13.9 \times (1, \dots, 2^6)$
2145 + 067	08-25-2002	0.42	0.18	-5	3.65	6.48	7.8	$23.5 \times (1, \dots, 2^7)$
2150 + 173	12-26-2002	0.66	0.18	-19	0.35	0.43	2.1	$6.2 \times (1, \dots, 2^5)$
2200 + 420	09-13-2003	0.27	0.19	13	3.27	4.40	11.2	$33.7 \times (1, \dots, 2^6)$
2227 - 088	09-13-2003	0.40	0.15	0	5.11	5.27	11.4	$34.1 \times (1, \dots, 2^7)$
2239 + 096	09-13-2003	0.88	0.24	-14	0.52	0.61	4.1	$11.9 \times (1, \dots, 2^5)$
2255 - 282	09-13-2003	0.41	0.15	-3	2.77	4.59	14.8	$42.9 \times (1, \dots, 2^6)$
2309 + 454	09-13-2003	0.72	0.27	-17	0.51	0.60	4.9	$12.3 \times (1, \dots, 2^5)$
2318 + 049	08-25-2002	0.42	0.18	-4	0.58	0.71	2.9	$8.7 \times (1, \dots, 2^6)$
2325 + 093	09-13-2003	0.38	0.17	-2	1.54	1.66	5.6	$16.4 \times (1, \dots, 2^6)$
2353 + 816	09-13-2003	0.46	0.26	62	0.96	0.93	4.0	$12.0 \times (1, \dots, 2^6)$

TABLE 3 — *Continued*

Source	Observation Epoch	Beam ^a			Flux Density			Contour Levels ^d (mJy bm ⁻¹)
		<i>a</i> (mas)	<i>b</i> (mas)	ϕ (°)	S_{peak} (Jy bm ⁻¹)	S_{total} ^b (Jy)	S_{rms} ^c (mJy bm ⁻¹)	

^a The restoring beam is an elliptical Gaussian with FWHM major axis *a* and minor axis *b*, with major axis in position angle ϕ (measured north through east).

^b The total image flux defined by the sum of the CLEAN components. In some cases this may be slightly less than the peak flux density due to the presence of components with negative amplitude in the CLEAN model.

^c The root mean square (rms) of the residuals of the final hybrid image.

^d Contours levels are represented by the geometric series 1, ..., 2^n , e.g. for $n = 5$ the contour levels would be $\pm 1, 2, 4, 8, 16, 32$.

TABLE 4
 SOURCE STRUCTURE INDICES.

Source	X band (8.4 GHz)			K band (24 GHz)			Q band (43 GHz)		
	N_{session}	SI_{min}	SI_{max}	N_{session}	SI_{min}	SI_{max}	N_{session}	SI_{min}	SI_{max}
0006+061	1	1	1
0007+106	1	1	1	6	1	2	1	1	1
0009+081	1	1	1	6	1	2	1	1	1
0016+731	1	1	1	4	1	2	2	1	1
0017+200	1	2	2	6	1	2	1	1	1
0019+058	3	1	1
0038-020	1	1	1
0046+316	1	2	2	6	1	2	1	1	1
0048-097	1	1	1	6	1	1	3	1	1
0054+161	1	1	1
0059+581	6	1	1	4	1	2
0104-408	1	1	1
0109+224	1	2	2	4	1	1
0110+495	3	1	2
0111+021	3	2	2
0119+041	3	2	2
0119+115	3	1	3	2	1	2
0119+247	3	2	2
0122-003	4	2	3	1	2	2
0123+257	1	2	2	4	1	1
0127+084	2	1	1
0133+476	1	1	1	5	1	1	2	1	1
0138-097	1	3	3	3	1	2	1	2	2
0149+218	2	2	2	10	1	2	4	1	1
0202+149	1	3	3	6	2	3	2	1	2
0202+319	1	1	1	3	1	1
0212+735	2	2	2	8	2	3	2	2	3
0213-026	3	2	2
0220-349	1	3	3
0221+067	2	2	2	6	1	2
0222+185	1	1	1
0224+671	1	3	3	6	1	3	3	2	2
0229+131	3	1	3	2	1	1
0234+285	1	1	1	6	1	3	2	2	2
0235+164	2	1	1	7	1	1	2	1	1
0237-027	3	1	2	1	1	1
0237+040	3	1	1	1	1	1
0239+108	1	3	3	6	1	2	2	1	1
0241+622	1	3	3	6	2	2	3	1	2
0250+320	1	1	1
0256+192	3	1	2
0300+470	2	2	2	10	1	2	4	1	1
0306+102	3	1	2	2	1	1
0309+411	1	1	1	3	2	2
0322+222	1	1	1	3	1	1
0333+321	3	1	2	2	1	1
0336-019	6	1	3	4	1	2
0340+362	1	2	2	5	1	2	1	1	1
0345+460	1	3	3	6	1	2	1	1	1
0346-279	1	2	2	6	1	2	1	1	1
0350+465	1	2	2	6	1	2	1	1	1
0354+231	3	1	1
0358+040	1	1	1	6	1	3	1	1	1
0358+210	1	1	1	3	1	1
0400+258	1	2	2	6	1	2	2	1	1
0402-362	1	1	1
0405-331	3	1	2
0405-385	1	2	2
0406+121	1	2	2
0409+229	1	3	3	2	1	2
0415+398	3	1	2
0420-014	3	1	1
0420+022	3	2	2
0422+004	3	1	1
0422-380	1	2	2
0425+048	1	1	1
0426+273	1	2	2	3	1	1
0426-380	1	1	1
0429+174	2	1	1
0430+052	3	2	3
0446+112	1	1	1	5	1	2	2	1	1
0450+013	1	1	1
0454-234	2	1	2	10	1	2	4	1	3
0458-020	2	1	2	10	1	1	4	1	1
0458+138	1	2	2	1	1	1

TABLE 4 — *Continued*

Source	X band (8.4 GHz)			K band (24 GHz)			Q band (43 GHz)		
	N_{session}	SI_{min}	SI_{max}	N_{session}	SI_{min}	SI_{max}	N_{session}	SI_{min}	SI_{max}
0459+135	3	1	1
0502+049	3	1	2
0506+056	1	2	2	6	1	2	1	1	1
0507+179	1	2	2	3	1	1
0511-220	3	1	2
0524+034	1	1	1	6	1	1	1	1	1
0528+134	1	1	1	5	1	3	2	2	2
0528-250	1	2	2
0534-340	1	1	1
0537-441	1	2	2
0544+273	1	2	2	4	1	1
0547+234	1	2	2	3	1	3
0549+192	1	2	2	1	1	1
0552+398	1	3	3	5	2	2	2	1	1
0554+242	1	2	2	3	1	3
0556+238	1	1	1	4	1	1	2	1	1
0601+245	1	3	3	1	2	2
0607-157	2	1	2	8	1	3	2	1	2
0611+131	1	1	1	3	1	2
0621+446	1	1	1
0639-032	1	2	2	4	1	2
0639+352	1	2	2
0642+449	1	1	1	4	2	2	2	2	3
0646-306	3	2	3	2	1	2
0648-165	2	1	1	10	1	2	4	1	3
0654+244	1	3	3	1	1	1
0707+476	3	1	2	1	3	3
0716+477	3	1	2
0721-071	1	2	2	4	1	2
0722+145	1	2	2	5	1	1	1	2	2
0725+219	1	2	2	2	1	2
0727-115	6	1	2	4	1	2
0728+249	1	2	2
0735+178	1	3	3	6	2	2	2	2	2
0736+017	3	1	2
0743-006	1	1	1	4	2	4	2	2	2
0745+241	1	2	2	6	1	2	2	1	1
0746+483	1	2	2	6	1	2	1	1	1
0748+126	2	1	1	8	1	2	2	1	1
0749+540	2	2	2	10	1	2	4	1	2
0754+100	2	2	2	10	1	3	4	1	2
0759+183	1	2	2	3	1	1
0804+499	2	1	2	10	1	2	4	1	1
0805-077	3	1	2
0805+410	1	1	1	5	1	1	2	1	1
0808+019	2	1	1	10	1	1	4	1	1
0812+367	3	2	2
0814+425	1	2	2	5	1	2	2	1	1
0820+560	1	3	3	4	2	2	2	1	1
0821+248	1	1	1	2	1	1
0821+394	1	1	1	3	1	1
0823+033	1	2	2	4	1	2	2	1	2
0827+243	1	2	2	4	1	2
0834-201	3	2	2
0834+250	1	2	2	3	1	2
0838+133	1	3	3	6	2	2	1	2	2
0839+187	1	4	4	2	1	2
0850+581	1	3	3	2	1	2
0851+202	1	2	2	5	1	2	2	1	2
0906+163	2	1	1
0912+029	3	1	2
0917+624	1	3	3	4	1	2	2	1	2
0923+392	1	3	3	4	3	3	2	4	4
0945+408	1	4	4	3	2	3
0953+254	2	3	3	10	1	2	4	1	2
0955+326	1	2	2	3	2	2
0955+476	2	2	2	1	1	1
1005+066	3	1	2
1012+232	3	2	3
1016-311	2	2	2
1020+400	3	1	2
1022+194	1	2	2	3	1	1
1022+237	1	1	1
1032-199	3	1	3
1034-293	2	2	3	9	1	2	3	1	3
1039+811	3	1	2	1	1	1

TABLE 4 — *Continued*

Source	X band (8.4 GHz)			K band (24 GHz)			Q band (43 GHz)		
	N_{session}	SI_{min}	SI_{max}	N_{session}	SI_{min}	SI_{max}	N_{session}	SI_{min}	SI_{max}
1045-188	2	2	3	10	1	2	4	1	2
1048-313	1	3	3
1049+215	3	1	2	1	1	1
1053+815	2	2	3	7	1	1	2	1	1
1055+018	1	2	2	8	1	2	3	2	2
1101+384	3	1	1
1113+087	2	2	2
1124-186	2	1	1	10	1	1	4	1	2
1128+385	3	1	2	1	1	1
1142+052	2	1	3
1144-379	1	1	1	1	2	2
1144+402	5	1	1	2	1	1
1147+245	1	2	2	3	1	2
1150+497	3	2	2
1150+812	1	3	3	3	3	3
1156+295	1	1	1	5	1	2	1	1	1
1207-319	1	2	2
1213-172	3	2	2
1236+077	3	1	1	1	3	3
1243-072	3	1	1	1	1	1
1256-220	1	1	1	6	1	2	1	1	1
1302-102	1	2	2	1	1	1
1308+326	2	2	3	10	1	2	4	1	2
1308+554	1	2	2	3	1	1
1313-333	1	3	3	5	1	3	2	2	2
1324+224	1	1	1	5	1	2	2	1	1
1334-127	1	2	2	5	1	2	2	1	1
1354-152	3	1	1	1	2	2
1357+769	2	1	1	1	1	1
1406-076	2	1	2	1	2	2
1406-267	1	2	2
1418+546	1	3	3	3	2	2
1435-218	3	1	2
1437-153	3	1	1
1451-375	1	1	1
1459+480	3	1	2
1502+036	2	1	1	1	2	2
1502+106	2	2	2	10	1	2	4	1	2
1504+377	1	2	2
1505+428	1	3	3	6	1	2	1	2	2
1511-100	1	3	3	6	1	2	3	1	2
1514+004	1	3	3	5	2	2	1	2	2
1514+197	3	1	1
1514-241	3	2	3
1519-273	3	1	1
1520+437	1	1	1
1546+027	1	2	2	5	1	2	2	1	1
1548+056	1	3	3	4	1	3
1606+106	1	3	3	5	1	2	2	1	2
1611+343	3	2	2	1	1	1
1617+229	1	2	2	6	1	2	1	1	1
1622-253	3	1	1
1622-297	3	1	2
1637+574	1	1	1	4	1	2	2	2	2
1638+398	1	1	1	5	1	2	2	1	1
1652+398	3	2	2
1656-075	3	1	3
1657-261	3	1	1
1705+018	3	1	1	1	1	1
1710-269	2	2	3
1717+178	3	2	2	1	1	1
1726+455	2	1	2	10	1	1	4	1	3
1730-130	2	2	2	9	1	2	3	1	2
1732+389	1	1	1	5	1	2	2	2	2
1738+476	3	1	2	1	1	1
1741-038	1	1	1	5	1	3	3	1	2
1741-312	1	3	3
1742-078	1	3	3	6	2	2	1	1	1
1749+096	1	1	1	5	1	2	2	1	1
1749+701	1	3	3	3	2	3
1751+288	3	1	1	1	1	1
1754+155	3	1	2
1800+440	3	1	1
1803+784	1	3	3	4	1	2	2	1	2
1817-254	2	1	1
1817+387	3	1	3

TABLE 4 — *Continued*

Source	X band (8.4 GHz)			K band (24 GHz)			Q band (43 GHz)		
	N_{session}	SI_{min}	SI_{max}	N_{session}	SI_{min}	SI_{max}	N_{session}	SI_{min}	SI_{max}
1829-106	2	2	3
1829-207	2	2	3
1830-211	2	2	2
1849+670	1	1	1	4	1	1	2	1	1
1901+319	3	1	3	2	1	1
1921-293	2	2	3	8	1	2	3	1	2
1928+154	3	1	2
1936-155	1	1	1	3	1	1	2	1	2
1946-200	1	2	2
1954-388	1	1	1
1958-179	2	1	1	1	1	1
2000+472	3	1	2
2008-159	2	1	1	10	1	2	4	1	2
2013+163	3	1	1
2021+317	3	2	3	2	1	1
2029+121	1	2	2
2037+511	3	1	2	1	1	1
2048+312	1	3	3	3	1	3
2054-377	1	1	1
2106-413	1	2	2
2113+293	3	2	2	1	1	1
2121+053	1	1	1	5	1	2	2	1	1
2126-158	3	1	3	1	3	3
2128-123	3	3	4
2131-021	1	3	3	5	2	2	2	2	2
2136+141	2	2	2	10	2	3	4	1	1
2143-156	1	2	2	3	1	1
2145+067	1	3	3	5	1	2	2	2	2
2150+173	1	3	3	4	2	2	1	1	1
2200+420	3	1	2	2	1	1
2201+171	3	1	2
2209+236	3	1	2
2214+350	3	1	2
2227-088	1	1	1	9	1	1	4	1	1
2239+096	1	2	2	6	1	2	1	2	2
2251+158	1	4	4	3	2	2
2254+024	3	1	1
2255-282	2	1	2	10	1	2	4	1	2
2306+095	1	2	2
2309+454	1	2	2	6	1	2	1	1	1
2318+049	1	1	1	5	1	1	2	1	1
2325+093	1	1	1	6	1	1	1	1	1
2335-027	3	1	1
2344+092	3	2	2
2346+385	3	1	2
2353+816	1	2	2	6	1	1	1	1	1
2355-106	3	1	1
2357-318	3	1	1

TABLE 5
SOURCE COMPACTNESS VS. SOURCE STRUCTURE INDEX.

Struc. Ind.	K Band (24 GHz)			Q Band (43 GHz)		
	\bar{N}_{sou}	Mean	Median	\bar{N}_{sou}	Mean	Median
1	84	0.89	0.90	74	0.87	0.87
2	131	0.79	0.80	48	0.74	0.75
3	40	0.70	0.70	9	0.71	0.71
4

TABLE 6
SOURCE POSITION UNCERTAINTIES VS. SOURCE STRUCTURE INDEX.

Struc. Ind.	N_{sou}	X band (8.4 GHz) ^a				K Band (24 GHz) ^b				
		Mean (mas)		Median (mas)		Mean (mas)		Median (mas)		
		$\alpha \cos \delta$	δ	$\alpha \cos \delta$	δ	$\alpha \cos \delta$	δ	$\alpha \cos \delta$	δ	
1	50	0.34	0.42	0.28	0.31	49	0.27	0.33	0.27	0.31
2	106	0.38	0.45	0.29	0.32	119	0.28	0.33	0.27	0.30
3	72	0.44	0.54	0.33	0.36	23	0.27	0.32	0.27	0.30
4	36	0.54	0.72	0.76	1.07

^a X band ICRF values taken from Fey & Charlot (2000)

^b K band formal errors used to compute the mean and median uncertainties were inflated so as to be comparable to the X-band ICRF values (see discussion in the text).